2016

Understanding catalytic pyrolysis of biomass for production of biofuels

Chamila Rajeeva Thilakaratne
Iowa State University

Understanding catalytic pyrolysis of biomass for production of biofuels

by

Chamila Rajeeva Thilakaratne

A dissertation submitted to the graduate faculty

in partial fulfillment of the requirements for the degree of

DOCTOR OF PHILOSOPHY

Major: Mechanical Engineering

Program of Study Committee:
Robert C. Brown, Major Professor
Jean-Philippe Tessonnier
Mark Mba Wright
Guiping Hu
Song-Charng Kong

Iowa State University

Ames, Iowa

2016

DEDICATION

Dedicated to my dear Ammi (Mom) and Appachchi (Dad).

TABLE OF CONTENTS

ACKNOWLEDGMENTS

First and foremost, I would to take this opportunity to express my gratitude to my supervisor Dr. Robert C. Brown for his unwavering trust, motivation, and support towards the successful completion of this work. I would like to thank my committee members Dr. Jean-Philippe Tessonnier, Dr. Mark Mba Wright, Dr. Guiping Hu and Dr. Song-Charng Kong for their guidance and support throughout my PhD program. I am grateful to the support and helpful discussions from Bioeconomy Institute staff members in particular Ryan Smith, Dr. Marjorie Rover, Dr. Xianglan Bai, Patrick Johnston, Patrick Hall, Dr. Jackie Baughman, Lysle Whitmer and Preston Gable. I would also like to thank my past and present BEI colleagues including (by alphabetical order of surnames) Sanaz Abdolmohammadi, Denis Bbosa, Karl Broer, Tristan Brown, Dustin Dalluge, Qi Dang, Tannon Daugaard, Bernardo Del-Campo, Andrew Friend, Preston Gable, Arpa Gosh, Martin Haverly, Tom Hoff, Matt Kieffer, Ashokkumar Sharma, Wenqi Li, Wenqin Li, Jake Lindstrom, Kwang-Ho Kim, Longwen Ou, Joseph Polin, Juan Proano, Fenglei Qi, Lysle Whitmer, Patrick Woolcock, Yuan Xue, Yanan Zhang and Yan Zheng. Their friendship and support makes my time at Iowa State University a wonderful experience. I am grateful to Gayan Abeykoon, Nuwan de Silva and Umayangani Wanninayake of the Chemistry Department of Iowa State University for the helpful discussions about reaction mechanisms proposed in this study. Last but not least, I would like to thank my wife Supipi, my family and my friends who constantly stood by me through my good and bad times.

ABSTRACT

Catalytic pyrolysis of biomass has been identified as one of the pathways to replace fossil fuel resources for transportation fuels and mitigate environmental impacts of fossil fuels. However, lack of technical and economic information on this technology has created uncertainty about the feasibility of this approach to biofuels. This dissertation helps to fill some of the gaps and advances of catalytic pyrolysis as an alternative approach to producing advanced biofuels.

First, techno-economics of a woody biomass, mild catalytic pyrolysis pathway for transportation fuels was investigated. This study detailed the process modelling, energy analysis, economic analysis and uncertainty analysis of this technology. Novel methods for heat exchanger network design, higher heating value (HHV) based energy analysis and uncertainty analysis was demonstrated in this study.

Second, techno-economics of microalgae catalytic pyrolysis to transportation fuels was analyzed mainly to investigate the influence of moisture in feedstock and energy integration of the process. This study provides details of different dewatering techniques and illustrates how process heat can be used to partially dewater feed algae. Moreover, low product yield was identified as the major contributor for high fuel selling price obtained for this pathway.

Lastly, as it is important to understand the reaction chemistries of lignocellulosic biomass conversion over zeolites, lignin and cellulose conversion during catalytic pyrolysis was analyzed in micro-scale reactor setup, where mass and heat transfer effects are negligible. Lignin model compound study performed using phenol and anisole showed that

phenolic functionalities play a major role in the formation of aromatics and coke over zeolites. Hydroxyl functionality promoted coke formation, while methoxy functionality contributed toward alkylating aromatics and reducing coke. From the cellulose study, it was found that acid sites on the external surface of zeolites plays a major role in coke formation due to lower spatial restriction and dehydrogenation compared to acid sites in the internal pores of zeolites. Impregnating acid into cellulose and pyrolyzing it over silylated zeolites was demonstrated as a combined homogeneous and heterogeneous acid-catalyzed pathway that significantly improved aromatic yield.

CHAPTER I INTRODUCTION

Renewable Biofuel Production

In 2014, US transportation sector was responsible for 28% of US energy demand with 92% of this provided from fossil fuel resources. This reliance on fossil fuels is a major concern with respect to securing sustainable sources of energy for our society.[1] Conventional fossil fuel resources are drastically depleting and predictions say it will only last for another few decades.[2, 3] Newer technologies such as fracking and oil shale conversion have emerged, especially in US, as alternatives for this problem. However there are significant uncertainties of the environmental impacts, in addition to eventual limitations of these resources.[2, 4] Petroleum is a net carbon emitter, increasing greenhouse gas (GHG) levels in the atmosphere, which in turn contributes to global warming.[2] Even with significant technological advancements, battery electric and hydrogen fuel-cell vehicles are deemed insufficiently mature to immediately address this problem.[2] Life cycle analysis (LCA) of these technologies demonstrate that fossil fuels will probably be used to generate the required electricity and hydrogen for these vehicles, adversely affecting GHG emissions.[2, 5] On other hand, the energy cost of these processes are high due to multiple energy conversion steps and low conversion efficiencies.[2, 6] These analyses suggest that petroleum based transportation systems will persist for many years. We need to find liquid fuel alternatives to replace gasoline, diesel, and aviation fuel.

Biomass-to-transportation fuels pathways offer attractive solutions by providing renewable alternatives to fossil fuel-based transportation fuels.[2] Biomass derived fuels are considered low carbon neutral because CO_2 is cycled between growing plants combustion emissions.[7] However, net carbon emissions are influenced by the biomass-to-fuel life cycle. For

example, fossil fuel usage to produce biofuels and building of soil carbon during plant growth would result in positive and negative contributions to net GHG emissions, respectively.[7] A variety of approaches to advanced biofuels have been developed in the past few decades for producing biofuels.[8] The following sections discuss these approaches for biofuels in following broader categories.

Bio-ethanol and Bio-diesel

Fermenting sugars and starch from biomass to produce ethanol has been known for thousands of years.[9] In Brazil today, nearly 20% of automobiles run on ethanol derived from sugar cane.[10] In the USA, ethanol is mostly produced from starch crops, particularly corn, which is blended with gasoline as an oxygenate additive.[11] Since its introduction in the 1970's, ethanol has gradually developed into a major source of transportation fuel, being blended with gasoline at a concentration of10% by volume (commonly known as E10 fuels) that can be used without any changes to the gasoline engine.[12] Recent developments in flex-fuel engines allow up to 85% (E85) ethanol blending to gasoline vehicles, equipped with specially designed engines to alter the combustion characteristics in varying blending ratios.[8, 12] Resistance has emerged for using corn as fuel, the argument being that using a crop that also supports the human food supply is "a crime against humanity".[8] Additional criticism emerged in the form of indirect land use change arguing that with the reduction of food supply (used to produce fuels) in developed countries, farmers in underdeveloped countries may use forest land to supplant the demand of the food, increasing the overall carbon footprint with these forests are burned.[8] As an alternative, US scientists have developed the lignocellulose based process to produce ethanol using agricultural residues as the feedstock.[8] This process has additional pretreatment and hydrolysis steps

compared to grain ethanol to recover cellulose from agricultural residues and to convert the cellulose to glucose, which can be converted via traditional sugar fermentation process.[8] The major shortcoming of cellulosic ethanol process is that this can only can supplant the gasoline fraction of the transportation fuels, requiring a bio-based alternative for diesel and aviation fuels.

Biodiesel production via lipid rich feedstocks has been identified as an approach to replace the diesel part of the transportation fuel requirement.[8] This process employs an alkaline treatment at mild temperatures to liberate triglycerides from lipids that can be further upgraded to biodiesel.[8] This rather simple process can be adopted to use in wide range of feedstocks that contain lipids.[8] However, due to economics of scale, major production of biodiesel is still based on food based feedstocks such as soy-oil and palm-oil, drawing wide criticism of this approach.[13] Advances are being made to develop a process that can convert cellulosic feedstocks to diesel fuels; however, commercial success has not yet been achieved.[14]

Thermochemical conversion of biomass

There are several types of thermochemical conversions pathways. Gasification employs heat at high temperatures (600-1000^{o}C) to convert biomass to gaseous intermediates.[15] The amount of air injected in to the reactor is controlled to obtain higher energy gases, consist of CO and H_2, that are converted to gasoline and diesel range fuels over a catalyst bed. [15] This approach has the advantage of being able to use a wide range of feedstocks including those that are difficult to convert using other methods. However, the complex and costly gas cleaning steps employed to prevent poising of downstream catalyst bed is a major drawback for this process. [15] This combined with high capital cost has slowed commercialization of this technology.[15]

Solvolysis converts biomass in to a liquid intermediate that can be upgraded to fuels.[15]. When solvolysis uses water as the solvent, it is an attractive technology for converting high moisture feedstocks such as algae, sludge derived from municipal waste systems, etc.[15] This approach has gained attention as costly biomass pretreatments steps such as drying and grinding can be avoided.[15] However, complexities of designing high pressure reactor with a continuous feeding system have posed serious challenges for the feasibility of solvolysis pathway.[15]

Fast pyrolysis uses rapid heating of biomass in the absence of oxygen to directly produce liquids. In the process, a majority of the biomass is converted to gaseous volatiles that are quickly condensed to a liquid called bio-oil.[15] This bio-oil can be hydroprocessed in an upgrading reactor to produce gasoline and diesel fuels.[15] Non-condensable gases produced in the conversion are mostly consumed for process heat. The process produces a carbonaceous residue known as bio-char that is often combusted for heat although several other applications such as soil amendments and producing activated carbon have been explored.[15] The optimal temperature range for process is 400-600^{o}C.[15] Pyrolysis occurs in an inert atmosphere; however, oxygen in the void spaces of biomass contributes to some of the CO and CO_2 found in the exhaust gases.[15] This process typically converts about 70% of biomass to bio-oil. Reactors are relatively simple to construct. Due to lower cost of handling liquid bio-oil intermediate, pyrolysis-based biomass conversion can be carried out in distributed units to reduce the transportation cost of the feedstock. One major problem associated with fast pyrolysis is the lower stability of the bio-oil caused by its higher water content, higher oxygen content and abundance of compounds with reactive functionalities.[15] To overcome these obstacles, scientists have investigated the use of catalysts in the process to deoxygenate and stabilize the bio-oil produced. Under these conditions the process is called catalytic pyrolysis, which is the focus of this dissertation.

Catalytic pyrolysis of biomass

Catalytic pyrolysis generally employs a heterogeneous catalyst in the pyrolysis reaction to obtain a higher quality pyrolysis liquid.[16] The catalyst helps to overcome the reaction energy barriers to deoxygenating pyrolysis-derived vapors.[17] Bio-oil from catalytic pyrolysis has fewer unstable and oxygenated polar compounds, allowing it to be more easily upgraded to fuels.[16] The process employs slightly higher temperatures (600^{o}C to 700^{o}C) compared to conventional pyrolysis. Special arrangements to regenerate catalyst over circulating fluidized bed reactors must be included.[17]

Several types of catalyst have been investigated including acidic metal oxides and zeolites, transition metals and its oxides precious metals, and basic oxides.[18] Acidic zeolites have been most commonly investigated.[19, 20] High aluminum content and smaller pores such as found in ZSM5 and Y zeolites generally produce the highest liquid yields from biomass pyrolysis.[19, 20] Zeolites are relatively inexpensive and robust compared to the acidic metal oxide catalysts.[21] They can be readily regenerated to remove deposits of coke.[21] They do not require hydrogen or other reactive agents and can be used at atmospheric pressure. Thus, zeolites can be viewed as a practical and convenient catalyst for biomass conversion reactions. Hydropyrolysis, another version of catalytic pyrolysis, adds hydrogen in the reactor, which helps deoxygenate the bio-oil.[22] Catalytic pyrolysis over zeolites is the major focus of this dissertation.

In one version of this catalytic pyrolysis, biomass is completely deoxygenated to hydrocarbons, typically aromatics such as benzene, toluene and xylenes (BTX), naphthalenes and olefins. This process is sometimes referred to as severe catalytic pyrolysis.[17] Anellotech, which employs severe catalytic pyrolysis technology, has developed a process for the one-step

production of aromatics from biomass with plans to produce BTX in commercial-scale units.[17] Cool Planet has proposed similar technology, although the catalytic bed is located downstream of the pyrolyzer.[23]

In mild catalytic pyrolysis, biomass is partially deoxygenated and the resultant bio-oil is upgraded using hydroprocessing.[17, 24] Mild catalytic pyrolysis has been proposed by KiOR, although this company recently went into bankruptcy.[24, 25] Mild catalytic pyrolysis benefits from the ability to use existing petroleum refining technologies, such as fluid catalytic cracking (FCC), hydrotreating, and hydrocracking, thereby lowering the investment risk of the catalytic pyrolysis process.[17, 24] Only few studies have been published on the techno-economics of catalytic pyrolysis. Part of this dissertation attempts to rectify this knowledge gap, which will assist in future commercialization efforts.

Microalgae conversion over zeolites during catalytic pyrolysis has received wide attention with its denitrification capabilities reported.[26, 27] However, high moisture content of the algae feedstocks has remained a major challenge for this technology to achieve commercial scale production.[28, 29] The energy requirement for moisture removal is daunting, requiring as much as 50% of the energy content of the biomass itself.[30] Several researcher have investigated production of aromatic hydrocarbons form pyrolysis of microalgae; however, no in-depth analysis on feedstock dewatering and energy integration aspects of this process have been reported.[26, 27]

One of the major reasons for the bankruptcy of KiOR was their inadequate knowledge of the chemistry of catalytic pyrolysis, especially involving coke formation. Investigating lignin and cellulose (as model biopolymers of biomass) conversion over zeolites are identified as important

steps in understanding the reactions in biomass catalytic pyrolysis. Cellulose represents the most abundant component in lignocellulosic biomass, while lignin represents the most recalcitrant component. One major problem identified with lignin pyrolysis is its reactive functionalities (mainly hydroxyl and methoxy groups), contributing to polymerization and coke generation and, in turn, lower product yields.[31] It is largely unknown how aromatics and coke are generated over zeolite acid sites. The literature investigates model compounds over zeolites, which show yields of different products and their selectivities; however, these studies do not provide specific mechanisms for these reactions. [32-35]

Dissertation scope

The objective of this dissertation is to explore biomass catalytic pyrolysis to produce biofuels. Both techno-economic analysis of these pathways and lab-scale experimental studies on the conversion of biomass model compounds over zeolites are explored.

This dissertation is organized into six chapters, with Chapter 1 serving as an introduction and literature search. Chapter 2 describes techno-economic analysis mild catalytic pyrolysis of woody biomass to hydrocarbon fuels. Process modelling, energy analysis, economic analysis and uncertainty analysis of this pathway were performed. Chapter 3 explores catalytic pyrolysis of microalgae to produce biofuels using the severe catalytic pyrolysis approach. Specifically, this chapter investigates the mechanical and thermal dewatering techniques and examines the possibility of using process-derived heat for dewatering microalgae. Chapters 4 and 5 discuss the chemistries of lignocellulose biomass conversion over zeolites during catalytic pyrolysis. These studies were performed in microscale pyrolysis reactors. Using phenolic model compounds, a mechanistic study is presented in Chapter 4 describing how hydroxyl and methoxy

functionalities influence aromatics and coke formation over zeolites. In Chapter 5, cellulose conversion is investigated, analyzing the influence of different types of acid sites and zeolite structures in the conversion to aromatic hydrocarbons. Furthermore, this study details a novel method to increase aromatic yields by combining acid impregnation and zeolite silylation treatments. General conclusions and directions for future work are discussed in Chapter 6.

Reference

1. EIA, Energy use for Transportaion, http://www.eia.gov/Energyexplained/?page=us_energy_transportation.
2. R. C. Brown and T. R. Brown, *Why are We Producing Biofuels?*, Brownia LLC, 2012.
3. J. H. Walsh, Parabolic Projection of World Conventional Oil Production Based on Year 2000 Resource Assessment of the US Geological Survey, Proceedings of the Canadian Association for the Club of Rome, Series, 2000.
4. C. W. Schmidt, *Environmental health perspectives*, 2013, **121**, a117.
5. H. Ma, F. Balthasar, N. Tait, X. Riera-Palou and A. Harrison, *Energy Policy*, 2012, **44**, 160-173.
6. S. G. Wirasingha, N. Schofield and A. Emadi, Plug-in hybrid electric vehicle developments in the US: Trends, barriers, and economic feasibility, Vehicle Power and Propulsion Conference, 2008. VPPC'08. IEEE, 2008.
7. F. Cherubini, *Renewable Energy*, 2010, **35**, 1565-1573.
8. R. C. Brown and T. R. Brown, *Biorenewable Resources: Engineering New Products form Agriculture*, John Wiley & Sons Inc., 2014.
9. P. E. McGovern, J. Zhang, J. Tang, Z. Zhang, G. R. Hall, R. A. Moreau, A. Nuñez, E. D. Butrym, M. P. Richards, C.-s. Wang, G. Cheng, Z. Zhao and C. Wang, *Proceedings of the National Academy of Sciences of the United States of America*, 2004, **101**, 17593-17598.
10. A. Hira and L. G. De Oliveira, *Energy Policy*, 2009, **37**, 2450-2456.
11. J. Goettemoeller and A. Goettemoeller, *Sustainable ethanol: biofuels, biorefineries, cellulosic biomass, flex-fuel vehicles, and sustainable farming for energy independence*, 2007.
12. S. Kim and B. Dale, *The International Journal of Life Cycle Assessment*, 2006, **11**, 117-121.
13. J. Tomei and P. Upham, *Energy Policy*, 2009, **37**, 3890-3898.
14. A. Yousuf, *Waste Management*, 2012, **32**, 2061-2067.
15. R. C. Brown, ed., *Thermochemical Processing of Biomass*, John Wiley and Sons, Ltd, 2011.
16. R. Thilakaratne, T. Brown, Y. Li, G. Hu and R. Brown, *Green Chemistry*, 2014, **16**, 627-636.
17. R. Thilakaratne, T. Brown, Y. Li, G. Hu and R. Brown, *Green Chemistry*, 2013.

18. D. C. Dayton, Catalytic Biomass Pyrolysis for Bio-Crude Production, , TC Biomass 2011, Chicago, 2011.

19. D. J. Mihalcik, C. A. Mullen and A. A. Boateng, *Journal of Analytical and Applied Pyrolysis*, 2011, **92**, 224-232.

20. A. Aho, N. Kumar, K. Eränen, T. Salmi, M. Hupa and D. Y. Murzin, *Fuel*, 2008, **87**, 2493-2501.

21. M. Guisnet and J. P. Gilson, *Zeolites for cleaner technologies*, Imperial College Press, 2002.

22. T. L. Marker, L. G. Felix, M. B. Linck and M. J. Roberts, *Environmental Progress & Sustainable Energy*, 2012, **31**, 191-199.

23. C. Planet, Product and Technology, http://www.coolplanet.com/how-it-works/GreenFuels.

24. KiOR, :http://www.kior.com/content/?s=6&s2=55&p=55&t=Virtual-Plant-Tour, Accessed April 1 2013.

25. J. Lane, Gusher! KiOR starts production of US cellulosic biofuels at scale, http://www.biofuelsdigest.com/bdigest/2012/08/16/no-eeyores-for-kior/.

26. K. Wang and R. C. Brown, *Green Chemistry*, 2013, **15**, 675.

27. I. V. Babich, M. van der Hulst, L. Lefferts, J. A. Moulijn, P. O'Connor and K. Seshan, *Biomass and Bioenergy*, 2011, **35**, 3199-3207.

28. M. T. Abayomi O. Alabi, Eric Bibeau, *Seed Science*, 2009.

29. P. Chen, M. Min, Y. Chen, L. Wang, Y. Li, Q. Chen, C. Wang, Y. Wan, X. Wang and Y. Cheng, *International Journal of Agricultural and Biological Engineering*, 2010, **2**, 1-30.

30. R. Thilakaratne, M. M. Wright and R. C. Brown, *Fuel*, 2014, **128**, 104-112.

31. R. Thilakaratne, J.-P. Tessonnier and R. C. Brown, *Green Chemistry*, 2016.

32. A. V. Friderichsen, E. J. Shin, R. J. Evans, M. R. Nimlos, D. C. Dayton and G. B. Ellison, *Fuel*, 2000, **80**, 1747 - 1755.

33. M. A. González-Borja and D. E. Resasco, *Energy & Fuels*, 2011, **25**, 4155-4162.

34. T. Prasomsri, A. T. To, S. Crossley, W. E. Alvarez and D. E. Resasco, *Applied Catalysis B: Environmental*, 2011, **106**, 204-211.

35. M. Akazawa, Y. Kojima and Y. Kato, *EC Agriculture* 2015, **1**, 67-85.

CHAPTER 2

MILD CATALYTIC PYROLYSIS OF BIOMASS FOR PRODUCTION OF TRANSPORTATION FUELS: A TECHNO-ECONOMIC ANALYSIS

A paper Published by *Green Chemistry*

Rajeeva Thilakaratne, Tristan R. Brown, Yihua Li, Guiping Hu, Robert C. Brown`

Abstract

A techno-economic analysis of mild catalytic pyrolysis (CP) of woody biomass followed by upgrading of the partially deoxygenated pyrolysis liquid is performed to assess this pathway's economic feasibility for the production of hydrocarbon-based biofuels. The process achieves a fuel yield of 17.7wt% and an energy conversion of 39%. Deoxygenation of the pyrolysis liquid requires 2.7wt% hydrogen while saturation of aromatic rings in the pyrolysis liquid increases total hydrogen consumption to 6.4wt%.

Total project investment is $457 million with annual operating costs of $142 million for a 2000 metric ton per day facility. A minimum fuel selling price (MFSP) of $3.69/gal is estimated assuming 10% internal rate of return. Twenty-nine percent of the capital outlay is the result of including a co-generation system to consume heat generated from burning part of the off-gases from pyrolysis and upgrading and all of the coke during regeneration of catalysts. Forty-five percent of the MFSP arises from the cost of biomass feedstock. Hydrogen required for the upgrading process is generated using the balance of the process off-gases.

The analysis reveals that an optimum design would include a cogeneration unit; however using natural gas for hydrogen generation is more favorable than using process off-gases as the feed. An uncertainty analysis indicates a probable fuel price of $3.03/gal, demonstrating the potential of the CP pathway as an alternative to petroleum-derived transportation fuels.

Introduction

Fast pyrolysis is the rapid heating of biomass in an oxygen-free environment to produce organic vapors and aerosols, which are recovered as liquid known as bio-oil or pyrolysis liquid. This liquid is similar in appearance to petroleum, but lower in quality due to its high oxygen and water content, high acidity, and instability during storage and upon heating.[1] During upgrading, unstable components of the pyrolysis oil tend to polymerize.[1] These compounds must be stabilized before further processing, but even this approach does not entirely produce a desirable feedstock for refining to fuel.[1, 2] Furthermore, hydroprocessing pyrolysis liquid produces large amounts of light off-gases due to the high level of oxygen in the pyrolysis liquid.[3] The result is diminished fuel yield and increased greenhouse gas (GHG) emissions.[3, 4]

As an alternative to this conventional approach to producing hydrocarbon fuels from fast pyrolysis, vapors released during pyrolysis can be exposed to a solid acid catalyst to obtain higher-quality pyrolysis liquid. Oxygenated polar compounds in the vapor are partially or fully deoxygenated through the acid activity encountered when the vapor passes through pores in the catalyst.[5] This reaction reduces the acidity and improves stability of the pyrolysis liquid compared to conventional (non-catalytic) pyrolysis liquid.[6] The most commonly-used catalyst is zeolite, a porous solid acid catalyst with an alumino-silicate structure.[5, 7-10] The main disadvantage of CP is the production of large amounts of coke resulting from the dehydration of

organic compounds by the acid catalyst.[11] The coke blocks active sites in the catalyst, requiring the periodic regeneration of the catalyst.[11] Two variations of CP are practiced, based upon the deoxygenation level achieved in the pyrolysis liquid. Under conditions of high acid site density or low space velocity, known as severe catalytic pyrolysis, vapors are completely deoxygenated. This typically yields aromatic compounds, especially benzene, toluene and xylene (BTX) although light olefins are also produced. This complete conversion of oxygenated molecules to hydrocarbons comes at the cost of relatively low yields of hydrocarbons and high rates of coking on the catalyst.[5] Under conditions of low acid site density and high space velocity, known as mild catalytic pyrolysis, only partial deoxygenation of the organic vapors occurs, although it has the advantages of higher yields of pyrolysis liquid and lower rates of catalyst coking compared to pyrolysis at higher acid strengths.[12] The main focus of this paper is mild catalytic pyrolysis for the production of bio-based transportation fuels.

Due to the oxygen remaining in the liquid product after mild catalytic pyrolysis (mild CP), the pyrolysis liquid requires additional hydroprocessing in order to meet transportation fuel standards.[12] At the same time, the improved stability of mild CP liquid makes it more suitable than conventional (non-catalytic) pyrolysis liquid for upgrading to transportation fuels.[12] Its light oxygenate content is minimal, which leads to lower GHG emissions in hydroprocessing and higher yields. The hydrogen requirement for the upgrading is expected to be low as well due to the lower oxygen content.[12]

The CP pathway has been employed at the commercial-scale, making it the first cellulosic biofuel pathway to reach this milestone.[13] The CP pathway benefits from its ability to use existing petroleum refining technologies, such as fluid catalytic cracking (FCC), hydrotreating,

and hydrocracking, thereby lowering the investment risk of the CP process.[14] Two companies are presently commercializing this pathway. KiOR is employing the mild CP and hydroprocessing pathway at a commercial-scale plant in Columbus, MS.[15, 16] Anellotech, which also employs CP, has developed a process for the one-step production of aromatics from biomass and has plans to produce BTX on a commercial-scale.[17]

To date, most published studies on CP have focused on complete deoxygenation of pyrolysis vapors to produce aromatic hydrocarbons.[10, 18-20] In the available literature on mild CP, Dayton et al.[21] report experimental work on mild CP and hydroprocessing and provide a summary of the pathway techno-economics. Zacher et al.[12] describe an experimental approach for a similar process but give no details on its techno-economics.

This paper presents the results of a techno-economic analysis (TEA) of the mild CP and hydroprocessing pathway. A 2000 metric ton per day (MTPD) CP and hydroprocessing facility is modeled to calculate its total project investment (TPI) and annual operating costs. Minimum fuel selling prices (MFSP) for the product gasoline and diesel fuel are estimated under a 10% internal rate of return (IRR). The results of this paper are presented in a format permitting comparisons with recent TEAs of other pyrolytic pathways, including fast pyrolysis and hydroprocessing,[4, 22] fast pyrolysis and integrated catalytic processing[23], and fast pyrolysis and FCC upgrading.[24]

Material and methods

Process model description

The base-case mild CP process model is developed using ChemCAD assuming an n^{th} plant design. Aspen Energy Analyzer is used to design the heat exchanger network (HEN). The model

Alternative designs such as using purchased hydrogen or natural gas for hydrogen generation and a design without cogeneration are also analyzed to investigate the optimum scenario consists of the key areas of feedstock pretreatment, catalytic pyrolysis, upgrading, hydrogen generation and co-generation, as illustrated in **Figure 1**. Alternative designs such as using purchased hydrogen or natural gas for hydrogen generation and a design without cogeneration are also analyzed to investigate the optimum scenario.

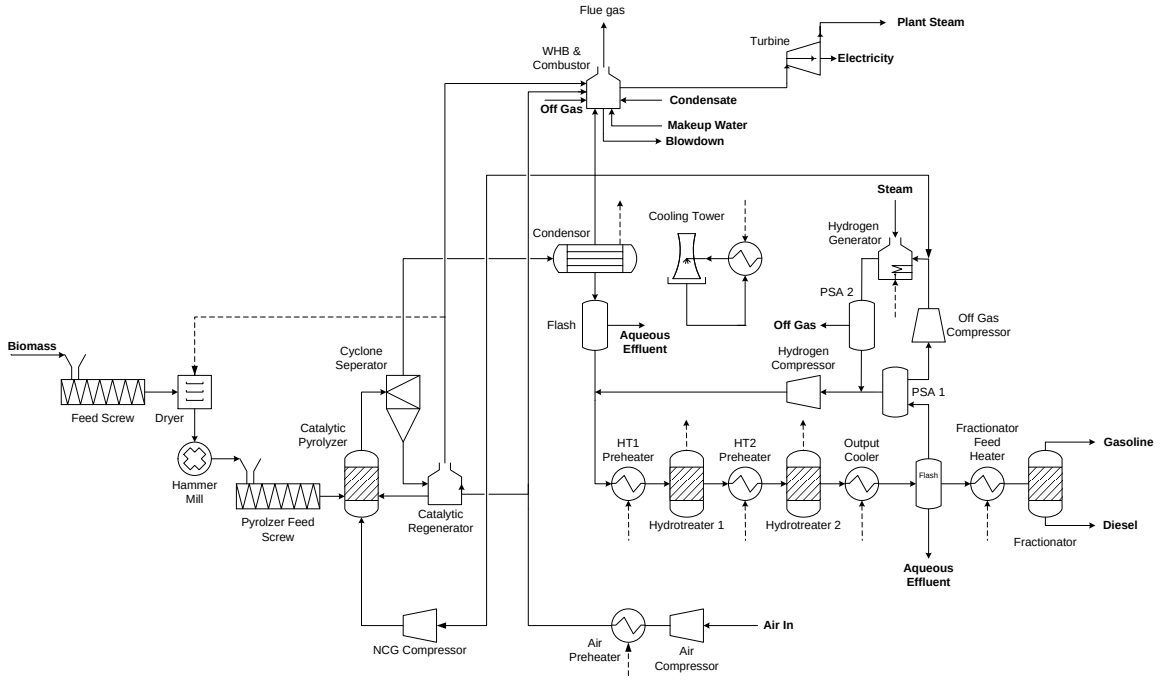

Figure 1. Simplified mild CP process flow diagram

Biomass feedstock

A wide variety of biomass can be employed as feedstock for CP. The particular selection depends upon availability, cost, pyrolysis conversion rates, and product yields. For this particular study, hybrid popular is selected as feedstock. In general, woody biomass achieves higher conversion rates relative to herbaceous feedstock because of its lower mineral content; minerals

in biomass reduce conversion rates by increasing gas and char generation.[25] The elemental analysis of the hybrid popular is assumed to be carbon:49.75 wt%; hydrogen: 5.52 wt%; nitrogen: 0.52 wt%;oxygen: 42.42 wt%; and ash: 2.03 wt%.[26] Molar balances on the pyrolysis process are used to back calculate char and coke yields.

Pretreatment

2000 MTPD of hybrid poplar feedstock is received in the pretreatment site with moisture content of 30% and in the form of two inch sieve size chips. The site consists of a storage system, conveyor system, dryer, and hammer mill.[27] Process (regenerator) flue gas is used in the dryer to reduce the moisture content of the biomass to 10%. The design uses a flue gas flow of 400,000 kg/hr and a dryer inlet temperature of 290^{o}C , obtained by diluting flue gas with an additional air stream.[27] The hammer mill grinds the dried biomass into a screen size of 2 mm before feeding it to the pyrolyzer.[27]

Pyrolysis

Solid biomass is converted to pyrolysis vapor at 500^{o}C and atmospheric pressure in a circulating fluidized-bed-type (CFB) pyrolyzer. Data for mild CP is scarcely reported in the literature; the yield data in **Table 1** comes from Dayton et al.[21]

The coke, char, catalyst, and heat-carrier sand are separated from the pyrolysis vapor in cyclones and the catalyst is regenerated in the combustor, where the coke and char are burned out. The heated catalyst and sand at 650^{o}C are recycled back to the pyrolyzer, where they act as heat carriers for the pyrolysis reaction.[28] The quantity of heat-carrier sand is sufficient to maintain the desired pyrolysis temperature. The CFB reactor configuration is extensively used in FCC processes in crude oil refineries; and is well suited for biomass CP as coke regeneration is

required for continuous operation. For circulation and fluidization, a fraction of the non-condensable gas (NCG) is used to maintain a superficial velocity of 4 m/s for a solid-flux rate of 110 kg/ms.[2, 28] This study assumes a catalyst and sand particle size of 50 microns.[28]

Table 1. Mild CP material balance [21]

Component	**Wt% of dry feed**
Coke and char	21.4
Water	26.1
Pyrolysis liquid (dry basis)	24.8
Gas compounds‡	25.64
Pyrolysis liquid compounds	
Furans	0.27
Aldehydes/Ketones	2.66
Phenols	6.15
Aromatic polyols	9.90
Sugars	0.05
Mono aromatics	1.40
Di-aromatics	3.17
Paraffins	0.13
Tetra-aromatics	1.05
Gas compounds	
H_2	0.12
CO	8.17
CO_2	11.29
CH_4	1.67
C_{2+}	2.64
NO_2	1.74

‡ Adjusted to obtain material balance

A multifunctional catalyst is used to obtain the pyrolysis liquid distribution in **Table 1**, which includes solid bases and transition metal oxides in addition to the acidic zeolite.[21] A mild CP catalyst-to-biomass ratio of 1:1 is maintained and this ratio is estimated by extrapolating experimental data from Zacher et al.[12] to match the 20 wt% oxygen in the pyrolysis liquid used in the analysis.

After removing the solids through cyclones, the pyrolysis vapor is recovered with a series of condensers, using cooling water at 30^{o}C. The remaining NCG is used for a variety of purposes: part is used to fluidize the pyrolysis bed, part is sent to the co-generation area, and the rest is sent to the hydrogen plant as feed. The cooled and condensed pyrolysis liquid has relatively low oxygen content (20%) compared to conventional fast pyrolysis liquid (40%), and it can be easily phase separated using a flash vessel to isolate the water-rich phase from the oil-rich phase. The water-rich portion, (aqueous phase) which contains negligible amounts of carbohydrates, is sent to the water treatment plant as waste. The oil-rich portion (oil phase) is sent to the upgrading section, where it is upgraded to gasoline and diesel.

Upgrading

Mild CP liquid's oxygen content must be reduced to negligible levels before it can meet transportation fuel standards.[29] The oxygen removal is done via two-stage hydrotreating using hydrogen over pressure of 50%.[29] In the first stage, hydrotreating is done in mild conditions of 200^{0}C and 1700 psi to stabilize the pyrolysis liquid.[30] The second stage completes the upgrading of the resultant oil to hydrocarbons, a process that requires more severe conditions of 400^{o}C and 1700 psi.[30]

Unfortunately, no detailed data is reported for hydroprocessing of mild CP oil. Scott et al.[31] report a product gas distribution for lignin hydroprocessing for a feed with oxygen content similar to this study (20% dry basis). In that study, 9.2 wt% of the feed is converted to gases. Zacher et al.[12] provide typical constituents in an upgraded oil of mild CP. When these assumptions are combined, mole-balance calculations provide a conversion of 78 wt% on a dry feed basis. The oxygen is removed from the oil mainly in the form of water (87%), with the rest leaving in the form of carbon dioxide. **Table 2** gives a detailed description of the material balance for the hydroprocessing step.

Following hydroprocessing, the upgraded pyrolysis liquid, now with negligible oxygen content, is phase separated using high-pressure and low-pressure flash chambers to obtain upgraded hydrocarbon oil, aqueous waste, and off-gases. The aqueous waste is directed to a waste water treatment plant, while the gases are used along with some of the NCG as feed for the hydrogen plant.

The upgraded hydrocarbon liquid is next sent to a debutanizer column where butane and other light gas components are separated from the top (70^{o}C) and the rest of the oil is recovered as bottom product (130^{o}C). The light gases are directed to the hydrogen plant as feed. Bottom product is then fed into a fractionator column to obtain gasoline from the top (170^{o}C) and diesel from the bottom (220^{o}C).

Table 2. Hydroprocessing material balance

Component	**Wt% of dry feed**
Feed hydrogen‡	6.4
Upgraded oil‡	78.2
Gas[31]	9.2
Water[a]	18.9
Upgraded oil [12]	
Aromatics	25.0
Cycloalkanes	50.6
Partially saturated aromatics	7.4
Olefins	2.4
Paraffins	14.6
Gas compounds[26]	
CO_2	3.35
CH_4	3.14
C_2H_6	0.96
C_3H_8	0.86
C_4H_{10}	0.91

‡ Calculated from the mole balance

Hydrogen generation

Hydrogen for the process is provided by steam reforming NCG and off-gases from hydroprocessing. After compression and desulfurification, these feed gases are subjected to adiabatic pre-reforming where components with two or more carbons are broken down to single carbon molecules.[34] In the reformer, most of the feed is converted to hydrogen, carbon monoxide, and carbon dioxide at 830^{o}C and 20 bars, using a steam-to-carbon ratio of 4:1.[32-34] A high-temperature-shift reactor at 521^{o}C is used to convert the majority of the carbon monoxide

and water to carbon dioxide and hydrogen.[32-34] Reforming is a highly endothermic reaction and the heat required for this conversion is provided through the combustion of some of the off-gases in a fired heater.

Co-generation

Overall the process produces excess heat, especially from the catalyst regeneration step. This heat is used to fuel a co-generation system that produces electricity and steam. High-pressure steam at 450^{o}C and 60 bars is generated from a waste-heat boiler, which uses excess heat from the catalyst regenerator and the off gas combustor.[33] A series of turbines uses a major portion of this high-pressure steam to generate power, while a small portion is used as process steam. The expanded steam is cooled and condensed at 0.1 bar and 46^{o}C and then recycled.[33] Boiler blow-down is assumed to be 0.3% of total steam generated.[33] A scrubber removes the gaseous sulfur and nitrogen constituents of the flue gas in the combustors.[34]

Utilities

The HEN is designed using Aspen Energy Analyzer and the stream data is provided by the ChemCAD model. A pinch temperature of 10^{o}C (DT min) is used for the design, targeting minimum annualized cost. Negligible heat losses are assumed for the heat exchangers in the process.

The cooling plant provides the necessary process cooling requirements, with water inlet and outlet at 30^{o}C and 40^{o}C, respectively.[33] The windage and blow-down rates were assumed at 1.15% and 0.14% of the total flow rate.[33]

The waste water plant converts the aqueous light components to methane and sludge, through an aerobic-anaerobic digestion system.[33] To reduce the complexity of the model, the waste-water-treatment (WWT) plant design is not included in this study; an assumption is made that waste water is treated in an outside facility.[33] A storage system, air compressor system, and fire extinguisher system are included in the cost estimation to improve the accuracy of the study.[33]

Techno-economics

The ChemCAD model provides a simplified representation of the mild CP pathway in order to obtain material and energy balances. Key process-unit costs are obtained from reliable sources on an installed basis, using model data to calculate the required scale. This approach is adopted to improve the accuracy of the cost estimation. After scaling, estimates based upon petroleum FCC units are used to obtain pyrolyzer-regenerator costs.[35] For hydroprocessing, high-end values of petroleum hydrotreater/hydrocracker units are used to meet the special metallurgy requirements for use with acidic pyrolysis liquid.[41] These values closely resemble an estimate provided for upgrading pyrolytic lignin in another report.[42] The co-generation system cost is obtained from a vendor quote and Aspen Energy Analyzer's steam-generation data is used for scaling.[33] Aspen Energy Analyzer also calculates the HEN cost, using stream data provided by the ChemCAD model. As the hydrogen plant uses process off-gases instead of natural gas as feed, volumetric scaling is done to obtain the installed plant cost, using estimates provided by Stanford Research Institute [34] (SRI) for a natural-gas steam-reforming hydrogen plant. Other equipment costs, such as those of distillation columns, flash tanks, compressors and motors are calculated using ChemCAD built-in costing after sizing and the rest is obtained from publically-

available literature.[4, 30, 33, 35, 43, 44] A fixed-factor method is used as described in **Table 3** to obtain TPI from total purchased equipment cost (TPEC) in order to avoid the significant variances reported for individual equipment factors.[37] Lang factor multiplier represents TPI/TPEC. TPEC is calculated using process model and Lang factor is used to obtain TPI allowing direct and indirect cost associated to installation as shown in **Table 3**. Finally, all prices are adjusted as necessary to reflect a 2011 basis year.

The biomass feedstock cost includes the costs of drying, grinding, and handling, with the assumption that drying heat is provided by coke combustion.[29] The base salaries are calculated using data from the Bureau of Labor Statistics.[41] The numbers of workers are assigned according to the nature of the work and the number and types of process units used. A discounted cash flow rate of return (DCFROR) spreadsheet developed by the National Renewable Energy Lab (NREL)[36] is used to calculate the MFSP as a function of operating and capital costs.

Transportation fuel prices employed in the spreadsheet exclude excise taxes in the amount of the average national excise taxes for both gasoline and diesel fuel. The key economic parameters are summarized as shown in **Table 3.**

Results and Discussion

Process results

The organic content of the aqueous phase of mild CP liquid is negligible (2.2wt %) because the zeolite catalyst converts most of the light oxygenates into aromatic hydrocarbons or coke. Yield of the oil phase is 24.2wt% of the dry biomass feed, with water retention of 6wt% of the oil-phase due to the moderate polarity of the oxygenated compounds. Hydroprocessing

Table 3. Assumed parameters for economic analysis[±]

Factor	Value	Factor	Value
General[36]			
Cost year	2011	Loan interest	8%
Equity	40%	Internal rate of return	10%
Loan term	10 years	Construction time	2.5 years
Loan interest	8%	Startup time	0.5 years
Internal rate of return	10%	Stream factor	90.1%
Income tax rate	39%	Plant life	30 years
Working capital	15% of fixed capital investment	Depreciation system	MACRS[‡] 7 years
Capital cost			
Scaling factor	0.6 [4]	Lang factor[37]	5.1
Variable operating cost			
Woody biomass[22]	$96.57/MT in 2011 dollars	Solid waste removal[4]	$36.98/MT
Pyrolysis catalyst[38]	$13/kg	Process water[33]	195.26 cents/1000 gal
Hydrotreating catalyst[38]	$40.15/kg	Fuel price[39]	$2.92/gal
Hydrogen plant catalyst[40]	$4.24/1000 scf of hydrogen	Electricity cost[40]	$6.16/kWh
Boiler chemicals[33]	$3.63/kg	Natural gas[40]	$5.11/1000 scf
Cooling tower chemicals[33]	$2.60/kg		
Fixed operating cost[36]			
Overhead	95% of labor cost	Maintenance	2% TPI
Insurance and tax	2% TPI		

[‡] Modified accelerated cost recovery system.
[±] All calculations including tax and depreciations are done in real terms (2011 dollars) due to the unpredictability of future inflation rates.

conversion is 73.4wt% of the feed on a wet basis. The hydrogen required for processing is comparatively high at 6.4wt% of the feed (versus ~5wt% for conventional pyrolysis), mainly due to higher aromaticity of the feed pyrolysis liquid and saturation of the aromatic rings in hydroprocessing. In comparison, the theoretical hydrogen requirement for deoxygenation is only 2.7% on a feed basis. Respective gasoline and diesel yields are 39.9 and 18.7 gallons per MT of dry biomass, which translates to an overall fuel yield of 17.7wt% in biomass basis. The hydrogen required for the process can be completely obtained by steam-reforming some of the process off-gases. The co-generation system generates 3.73MW of excess electricity while supplying the steam and electricity required for the process.

Economic results

This study interprets fixed capital investment (FCI) as the installed equipment cost, which is 4.28 times the TPEC. The calculated MFSP of the analysis is $3.69/gal (**Table** 4), which is considerably higher than the projected 20-year average petroleum-based gasoline price of $2.92/gal.[39]

A major contribution to the capital cost comes from the co-generation unit followed by hydrogen generation, pyrolysis and hydroprocessing. At $111 million, the co-generation incurs a capital cost equivalent to $2337 per kilowatt of electricity produced. The compressor costs included in the main areas add up to $56.8 million, which also represents a significant portion of the TPI. The cost of the biomass feedstock is the most significant operating cost, representing 45% of the total operating cost. Selling the excess electricity to the grid provides a byproduct credit of $15.6million/year. **Figure 2** illustrates the degree to which various processing steps contribute to the MFSP. A major portion comes from the cost of biomass, which contributes

approximately 45% of the MFSP. The co-generation plant's contribution to the MFSP is negative, providing an overall reduction in MFSP.

Table 4. Summary of key results

Total Purchased equipment cost (TPEC)	100% TPEC	89.7	$ million
Direct installed cost (DIC)	302% TPEC	270.9	$ million
Indirect costs (TIC)	126% TPEC	79.8	$ million
Fixed capital investment (FCI)	428% TPEC	384.2	$ million
Working capital	15% FCI	67.8	$ million
Land	6% FCI	5.4	$ million
Total project investment (TPI)	510% TPEC	457.4	$ million
Annual operating cost		142.1	$ million /year
Fuel Yield		38.5	million gal/year
		58.6	Fuel gal/MT of dry biomass
		17.7	wt% of dry biomass
MFSP		3.69	$/gal fuel

Source [37, 41]

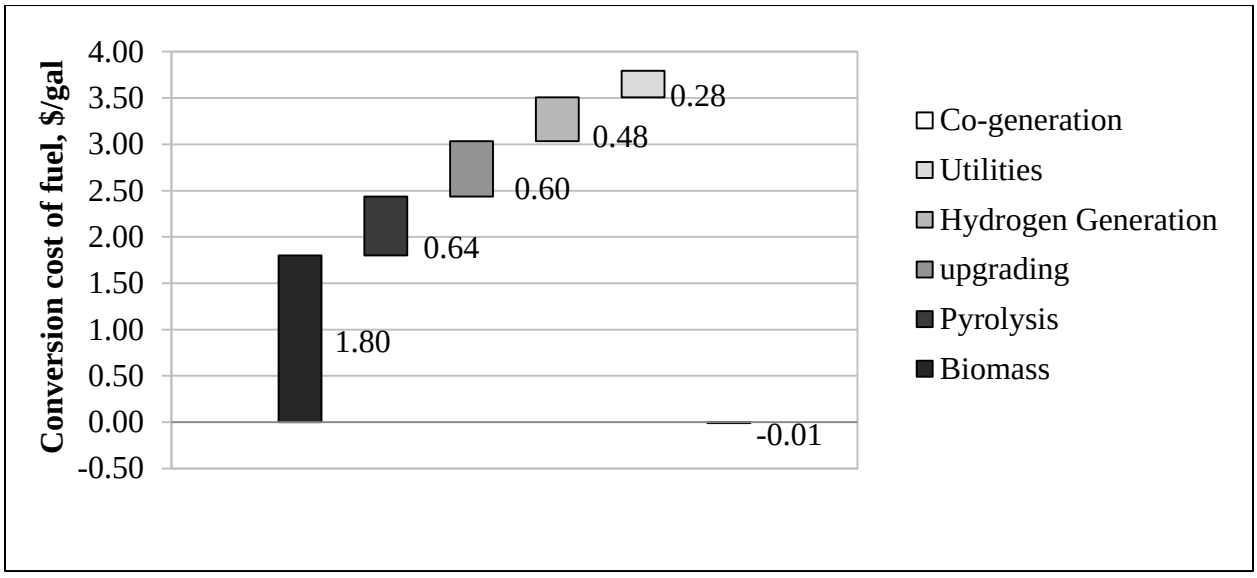

Figure 2. Contribution of various cost categories to MFSP

Analysis for optimum design

A design without a hydrogen plant would result in a MFSP of $4.15/gal, the increase is due to the cost of purchasing hydrogen at $1.82/kg.[42] If natural gas is used instead of process off-gases to produce hydrogen, the capital investment of the hydrogen plant would be reduced because the volumetric flow rate of natural gas through the hydrogen plant would be substantially reduced compared to the off-gases from the process. In addition, under this scenario, the co-generation system expands to accommodate the excess off-gases coming from the process. This scenario gives a reduced MFSP of $3.46/gal, mainly due to the additional electricity generation and hydrogen plant cost reduction.[39] When single-stage hydroprocessing is used, the analysis shows a marginal cost advantage, giving an MFSP of $3.59/gal.

The cogeneration plant is intended to use the excess heat in the process to generate excess electricity for an additional income. This benefit, however, incurs additional capital costs, equivalent to adding a power plant to the process. When the co-generation unit is not included, the process off-gas and NCG can be sold to an external party at an assumed price of $0.66/1000 scf due to the lower energy density of the lower quality gas (6.9 MJ/kg). The process heating requirement can be met in the absence of a co-generation plant with a smaller boiler at a cost of $35 million. Considering all of these variables, our analysis shows that eliminating the co-generation plant decreases the MFSP marginally to $3.64/gal with a reduced TPI of $357 million. However, the uncertainty of selling process off-gases at the assumed price would justify the inclusion of a co-generation unit in an optimum design scenario.

It is inferred from the analysis that an optimum design would contain a co-generation unit, while hydrogen required for the process is generated in a hydrogen plant using natural gas as the feed.

Energy flow

Figure 3 shows the conversion of input energy: biomass high heating value (HHV) in the form of sensible heat and the HHV of the streams. HHV of the stream is obtained from the Chemcad process model stream properties. Sensible heat is calculated as the enthalpy of the stream minus the enthalpy of the stream at the reference state of 25^{o}C and 1 atm.

Overall, the rate of energy conversion to fuel (39%) is several times higher than the mass conversion rate of 17.7 wt%. Process energy balance can be obtained by adding up HHV losses (pyrolysis and hydroprocessing) and HHV gains (hydrogen generation) in each process streams to the energy flow shown in **Figure 3**. Process energy conversion rate is comparable to the cellulosic ethanol (44%) and starch ethanol pathways (38%).[33, 43] When the combination of fuel and power output is considered, mild CP and cellulosic ethanol pathways has energy conversion rates of 46.6% and 47.4% respectively. The process yields 61.1 gasoline gallon equivalent (GGE) per MT of biomass, which is higher than for corn ethanol (57.9 GGE/MT) and lower than for starch ethanol (87.6 GGE/MT).[33, 43] The heat of reaction for catalytic pyrolysis is slightly endothermic at 32.3 kJ/kg.

Sensitivity analysis

Sensitivity analysis for MFSP is carried out for several reasons. First, several assumptions were made due to the scarceness of data on mild CP that introduced uncertainty into the analysis.

Second, because of the novelty of the process, a conservative approach is used in calculating the base-case MFSP that results in a relatively high MFSP. Third, sensitivity analysis is employed to determine which factors have the most influence on the MFSP.

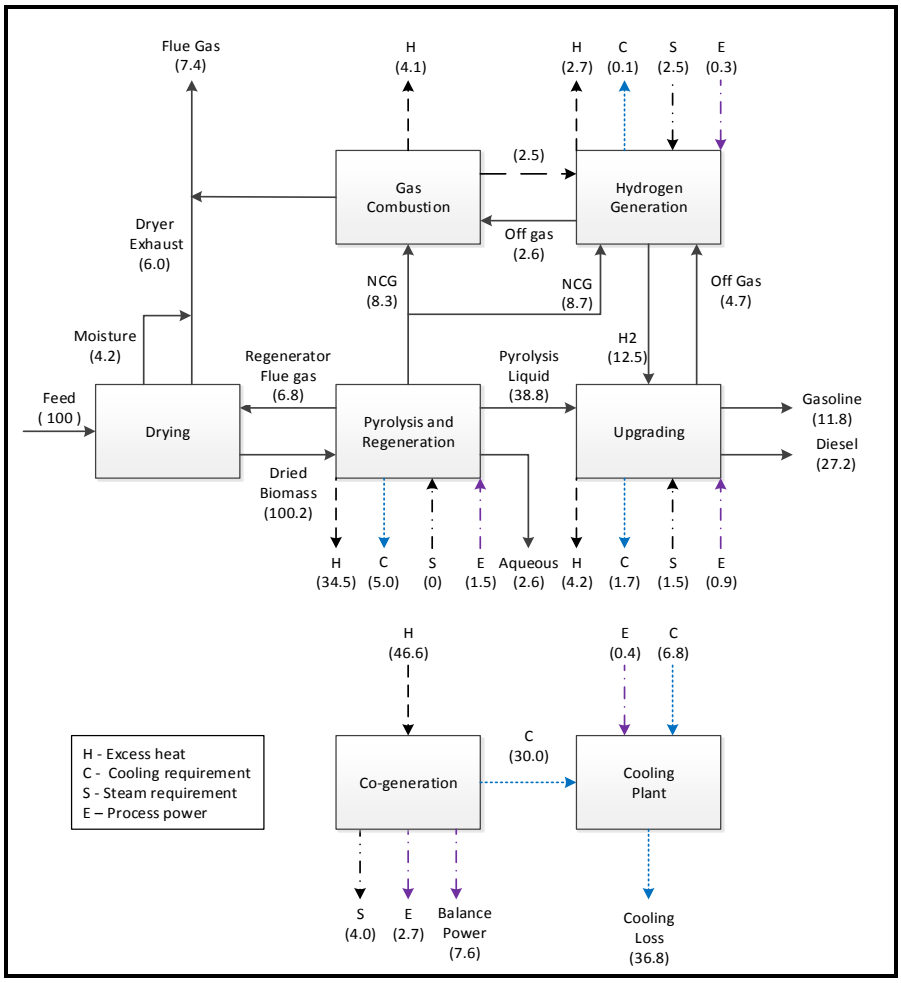

Figure 3. Energy flow (HHV + sensible energy) for process streams as a percentage of biomass HHV

The sensitivity analysis is conducted by developing a +/- 20% range of values around each base case parameter employed in the TEA. MFSPs are calculated for the base case, +20%, and -20% assumptions for each parameter. The parameters are then ranked according to the sensitivity of the MFSP to the changes for each. **Figure 4** presents the parameters to which the MFSP is most sensitive according to degree of sensitivity.

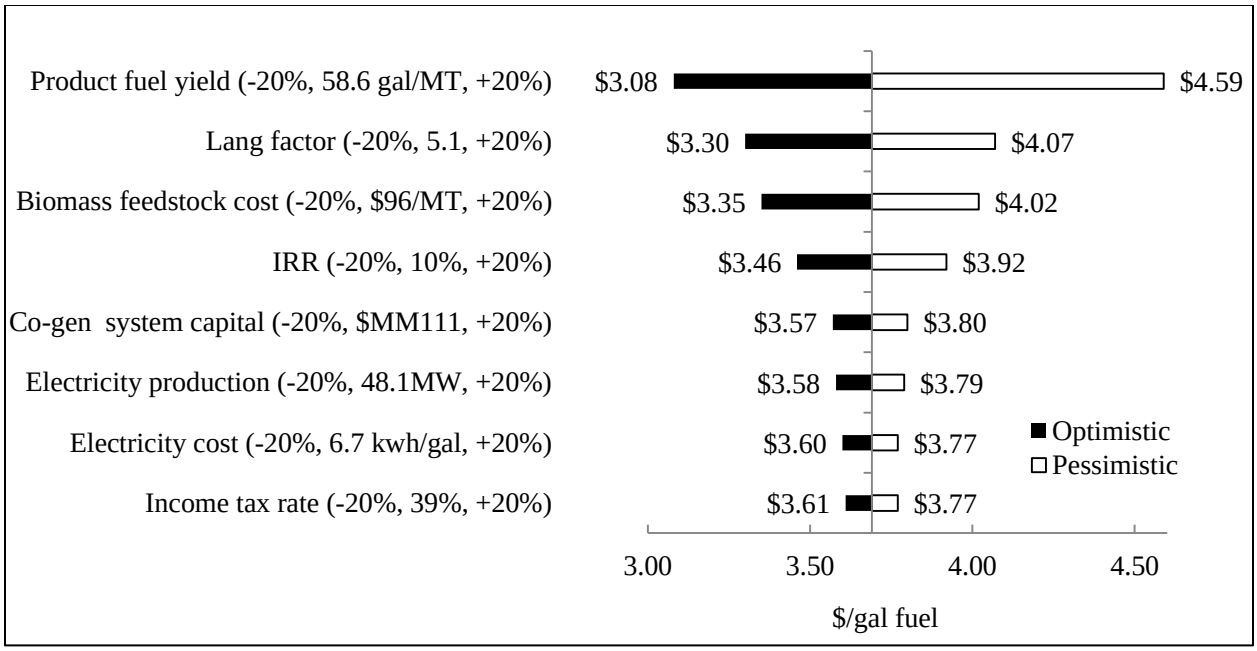

Figure 4. Sensitivity analysis for MFSP

Uncertainty analysis

Detailed examination of the parameters, to which the MFSP is identified by the sensitivity analysis as being most sensitive to, is carried out to quantify the uncertainty of the MFSP. Uncertainty of using co-generation is discussed in detail in the optimum design analysis section.

For the base case, a conservative biomass conversion rate of 24.2wt % is assumed for pyrolysis liquid containing 20wt% oxygen. When the highest reported yield rates for pyrolysis liquid (30wt%) with similar oxygen content (21wt%) are assumed, the analysis gives an overall conversion rate of 22.0wt%.[8] KiOR, which operates the world's first commercial-scale mild CP facility, claims to achieve 67 gal/MT at present and expects this to increase to 92 gal/MT in the future.[15] Using these claims in our analysis generates MFSPs of $3.23/gal and $2.37/gal, respectively, for the present and anticipated yields of product.

Our base case analysis generates a Lang factor of 5.1, which is a conservative value for a solid-fluid processing plant.[37] A Lang factor of 5.46 is reported for fast pyrolysis and hydroprocessing, which is similar to mild CP and hydroprocessing.[4] More recent methods, such as one developed by Guthrie, promise to improve accuracy by using different factors for different equipment.[44] However, statistically derived factors could provide better estimations by lowering uncertainties involved. Brennan et al.[44] provide a statistical analysis and describe a factored approach for equipment classes. They argue that installed cost may potentially vary more with equipment value than with equipment type.[44] In general, the Lang factor is relatively high for smaller scale facilities due to economies of scale, which generate lower scaling factors for larger capacities and higher scaling factors for smaller capacities.[44] When the installation factors used in this analysis are assumed for each equipment category, this analysis generates a TPI of $279 million and a Lang factor of 3.05.

The total cost of the dried and ground woody biomass used in this analysis is assumed to be $96.6/MT in 2011 dollars. The breakdown allows $17.9/MT for payment to the biomass grower and $29.9/MT for processing at the plant.[26] The Idaho National Lab (INL) provides a sensitivity analysis for dried (but not ground) woody biomass without grower payment, reporting a cost variance from $43.1 to $67.7 (in 2011 dollars).[27] When drying cost of $5.1 is deducted and plant processing costs and grower payment costs are added, fully processed biomass cost is estimated between $85.8 and $110.4/MT in 2011 dollars.[27]

Most probable fuel price and range

To determine the fuel price range, we first estimate the lowest possible fuel price. Using the most optimistic conditions obtained from uncertainty analysis (**Table 5**) the optimum design

(which includes a natural gas hydrogen generation unit and a cogeneration unit) generates a minimum MFSP of $2.17/gal. Next, we estimate the maximum MFSP of $4.07/gal for the optimum design using the pessimistic conditions of the uncertainty analysis (**Table 5**). Finally, to obtain the most probable fuel price, Monte-Carlo analysis is carried out in the range of pessimistic to optimistic (**Table 5**), assuming a normal distribution for each parameter. This analysis produces a median MFSP of $3.03/gal, as shown in **Figure 5**. This value can be projected as the most probable fuel price for this analysis.

Table 5. Distribution characteristics of most sensitive parameters for MFSP

	Distribution shape	**Optimistic case**	**Base case**	**Pessimistic case**
Product yield	Normal	22%	17.7%	17.7%
Lang factor	Normal	3.05	5.1	5.46
Biomass cost	Normal	$85.8/MT	$96.6/MT	$110.4/MT

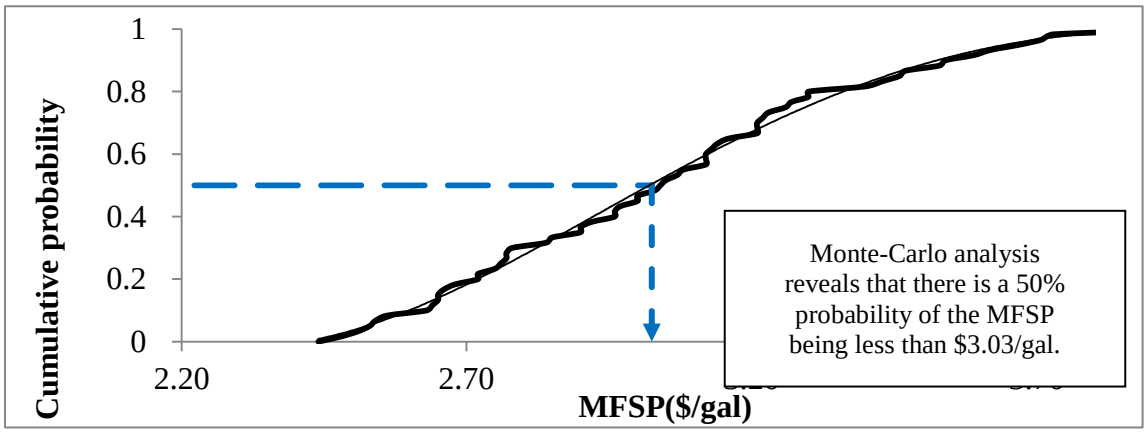

Figure 5. Monte-Carlo analysis for most probable fuel price

Conclusion

The analysis shows that transportation-range fuels can be obtained from mild catalytic pyrolysis (CP) of biomass with subsequent hydroprocessing of the product pyrolysis. The

process gives a product fuel yield of 58.6gal/MT of biomass which is equivalent to a mass conversion rate of 17.7wt%. The energy conversion to fuels is 39% of biomass high heating value (HHV). This pathway has a gasoline gallon equivalent (GGE) value of 61.1 for MT of biomass, a value higher than cellulosic ethanol pathway.

The 2000 metric ton per day facility incurs a total project investment of $457 million and an annual operating cost of $142 million. When a conservative approach is used, base-case analysis results in a minimum fuel selling price (MFSP) of $3.69/gal. Cogeneration unit cost and feedstock cost dominate the total project investment (TPI) and operating costs respectively, but the MFSP is mostly influenced by fuel yield. An optimum design would include a cogeneration unit. In such a design, hydrogen plant included in the process generates hydrogen required for the process using natural gas as the feed. Purchasing hydrogen for direct use is even more unfavorable at current hydrogen prices. A sensitivity analysis using a +/-20% range around the base case values identifies fuel production rate, installation factor, biomass feedstock cost, and co-generation capital cost as having the greatest impact on MFSP. Monte-Carlo analysis is carried out using these parameters to calculate a most probable fuel price of $3.03/gal, which is only slightly higher than the twenty-year average for gasoline price. Accordingly, mild CP has emerging promise for the production of advanced biofuels.

Acknowledgement

The authors would like to acknowledge financial support from the U.S. Department of Energy (Contract No.: 11.2.2.4 - 24444). The authors would also like to thank Sue Jones and Aye Meyer at the PNNL for useful discussions and Joy Graveline for editing this paper.

Reference

1. R. H. Venderbosch, A. R. Ardiyanti, J. Wildschut, A. Oasmaa and H. J. Heeres, *Journal of Chemical Technology & Biotechnology*, 2010, **85**, 674-686.
2. Q. Zhang, J. Chang, T. Wang and Y. Xu, *Energy Conversion and Management*, 2007, **48**, 87-92.
3. D. D. Hsu, *Biomass and bioenergy*, 2012, **45**, 41-47.
4. M. M. Wright, D. E. Daugaard, J. A. Satrio and R. C. Brown, *Fuel*, 2010, **89**, S2-S10.
5. Y. T. Cheng, J. Jae, J. Shi, W. Fan and G. W. Huber, *Angew Chem Int Ed Engl*, 2012, **51**, 1387-1390.
6. S. D. Stefanidis, K. G. Kalogiannis, E. F. Iliopoulou, A. A. Lappas and P. A. Pilavachi, *Bioresour Technol*, 2011, **102**, 8261-8267.
7. C. A. Mullen, A. A. Boateng, D. J. Mihalcik and N. M. Goldberg, *Energy Fuels*, 2011, **25**, 5444-5451.
8. A. A. Lappas, K. G. Kalogiannis, E. F. Iliopoulou, K. S. Triantafyllidis and S. D. Stefanidis, *Wiley Interdisciplinary Reviews: Energy and Environment*, 2012, **1**, 285-297.
9. R. French and S. Czernik, *Fuel Processing Technology*, 2010, **91**, 25-32.
10. T. R. Carlson, T. P. Vispute and G. W. Huber, *ChemSusChem*, 2008, **1**, 397-400.
11. H. Zhang, R. Xiao, D. Wang, Z. Zhong, M. Song, Q. Pan and G. He, *Energy & Fuels*, 2009, **23**, 6199-6206.
12. A. Zacher, D. Santosa and D. Elliott, Mild Catalytic Fast Pyrolysis of Biomass and Catalytic Hydrotreating to Liquid Transportation Fuels, TC Biomass 2011, Chicago, 2011.
13. T. R. Brown and R. C. Brown, *Biofuels, Bioproducts and Biorefining*, 2013, DOI: 10.1002/bbb.1387.
14. KiOR, :http://www.kior.com/content/?s=6&s2=55&p=55&t=Virtual-Plant-Tour, Accessed April 1 2013.
15. J. Lane, No Eeyores for KiOR, http://www.biofuelsdigest.com/bdigest/2012/08/16/no-eeyores-for-kior/.
16. J. Lane, Gusher! KiOR starts production of US cellulosic biofuels at scale, http://www.biofuelsdigest.com/bdigest/2012/08/16/no-eeyores-for-kior/.
17. J. Lane, Anellotech and the advent of Green Enes, http://www.biofuelsdigest.com/bdigest/2013/03/10/anellotech-and-the-advent-of-the-green-enes/.
18. T. R. Carlson, Y. T. Cheng, J. Jae and G. W. Huber, *Energy & Environmental Science*, 2011, **4**, 145.
19. H. Zhang, T. R. Carlson, R. Xiao and G. W. Huber, *Green Chemistry*, 2012, **14**, 98.
20. D. L. Compton, M. A. Jackson, D. J. Mihalcik, C. A. Mullen and A. A. Boateng, *Journal of Analytical and Applied Pyrolysis*, 2011, **90**, 174-181.
21. D. C. Dayton, Catalytic Biomass Pyrolysis for Bio-Crude Production, , TC Biomass 2011, Chicago, 2011.

22. T. R. Brown, R. Thilakaratne, G. Hu and R. C. Brown, *Fuel*, 2013, **106**, 463-469.

23. T. R. Brown, Y. Zhang, G. Hu and R. C. Brown, *Biofuels, Bioproducts and Biorefining*, 2012, **6**, 73-87.

24. Y. Zhang, T. R. Brown, G. Hu and R. C. Brown, *Chemical Engineering Journal*, 2013, DOI: 10.1016/j.cej.2013.1001.1030.

25. P. R. Patwardhan, J. A. Satrio, R. C. Brown and B. H. Shanks, *Bioresource Technology*, 2009, **101**, 4646-4655.

26. DOE, Biomass Feedstock Composition and Property Database, http://www.afdc.energy.gov/biomass/progs/search1.cgi., Accessed November 2012.

27. E. M. Searcy and J. R. Hess, *Uniform-Format Feedstock Supply System: A Commodity-Scale Design to Produce an Infrastructure-Compatible Biocrude from Lignocellulosic Biomass*, Report INL/EXT-10-20372, Idaho National Laboratory, USA, 2010.

28. J. R. Grace, A. A. Avidan and T. M. Knowlton, in *Circulating Fluidized Beds*, Chapman & Hall, London, UK, 1 edn., 1997, ch. 4, p. 131.

29. D. C. Elliott, T. R. Hart, G. G. Neuenschwander, L. J. Rotness and A. H. Zacher, *Environmental Progress & Sustainable Energy*, 2009, **28**, 441-449.

30. S. Jones, J. Holladay, C. Valkenburg, D. Stevens, C. Walton, C. Kinchin, D. Elliott and S. Czernik, *Production of Gasoline and Diesel from Biomass via Fast Pyrolysis, Hydrotreating and Hydrocracking: a design case*, Report PNNL-18284, Pacific Northwest National Laboratory, USA, 2009.

31. J. Piskorz, P. Majerski, D. Radlein and A. C. Scott, *Fuels Energy & Fuels* 1989, **3**, 723,726.

32. J. C. Molburg and R. D. Doctor, Hydrogen from Steam-Methane Reforming with CO2 Capture, 20th Annual International Pittsburgh Coal Conference, 2003.

33. D. Humbird, R. Davis, L. Tao, C. Kinchin, D. Hsu, A. Aden, P. Schoen, J. Lukas, B. Olthof, M. Worley, D. Sexton and D. Dudgeon, *Process Design and Economics for Biochemical Conversion of Lignocellulosic Biomass to Ethanol*, Report NREL/TP-5100-47764, National Renewable Energy Laborotary, USA, 2011.

34. EPA, in *Air pollution control permit for KiOR Inc, Permit No. 1680-00073*, Environmental protection agency, 2011.

35. R. A. Meyer, in *Handbook of Petroleum Refining Processes*, McGraw Hill, New York, 3rd edn., 2004, ch. 3, p. 68.

36. NREL, in *DCFROR based spreadsheet for calculating minimum fuel selling price*, National Renewable Energy Laboratory, USA, 2011.

37. M. S. Peters, K. D. Timmerhaus and R. E. West, in *Plant design and economics for chemical engineers*, McGraw-Hill, Newyork, 5th edn., 2003, ch. 6, pp. 250-251.

38. SRI, *PEP Yearbook International 2007*, SRI International, United States, Menlo Park, CA, 2007.

39. EIA, Projected gasoline and diesel prices, Annual Energy Outlook 2011, http://www.eia.gov/forecasts/archive/aeo11/source_oil.cfm.

40. EIA, Annual average natural gas price 2011, http://www.eia.gov/totalenergy/data/monthly/pdf/sec9_15.pdf.

41. T. R. Brown and R. C. Brown, *RSC Advances*, 2013, **3**, 5758.

42. R. A. Meyer, in *Handbook of Petroleum Refining Processes*, McGraw Hill, New York, 3rd edn., 2004, ch. 7, p. 33.

43. J. R. Kwiatkowski, A. J. McAloon, F. Taylor and D. B. Johnston, *Industrial Crops and Products*, 2006, **23**, 288-296.

44. D. J. Brennan and K. A. Golonka, *Chemical Engineering Research and Design*, 2002, **80**, 579-586.

CHAPTER 3

A TECHNO-ECONOMIC ANALYSIS OF MICROALGAE REMNANT CATALYTIC PYROLYSIS AND UPGRADING TO FUELS

A paper Published by *Fuel*

Rajeeva Thilakaratne, Mark M. Wright, and Robert C. Brown

Abstract

Microalgae have been proposed as potentially promising feedstock for the production of renewable transportation fuels. The plants are intriguing for their capacity to serve both as a source of renewable carbon fuels and as a powerful tool for carbon sequestration. Microalgae remnant, a low-cost by-product of microalgae lipid extraction, is a particularly appealing candidate for these processes. Through catalytic pyrolysis, microalgae remnant is capable of producing aromatic hydrocarbons that could be used for the production of drop-in biofuels. One of the most challenging barriers to this promising pathway is the high moisture content of harvested microalgae.

The goal of this study is to compare the economics of two catalytic pyrolysis pathways for the production of drop-in biofuels, each pathway employing its own distinct method of feedstock dewatering: thermal drying or partial mechanical dewatering. The study presents chemical process models, capital expense and operating cost estimates, and sensitivity analyses of both scenarios.

Results indicate that thermal drying prior to catalytic pyrolysis (TDCP) incurs capital costs similar to those incurred in partial mechanical dewatering prior to catalytic pyrolysis (MDCP) ($346 million vs. $409 million). TDCP and MDCP yield minimum fuel-selling prices (MFSPs) of $1.80/liter and $1.49/liter, respectively. Energy analysis shows that TDCP achieves 16.8% energy efficiency and MDCP achieves 26.7% efficiency.

Introduction

Global environmental concerns about atmospheric carbon levels have prompted interest in both reducing atmospheric CO_2 levels and increasing the use of renewable carbon fuels in the energy sector. Both objectives can be accomplished through the cultivation and conversion of microalgae biomass. In the 1970s, the U.S. Department of Energy extensively researched the growth and conversion of microalgae for transportation fuels.[1] At that time, it was determined that the costs to produce transportation fuels from microalgae rendered the process economically infeasible. Today, innovative approaches to microalgae growth and conversion have renewed interest in algae biofuels[1, 2], but the question of economic feasibility remains. Despite the increase in algae-related publications, few papers effectively address this key question of the economic costs of producing algae biofuels.

The cost estimates given in the literature vary greatly in their level of detail. Some provide single value estimates and others give complete process and economic analyses. Lundquist et al. [1] published that algae biofuel costs would range from $0.17/liter to $2.09/liter. Ayobi et al. [2] suggested a cost range of $0.88/liter to $24.60/liter. There are several reasons for the wide range of prices given in the literature, but the primary driver of these wide variations is the wide variations found in the combined costs of algae cultivation, extraction, and pretreatment.

Published algae biomass costs vary from $0.35/kg to $7.32/kg, depending on algae strain, cultivation and extraction methods, and facility locations.[2]

Algae are microscopic in nature and account for most of the organic matter found in aquatic cultures. The surface-to-volume ratio of algae is very high, which results in rapid nutrient and CO_2 uptake and a fast growth rate.[2] Microalgae are suitable for numerous applications such as livestock and aquaculture feed [2] but their high processing costs have discouraged widespread commercialization.[2]

Similarly, algal biomass is suitable for conversion to liquid fuels through various processes. Lipids extracted from algae can be transesterified to biodiesel [3] or hydroprocessed to green diesel. Whole algae or algae remnant can be hydrothermally processed [4] or dried and pyrolyzed [5] to produce bio-oil suitable for hydroprocessing to renewable gasoline or diesel. Whole algae or algae remnant can also be gasified and the resulting syngas can be catalytically synthesized to liquid fuels.[6] The technology for upgrading lipids to fuels has already been developed for vegetable oils and animal fats [4, 7], but algal lipids are currently too expensive to process with this method due to their high processing costs. The conversion of whole algae and algae remnant to fuels, which contain large amounts of protein and carbohydrate as well as lipids, is still under development.

Recently-developed methods for extracting lipids from wet algal biomass have yielded wet algae remnant as a by-product.[6] Algae remnant can be converted to methane through anaerobic digestion or it can be sold as a protein supplement for animal feed.[2] However, its greatest value may lie in its thus-far-undeveloped potential to serve as a low cost feedstock for biofuel production. Direct liquefaction, such as that accomplished through catalytic fast pyrolysis and

hydrothermal processing, is capable of thermally converting algae remnant into an intermediate oil suitable for upgrading to naphtha and diesel biofuels.[5, 8, 9] The major technical challenges for this approach are the high moisture and nitrogen contents of algae remnant.

Catalytic pyrolysis offers a distinct advantage for algae processing: its zeolite catalysts are capable of reducing heteronuclear nitrogen to negligible levels.[8] Unfortunately, high moisture levels impede the catalytic pyrolysis process. Hence, effective water management is a key challenge for the conversion of algae remnant, which typically contains approximately 80wt% moisture.[3,10] This study investigates the performance of two water removal approaches: thermal drying and partial mechanical dewatering.

The purpose of this paper is to conduct a techno-economic analysis (TEA) of the catalytic pyrolysis of microalgae remnant for the production of biofuels that provide information to compare it to alternative algae conversion pathways. The paper will accomplish these objectives through the following five steps. It will: 1) describe two base case scenarios, each employing a different dewatering technique; 2) develop chemical process models for algae-to-biofuel conversion; 3) estimate the profitabilities of each scenario; 4) conduct energy flow analysis; and to 5) conduct a sensitivity analysis of the process and economic models.

Methods

The conversion of algae remnant to biofuels requires six primary conversion steps and three auxiliary processing units. The primary conversion steps include pretreatment and drying, catalytic pyrolysis, benzene-toluene-xylene (BTX) separation, hydroprocessing, and fractionation. Pretreatment involves feedstock drying to 10wt% moisture content and feedstock

grinding to 1 mm diameter. Catalytic pyrolysis takes place in a reactor operating at about 700°C, atmospheric pressure, and without air or oxygen addition. In the pyrolysis, s solid carbonaceous particles (bio-char) are separated from the effluent stream and oil recovery is accomplished through the rapid condensation of pyrolysis oils (bio-oils). BTX separation uses distillation to recover a BTX mixture from the pyrolysis oil. Finally, heavy oil catalytic upgrading is accomplished through hydroprocessing and fractionation to gasoline and diesel range blend stock fuels. Auxiliary process units include a heat recovery and steam generation (HRSG) boiler unit, steam methane reforming (SMR) unit and a cooling plant. Algae cultivation and wastewater treatment facilities are assumed to be beyond the boundaries of the processing facility. **Figure 1** and **Figure 2** show a process block diagram and simplified flow diagram of the conversion system.

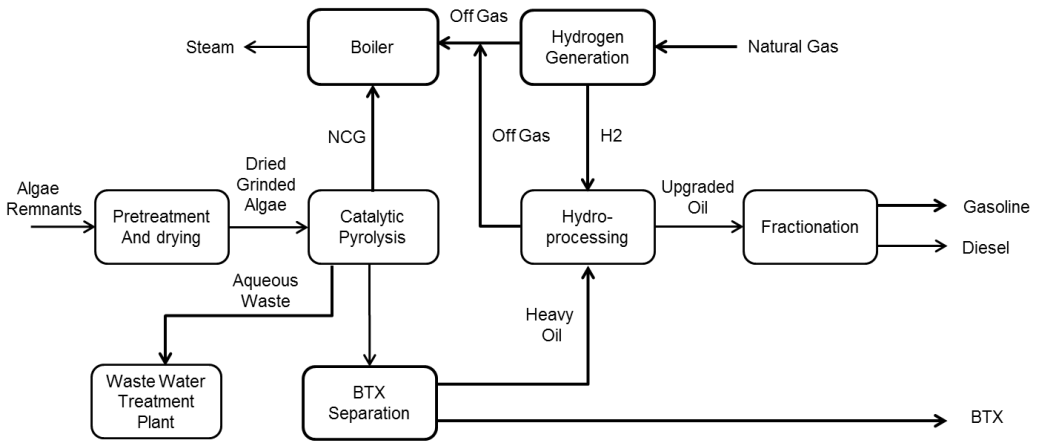

Figure 1. Process block flow diagram for microalgae remnant catalytic pyrolysis and upgrading to drop-in transportation fuels

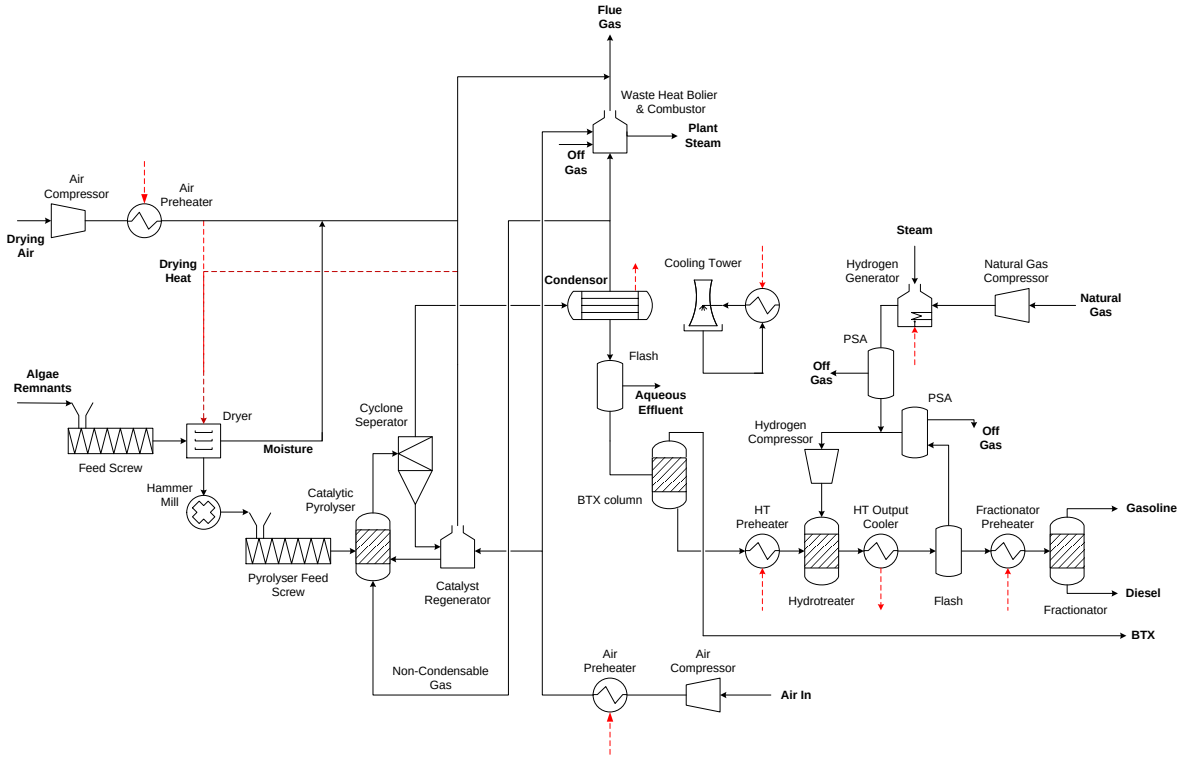

Figure 2. Simplified process flow diagram of microalgae remnant catalytic pyrolysis system for drop-in transportation fuel production

This study compares two microalgae drying technologies: thermal drying and partial mechanical dewatering. Thermal drying takes place at 290°C using hot air to reduce moisture content from 80 wt% to 10 wt%. This method requires significant energy input. Mechanical dewatering is an alternative technique that can reduce moisture content with a lower energy cost. The technique has been suggested as a possible alternative for thermal drying of wet lignin residue in the cellulosic ethanol pathway, but it has never been demonstrated for microalgae drying.[10] Unbound water can be removed with mechanical dewatering, but the cell bound water is difficult to remove completely with this method; subsequent thermal drying is required to reduce water levels to the levels required for catalytic pyrolysis. Microalgae have a large amount of cell bound water. Therefore, in this study, mechanical dewatering is applied until moisture is reduced to 60 wt% and then thermal drying will be used to achieve the requisite

Table 1. Material balance of algae remnant catalytic pyrolysis at 700^{o}C and atmospheric pressure[7]

Component	**Wt% of dry feed**
Coke and char‡	29.95
Water‡	14.64
Pyrolysis liquid (dry basis)	10.64
Gas compounds‡	28.64
Ash	16.13
Bio-oil compounds	
Benzene	2.13
Toluene	2.98
Xylene	2.47
Propyl-benzene	0.01
1-Ethyl-2-methyl-benzene	0.15
Trimethyl-benzene	0.23
4-Ethyl-1,2-dimethyl-benzene	0.02
Indan	0.11
1-Propynyl-benzene	0.16
1,Methyl-indan	0.10
Naphthalene	0.85
2-Methyl-naphthalene	0.89
Ethyl-naphthalene	0.04
Dimethyl-naphthalene	0.27
Fluorene	0.01
Anthracene	0.06
2-Methylanthracene	0.04
Gas compounds‡	
Carbon Dioxide	16.01
Carbon Monoxide	5.00
Ammonia	5.97
Hydrogen Cyanide	1.66

‡ Adjusted to obtain material balance

10 wt% moisture content. Mechanical dewatering of algae is a novel technology with limited commercial history. Various lab and pilot scale types of equipment have been investigated. The mechanical dewatering methods explored in literature include filter and belt presses, membrane technologies, and pressurized air and vacuum systems.

This study employs a belt dryer mechanical dewatering technique with pressurized air to drive away moisture. This method has been proposed for dewatering lignin residue slurries from the cellulosic ethanol conversion process.[10] In this process, lignin residue is dewatered from 87 wt.% moisture to 65 wt.% moisture, levels that closely resemble the mechanical dewatering requirement in this study.[10]

The literature includes few studies on microalgae catalytic pyrolysis. Thangalazhy-Gopakumar et al.[11] processed catalytic pyrolysis of Chlorella vulgaris microalgae using HZSM5 catalyst and claimed to obtain higher quality pyrolysis oil. Babich et al.[12] employed the same strain of microalgae with Na_2CO_3 catalyst to improve the stability of the pyrolysis oil. In this study, we employ results published by Wang and Brown[8] for catalytic pyrolysis using Chlorella microalgae.

Microalgae remnant is the raffinate that remains after lipids are extracted from the feed. Microalgae catalytic pyrolysis typically yields more solid carbon products (coke and biochar) than are produced in conventional pyrolysis. The most significant difference, observed, however, has to do with the behavior of the nitrogen. In microalgae catalytic pyrolysis, virtually all of the nitrogen in the feed is converted to gaseous compounds and char, providing a highly desirable nitrogen-free liquid oil product.[8] **Table 1** shows the base data for catalytic pyrolysis yields on a weight basis.

The composition of catalytic pyrolysis oils varies depending upon feedstock and processing conditions. There is insufficient data available to adapt the process models to different conditions. In this study, we employ the bio-oil composition provided by Wang and Brown for catalytic pyrolysis of Chlorella Vulgaris, a lipid-lean microalgae strain that has similarities to the composition of microalgae remnants.[8] (see **Table 2** for Chlorella Vulgaris characterization details).

Table 2. Characterization of Chlorella Vulgaris[8]

Proximate Analysis	**(Wt%)**
Moisture	6.18
Volatiles	66.56
Fixed carbon	11.62
Ashes	15.64
Elemental Analysis	**(Wt%)**
C	42.54
H	6.77
N	6.64
O	27.95
Biochemical Composition	**(Wt%)**
Total fatty acids	4.68
Proteins	42.51
Carbohydrates	20.99

Compared to bio-oils from woody or herbaceous biomass, traditional algae oils have higher amounts of nitrogen-containing compounds. Since nitrogen can be detrimental to catalyst activity and catalyst lifetime, algae-derived bio-oils present additional upgrading challenges. Nitrogen removal is one of the major costs associated with upgrading whole algae oils. However, the catalytic approach described here reduces the nitrogen of the algae bio-oil by converting nitrogen

to gaseous ammonia and char. Primary products from algae bio-oil upgrading include BTX and heavier polyaromatics. The BTX is separated using a distillation column, and the remaining heavy ends are hydroprocessed to obtain gasoline and diesel fuel blend stock. In heavy oil upgrading, it is assumed that mass conversion to gas molecules is 1.39 wt%, a value obtained from similar petroleum hydrotreating units.[13] Upgraded heavy oil product composition is assumed to be similar to that reported for the mildly cracked bio-oil upgrading process.[14] **Table 2** shows the calculated material balance for the upgrading step, when the above assumptions are employed.

Table 3. Material balance for algae heavy oil upgrading

Component	**Wt% of dry feed**
Feed hydrogen	6.96
Upgraded oil	105.88
Gas	1.39
Upgraded oil	
Aromatics	25.0
Cyclic hydrocarbons	50.6
Hydrated aromatics	7.4
Olefins	2.4
Paraffins	14.6
Gas compounds	
Ethane	0.67
Propane	0.36
Butane	0.36

A catalytic pyrolysis facility requires several auxiliary units: HRSG, SMR, cooling water plant, and wastewater treatment. The HRSG converts noncondensable gases and a portion of bio-char into process steam and electricity. Merchant natural gas can be purchased to meet additional

facility energy demand. The SMR generates hydrogen from natural gas, but biomass could serve as an alternative hydrogen source.[15-17] According to the model, bio-oil heavy end upgrading employs a calculated 0.12 kg H_2/kg of liquid input.

Pyrolysis oil aqueous phase effluents account for most of the wastewater generated at the facility. Wastewater management would be important to the overall sustainability of the algae conversion system. Wastewater from the pyrolysis section contains large quantities of dissolved ammonia (5.97 wt%) and hydrogen cyanide (1.66 wt%) that will require neutralization. Due to limited public information about the treatment costs of this type of effluent, the design employs an operating cost of $0.09/kg of chemical oxygen demand (COD) treated [13]. A recovery unit can be included to extract the ammonia from wastewater, but this alternative is not explored in this analysis.[8]

Economics

The analysis uses economic assumptions similar to those provided in previous biofuel techno-economic analyses.[10, 14, 15, 18-26] Heat and mass balances are obtained from a ChemStations ChemCAD^{TM} model in order to calculate equipment capital and operating costs. These are then used in a discounted cash flow rate of return (DCFROR) spreadsheet analysis to obtain the minimum fuel-selling price for this pathway. Wet (80 wt% moisture) algae remnant feedstock cost is assumed at $66/metric tonne (MT) based on a 2011 average reported value for wet distilleries grains.[27] Capital and operational costs of mechanical dewatering are calculated using reported values for lignin slurry dewatering in cellulosic ethanol process.[10] The pyrolyzer cost is based on the cost of the Evergent circulating bed pyrolyzer.[28] An estimate provided by Idaho National Laboratory is used to obtain the feedstock rotary dryer costs [29]. Hydrotreater

capital cost is calculated using a value of $3500 per input liquid barrel as reported for a 50,000 barrels per standard day (BPSD) petroleum refinery hydrocracker unit.[30]

Financial assumptions include 40% equity with a 7.5% loan interest rate and 10-year loan term. Equipment costs depreciate at a double-declining rate over seven years for the general plant, with zero equipment salvage value. The income tax rate is 39%, and the internal rate of return is 10% over a 30-year project lifetime. The facility construction period is three years with capital expenditure percentages of 32%, 60%, and 8% in the first, second, and third years, respectively. Revenues, variable costs, and fixed costs are 50%, 75%, and 100% of their respective full capacity values during the startup period of half a year. MFSP is calculated for cumulative gallons of all three co-products (gasoline, diesel, and BTX) as individual credit differences for these co-products are assumed negligible.

Results and Discussion

Study results indicate that a 2000 metric tonne per day (MTPD) microalgae catalytic pyrolysis facility can produce 21.4 million gallons of biofuel per year at a cost of $6.80 per gallon ($1.80 per liter) or $5.61 per gallon ($1.49 per liter) with thermal drying or partial mechanical dewatering, respectively. Total project investment costs are $346 million for the TDCP scenario and $409 million for the MDCP scenario. **Table 4** shows a summary of the process and economic results.

These results suggest that investing in the mechanical dewatering equipment could reduce algae remnant biofuel costs. Natural gas input for heating and drying contributes to the increase

in the operational costs in TDCP scenario, which leads to a higher MFSP value calculated for this case.

Table 4. Summary process and economic cost comparison of 2000 metric tonne per day thermal drying and mechanical dewatering catalytic pyrolysis biorefinery scenarios

Catalytic Pyrolysis Scenario Costs ($ million)		**TDCP**	**MDCP**
Total Purchased Equipment Cost (TPEC)	100% TPEC	67.8	80.2
Direct Installed Cost (DIC)	302% TPEC	204..8	242.3
Indirect Costs (TIC)	126% TPEC	60.4	71.4
Fixed Capital Investment (FCI)	428% TPEC	290.3	343.4
Working Capital	15% FCI	51.2	60.6
Land	6% FCI	4.1	4.8
Total Project Investment (TPI)	510% TPEC	345.6	408.8
Natural Gas Input for Heating and Drying (MTPD)		14.0	0
Natural Gas Input for Hydrogen Generation (MTPD)		0.6	0.6
Annual operating cost ($ million)		145.8	120.8
BTX Yield (Fuel gal/MT of dry biomass)		25.9	25.9
Gasoline Yield (Fuel gal/MT of dry biomass)		4.2	4.2
Diesel Yield (Fuel gal/MT of dry biomass)		2.5	2.5
Fuel Yield (million gal/year)		21.4	21.4
Fuel Yield (Fuel gal/MT of dry biomass)		32.6	32.6
Fuel Yield (wt% of dry biomass)		10.7	10.7
Energy conversion efficiency (% from biomass HHV)		16.8	26.7
MFSP ($/liter fuel)		1.80	1.49

Figure 3 shows that the MDCP scenario has co-generation equipment costs of $67.8 million compared to less than $1 million for the TDCP scenario. The higher cost is primarily due to the purchase of power generation units to convert excess heat into electricity. The additional

investment yields a $0.11 per liter electricity credit and somewhat offsets the disadvantage of higher capital in the MDCP scenario.

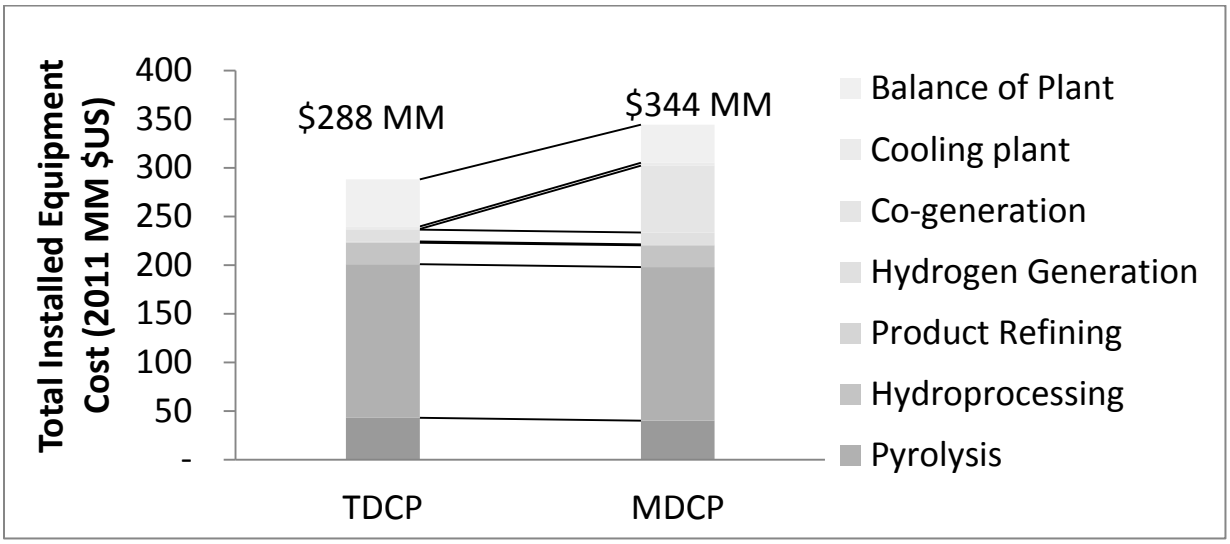

Figure 3. Total installed equipment costs (TIC) for the thermal drying (TDCP) and mechanical dewatering (MDCP) catalytic pyrolysis scenarios

Pyrolysis equipment accounts for most of the total facility cost with a $158 million total. Cost for co-generation is the second largest expenditure for the MDCP scenario at $68.8 million. Both TDCP and MDCP scenarios has comparatively similar pretreatment equipment capital costs. The mechanical drying equipment costs amounts to $21 million for belt dryer system installed. The thermal drum dryer in TDCP scenario has a capital cost of $27 million. Balance of plant (BOP) costs includes utility, storage, and material handling equipment.

Figure 4 shows a breakdown of microalgae biofuel production costs for the TDCP and MDCP scenarios. Feedstock costs and capital charges contribute the most to the MFSP of algae remnant biofuels. Wastewater treatment and catalyst costs individually contribute relatively small quantities; however, these costs are subject to high uncertainty because they are dependent upon on regulatory requirements and market conditions. The MDCP scenario benefits from

excess power generation while the TDCP scenario requires natural gas import for process heat. The major operation cost associated of water removal would be $0.17/liter natural gas usage costs for TDCP scenario versus $0.05/liter of electricity costs for air compression in MDCP. The BTX mixture obtained from the process is priced at the gasoline price. An investment in further separation units to obtain benzene, toluene, and xylene could result in more favorable economics because these chemicals have higher market prices than gasoline. The overall economics of the two pathways could improve by including an ammonia recovery unit assuming the additional capital cost for such unit is not significant.

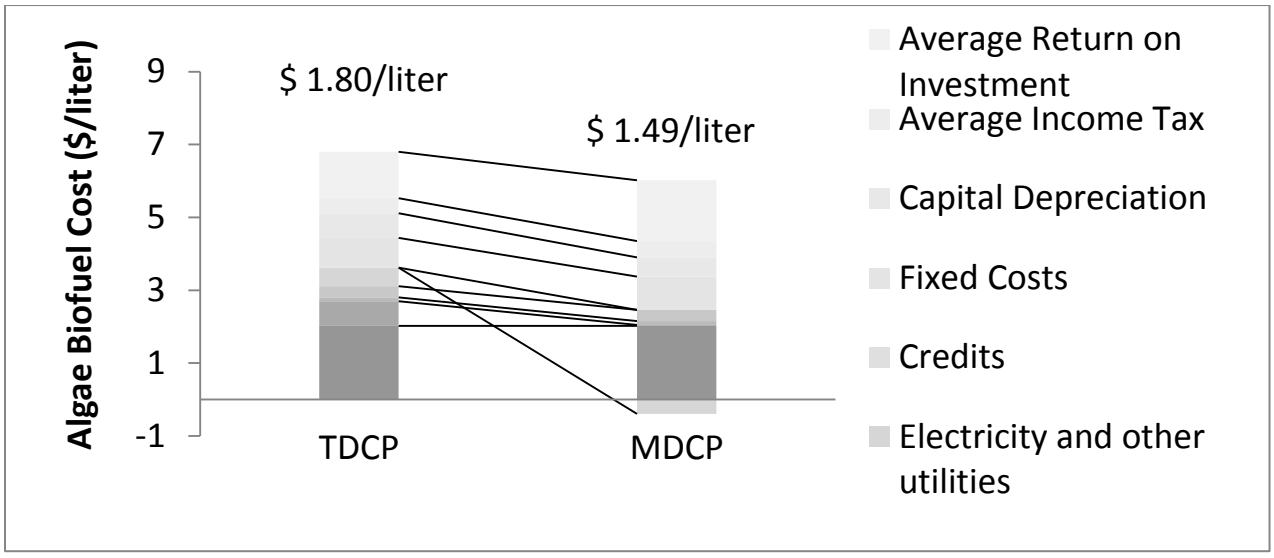

Figure 4. Algae biofuel production costs for the thermal drying (TDCP) and mechanical dewatering (MDCP) catalytic pyrolysis scenarios based on 20-year discounted cash flow rate of return analysis with 10% internal rate of return, 2000 MT per day capacity, and feedstock cost of $66/MT of microalgae

Energy Flow Analysis

Energy flows in the two scenarios are illustrated in **Figure 5** and **Figure 6** in the form of combined sensible heat and high heating value (HHV) of the streams as a percentage of the input

biomass HHV. A summary of normalized energy inputs, outputs, and the energy efficiency for the TDCP and MDCP scenarios is provided in **Table 5**. The energy efficiency for the TDCP scenario is 16.8%, which is lower than the 26.7% efficiency of the MDCP scenario. The MDCP scenario energy efficiency benefits from a net generation of electricity and the availability of sufficient internal energy sources.

Table 5. Summary of normalized energy inputs, outputs, and overall energy efficiencies for the thermal drying (TDCP) and mechanical drying (MDCP) catalytic pyrolysis scenarios

Energy Flows	**TDCP**	**MDCP**
	Inputs	
Biomass	100	100
Natural gas for hydrogen	1	1
Fired heat	23.4	0
Natural gas for fired heat‡	31.2	0
Electricity	4.8	0
Total input energy	137	101
	Outputs	
BTX	18.6	18.6
Gasoline	2.8	2.8
Diesel	1.6	1.6
Electricity	0	4
Total output	23	27
Efficiency	16.8	26.7

‡ For fired heaters thermal efficiency of 75% is assumed

The overall process energy balance can be obtained by tallying the HHV losses and gains in each conversion unit with the assumption that stray heat losses are negligible. ChemCad™ process model stream properties are used to obtain the HHV of the streams. Sensible heat is calculated as the enthalpy of the stream minus the enthalpy of the stream at the reference state of 25^0C and 1 atmospheric pressure. The overall energy conversion for fuels is 23% in both cases. In the TDCP scenario, most of the energy (76.3%) is converted to flue gas whereas flue gas represents only 33% of the input energy in the MDCP scenario. The MDCP scenario generates

excess electricity of 4%, while the TDCP scenario requires fired heat (23.4 %) and external electricity (4.8%) to sustain the process. Energy flow analysis shows that in both scenarios most of the unconverted feedstock energy can be used to dry the feedstock. However, the MDCP scenario saves sufficient energy to generate excess electricity.

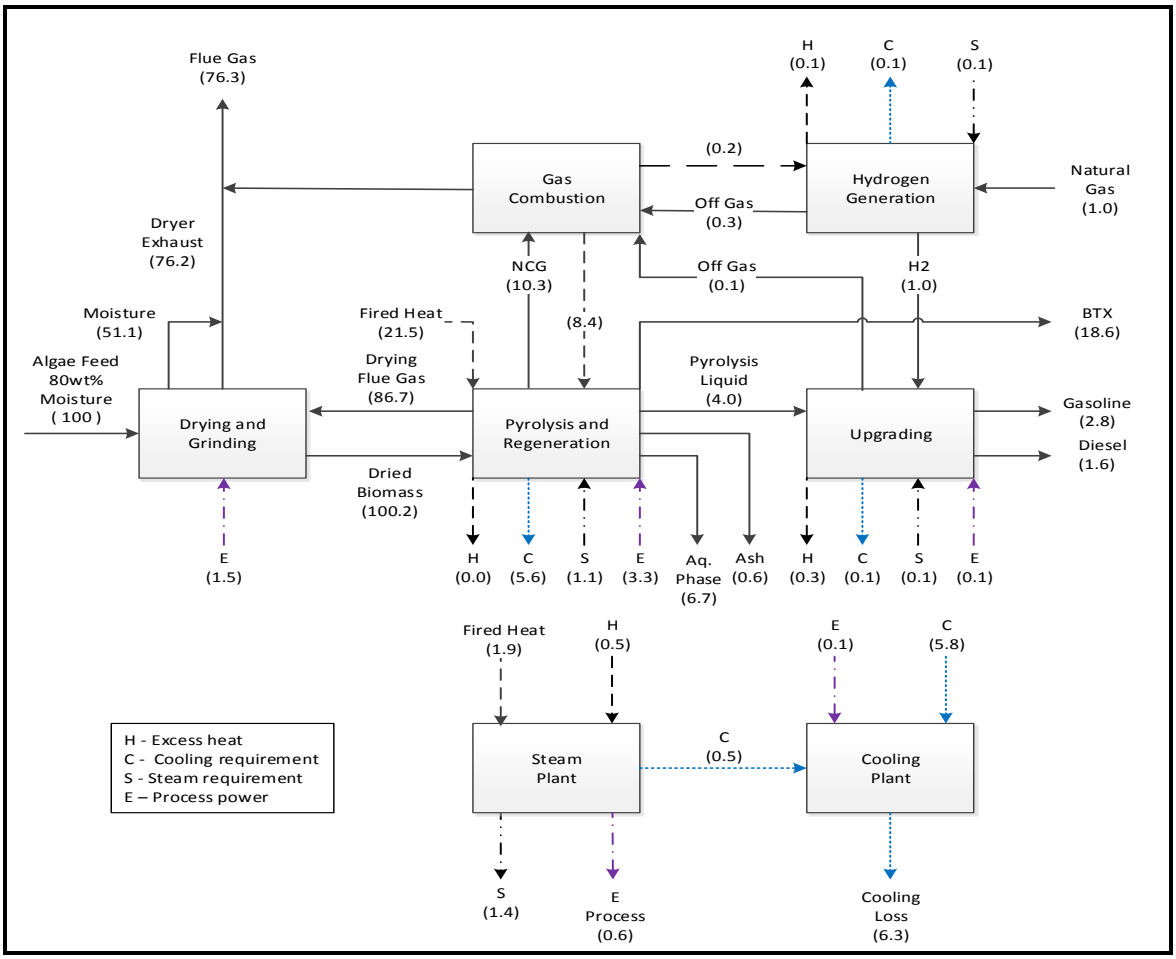

Figure 5. Energy flow (HHV + sensible energy) for thermal drying (TDCP) scenario process streams as a percentage of biomass HHV

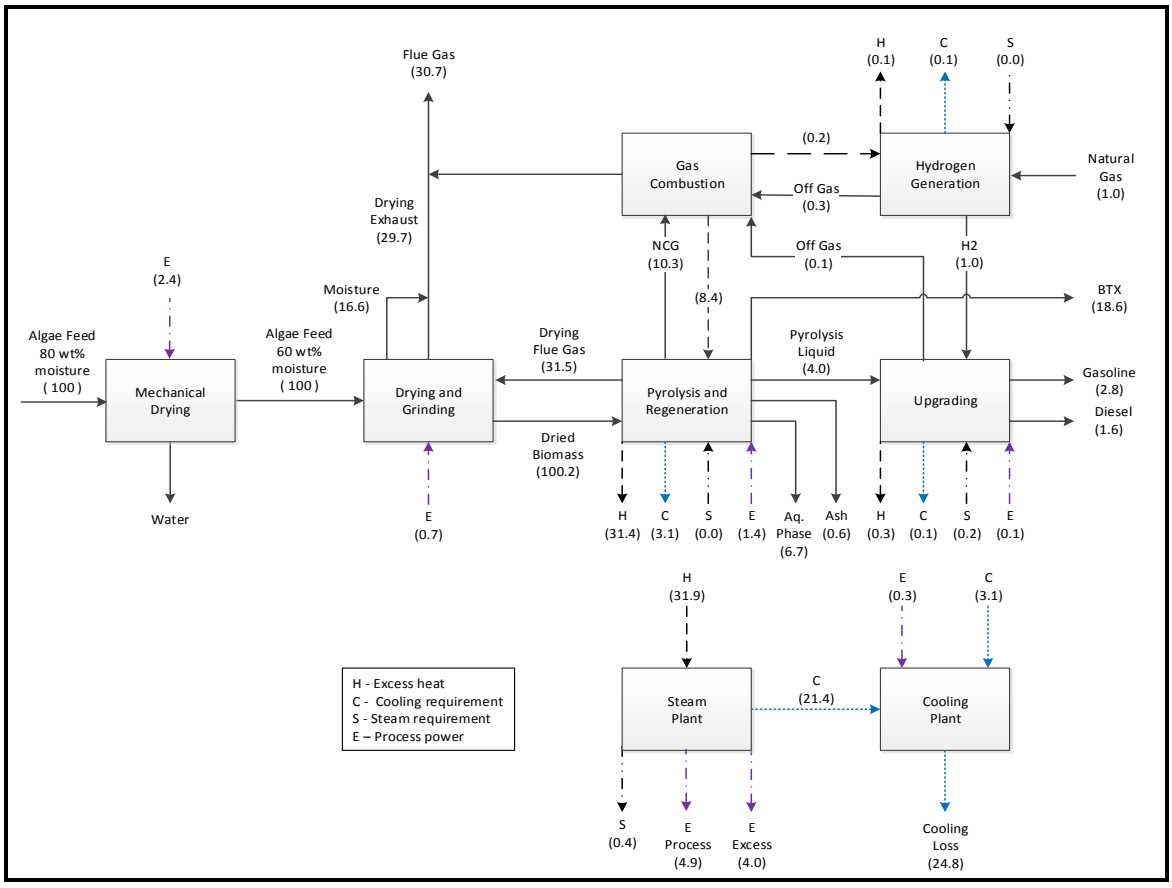

Figure 6. Energy flow (HHV + sensible energy) for mechanical dewatering (MDCP) process streams as a percentage of biomass HHV

Sensitivity Analysis

This study evaluates the impact of several variables on the biofuel MFSP. These variables include: product yield, feedstock cost (the feedstock cost for MDCP scenario includes the mechanical dewatering cost), total capital cost, Internal Rate of Return (IRR), catalytic pyrolysis reactor cost, natural gas use, electricity use, income tax rate, and pretreatment capital. The analysis changes the base assumption of each variable by ±20%. **Figure 7** and **Figure 8** show the results of the sensitivity analysis for the TDCP and MDCP scenarios respectively.

Sensitivity results indicate that ±20% variations in the overall product yield have a higher impact than a similar change in other key economic and technical factors for both the TDCP and MDCP scenarios. A 20% increase in product yields lowers the MFSP to $1.51/liter for the TDCP scenario and $1.21/liter for the MDCP scenario. Feedstock and total capital costs are the next two most significant factors that influence MFSP cost. A ±20% change in these three factors alters the MFSP by more than 7%. The remaining factors have either relatively small impact on the MFSP or relatively low uncertainty (i.e., electricity prices, which are regulated in the U.S.). This analysis indicates that a significant fuel price reduction can be achieved with a relatively small increase in product yield or, to a lesser extent, a relatively small decrease in microalgae feedstock cost.

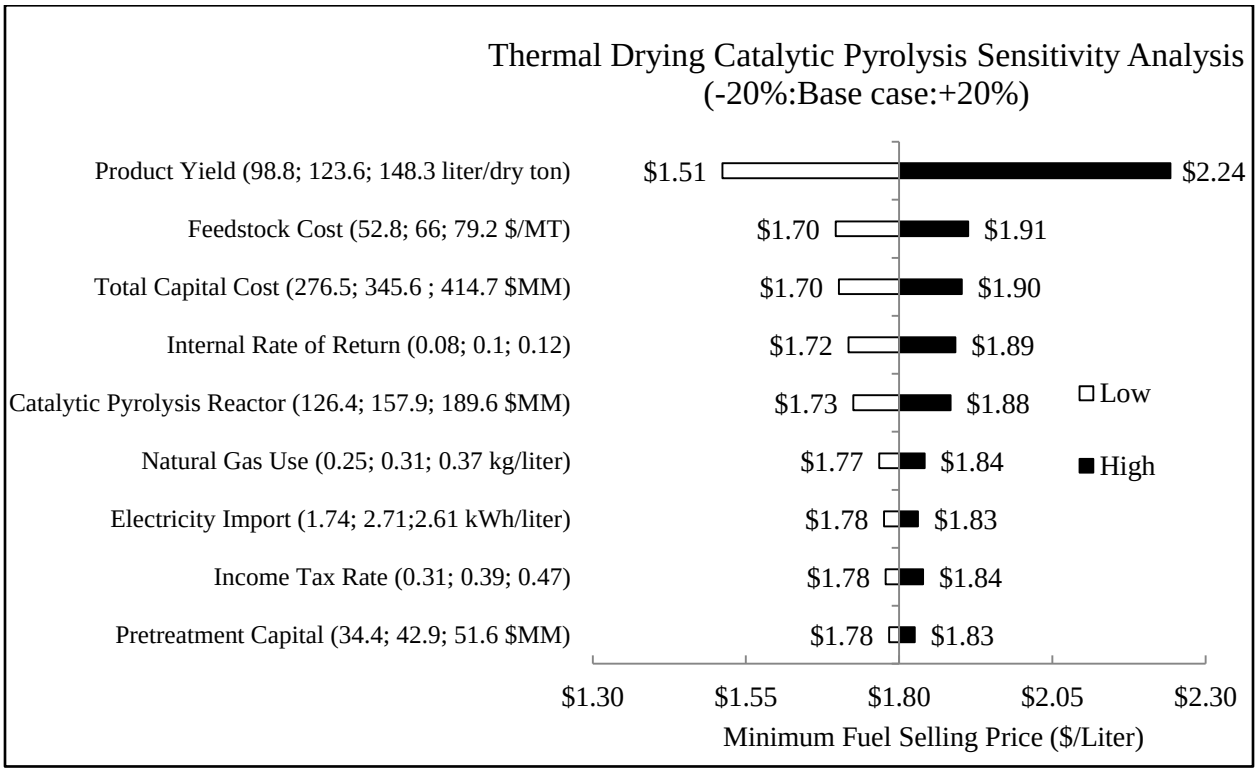

Figure 7. Economic and process sensitivity analysis results for thermal drying catalytic pyrolysis (TDCP) algae biofuel production based on ±20% variability

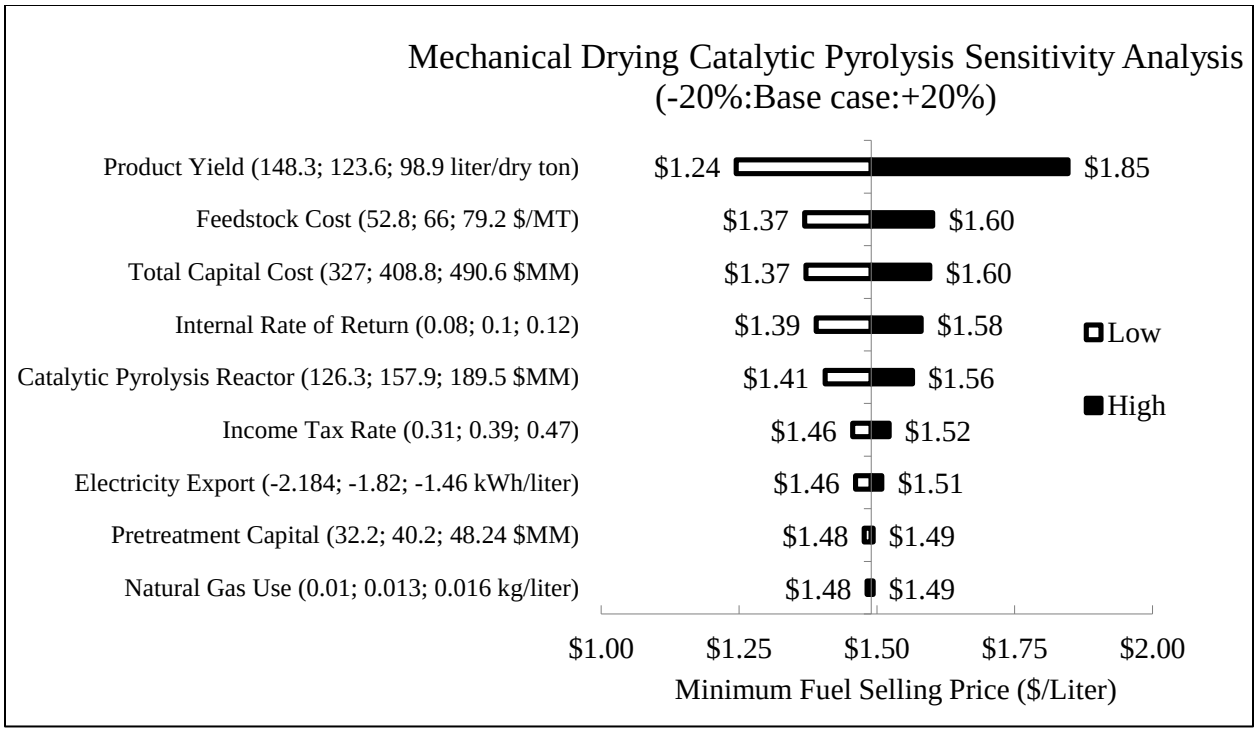

Figure 8. Economic and process sensitivity analysis results for mechanical dewatering catalytic pyrolysis (MDCP) algae biofuel production based on ±20% variability

The sensitivity analysis in this study does not include other key factors of algae biofuel production, including factors related to algae growing and harvesting, which have high levels of uncertainty. Data availability for these factors limits the ability to quantify their impact on algae biofuel prices. However, the base case analysis suggests that large variations in factors like wastewater treatment may not significantly change the MFSP. Large variations in algae production costs would likely be a reflection of the wider range of feedstock costs, which impact the MFSP significantly. Future studies could attempt to address these variable uncertainties as data become publicly available.

Conclusion

Microalgae remnant is a potential feedstock for the production of transportation fuels via catalytic pyrolysis and upgrading. However, there is limited information about the economics for this pathway in the public literature. The objective of this study was to develop a techno-economic assessment of two microalgae remnant biofuel scenarios using two distinct water removal methods: thermal drying and partial mechanical dewatering.

The analysis revealed that catalytic pyrolysis and subsequent upgrading of microalgae remnant at a dry feed rate of 2000 MTPD yields a mixture of BTX (25.9 gal/MT), diesel (4.2 gal/MT), and gasoline (2.5 gal/MT). Two scenarios of thermal and mechanical water removal methods were investigated in this study. At 10% IRR, thermal drying (TDCP) and mechanical dewatering (MDCP) scenarios resulted in minimum fuel selling prices of $1.80/liter and $1.49/liter, respectively. The operating costs of the two scenarios were $145.8 million/year and $120.8 million/year, respectively. (The higher operating cost for the TDCP scenario was due to a higher natural gas input required for feedstock drying.) The capital costs were $346 million and $409 million for TDCP and MDCP, respectively, where the higher capital cost for the MDCP scenario was mainly due to the cogeneration unit incorporated in the process. The energy flow analysis reveals that net energy conversion is unfavorable in the TDCP scenario while it is favorable for the MDCP scenario. Energy analysis also shows that most of the feedstock energy can be successfully used in thermal drying of wet feedstock, while incorporating mechanical dewatering further improve the economics of the pathway. Further analysis can focus on finding out the ideal mechanical dewatering requirement to achieve optimum process economics. Future

work could also investigate the separation of the BTX mixture fractionation and ammonia recovery from wastewater to assess the expected improvements in overall process economics.

Acknowledgements

The authors would like to acknowledge financial support from the U.S. Department of Energy (Contract No.: 11.2.2.4 - 24444). The authors would also like to thank Sue Jones and Aye Meyer from Pacific Northwest National Laboratory for useful discussions and Joy Graveline for editing this paper.

Reference

1. C. W. T.J.Lundquist, N.W.T.Quinn, J.R.Benemann, Energy Bioscience Institue, University of Califonia, Berkerly, Califonia, 2010.
2. M. T. Abayomi O. Alabi, Eric Bibeau, *Seed Science*, 2009.
3. M. J. Haas and K. Wagner, *European Journal of Lipid Science and Technology*, 2011, **113**, 1219-1229.
4. H. Maula, Neste Oil Corporation. , 2013.
5. K. Wang, R. C. Brown, S. Homsy, L. Martinez and S. S. Sidhu, *Bioresour Technol*, 2013, **127**, 494-499.
6. D. F. Ryan Davis, Edward D. Frank,Mark S. Wigmosta and A. M. C. Andy Aden, Philip T. Pienkos,Richard J. Skaggs, Erik R. Venteris,Michael Q. Wang, INL/NREL/PNNL, U.S. Department of Energy Biomass Program, 2012.
7. J. Hill, E. Nelson, D. Tilman, S. Polasky and D. Tiffany, *Proceedings of The National Academy of Sciences*, 2006.
8. K. Wang and R. C. Brown, *Green Chemistry*, 2013.
9. P. J. Valdez, J. G. Dickinson and P. E. Savage, *Energy & Fuels*, 2011, **25**, 3235-3243.
10. D. Humbird, R. Davis, L. Tao, C. Kinchin, D. Hsu, A. Aden, P. Schoen, J. Lukas, B. Olthof, M. Worley, D. Sexton and D. Dudgeon, *Process Design and Economics for Biochemical Conversion of Lignocellulosic Biomass to Ethanol*, Report NREL/TP-5100-47764, National Renewable Energy Laborotary, USA, 2011.
11. S. Thangalazhy-Gopakumar, S. Adhikari, S. A. Chattanathan and R. B. Gupta, *Bioresource Technology*, 2012, **118**, 150-157.

12. I. V. Babich, M. van der Hulst, L. Lefferts, J. A. Moulijn, P. O'Connor and K. Seshan, *Biomass and Bioenergy*, 2011, **35**, 3199-3207.

13. R. A. Meyer, in *Handbook of Petroleum Refining Processes*, McGraw Hill, New York, 3rd edn., 2004, ch. 8, p. 52.

14. R. Thilakaratne, T. Brown, Y. Li, G. Hu and R. Brown, *Green Chemistry*, 2013.

15. UOP, *Opportunities for biorenewable in oil refineries, Final technical report*, 2005.

16. M. M. Wright, Y. Román-Leshkov and W. H. Green, *Biofuels, Bioproducts and Biorefining*, 2012, **6**, 503-520.

17. S. Czernik, R. Evans and R. French, *Catalysis Today*, 2007, **129**, 265-268.

18. EIA, Anual average electricty price 2007, http://www.eia.gov/totalenergy/data/monthly/pdf/sec9_11.pdf.

19. EIA, Annual average natural gas price 2011, http://www.eia.gov/totalenergy/data/monthly/pdf/sec9_15.pdf.

20. SRI, *Hydrogen Production from Natural Gas, PEP Yearbook International 2007*, SRI International, United States, Menlo Park, CA, 2007.

21. SRI, *PEP Yearbook International 2007*, SRI International, United States, Menlo Park, CA, 2007.

22. M. M. Wright, D. E. Daugaard, J. A. Satrio and R. C. Brown, *Fuel*, 2010, **89**, S2-S10.

23. T. R. Brown, R. Thilakaratne, G. Hu and R. C. Brown, *Fuel*, 2013, **106**, 463-469.

24. T. R. Brown, Y. Zhang, G. Hu and R. C. Brown, *Biofuels, Bioproducts and Biorefining*, 2012, **6**, 73-87.

25. M. S. Peters, K. D. Timmerhaus and R. E. West, in *Plant design and economics for chemical engineers*, McGraw-Hill, Newyork, 5th edn., 2003, ch. 6, pp. 250-251.

26. J. R. Grace, A. A. Avidan and T. M. Knowlton, in *Circulating Fluidized Beds*, Chapman & Hall, London, UK, 1 edn., 1997, ch. 4, p. 131.

27. USDA, 2011.

28. Evergent, 2013.

29. INL, personal communication.

30. R. A. Meyer, in *Handbook of Petroleum Refining Processes*, McGraw Hill, New York, 3rd edn., 2004, ch. 7, p. 33.

CHAPTER 4

CONVERSION OF METHOXY AND HYDROXYL FUNCTIONALITIES OF PHENOLIC MONOMERS OVER ZEOLITES

A paper Published by *Green Chemistry*

Rajeeva Thilakaratne , Jean-PhilippeTessonnier , Robert C. Brown

Abstract

This study investigates the mechanisms of gas phase anisole and phenol conversion over zeolite catalyst. These monomers contain methoxy and hydroxyl groups, the predominant functionalities of the phenolic products of lignin pyrolysis. The proposed reaction mechanisms for anisole and phenol are distinct, with significant differences in product distributions. The anisole mechanism involves methenium ions in the conversion of phenol and alkylating aromatics inside zeolite pores. Phenol converts primarily to benzene and naphthalene via a ring opening reaction promoted by hydroxyl radicals. The phenol mechanism sheds insights on how reactive bi-radicals generated from fragmented phenol aromatic rings (identified as dominant coke precursors) cyclize rapidly to produce polyaromatic hydrocarbons (PAHs). Resulting coke yields were significantly higher for phenol than anisole (56.4% vs. 36.4 %) while carbon yields of aromatic hydrocarbons were lower (29.0% vs. 58.4 %).

Water enhances formation of hydrogen and hydroxyl radicals, thus promoting phenol conversion and product hydrogenation. From this finding we propose phenol-water-zeolite

combination to be a high temperature hydrolysis system that can be used to generate both hydrogen and hydroxyl radicals useful for other kinds of reactions.

Introduction

Zeolites are widely used as catalysts to refine crude petroleum to hydrocarbon fuels. They are also recognized for their ability to convert carbohydrate-derived compounds from biomass into aromatic hydrocarbons during pyrolysis.[1-8] ZSM-5 zeolite was reported to be the best in achieving high conversions to aromatic hydrocarbons, mainly due to its unique structure and acid sites.[1,9]

Despite already having an aromatic structure, lignin in biomass presents a unique challenge to upgrading via pyrolysis. This is mainly due to the recalcitrant bonds formed from repolymerizing phenolic intermediates produced from lignin during pyrolysis conversion.[10-12] Processes with high ionic energies such as that occur during catalytic process are required to deconstruct and deoxygenate these condensed bonds formed from lignin.[13, 14] However, the literature reports poor yields of hydrocarbons for pyrolysis of lignin and upgrading lignin derived bio-oil in the presence of zeolites with high coke (carbonaceous material produced on the surface of the catalyst) generation cited as the reason for this inferior performance.[13, 14]

Catalytic pyrolysis of biomass over zeolites is generally considered to occur in two steps: 1) depolymerization and devolatilization; and 2) catalytic conversion of volatiles to hydrocarbons.[15,16] Depolymerization produces phenolic monomers containing hydroxyl, methoxy, carbonyl, vinyl and methyl functionalities and these are abundant in bio-oil obtained from fast pyrolysis of biomass.[10] Of these, hydroxyl and methoxy functionalities are most commonly produced from lignin and are thought to be the driving force of the reactivity of lignin

and lignin-derived products.[17] In this study we analyze catalytic upgrading of anisole and phenol using ZSM-5 zeolites to understand the conversion of lignin-derived phenolic monomers with the aim of reducing coke generation and increasing the yield of aromatic hydrocarbons.

Zhu et al.[18] describe high temperature non-catalytic decomposition of phenol to its keto-isomers while Friderichson et al.[19] explain how polyaromatic hydrocarbons (PAHs) are formed from anisole. Hemings et al.[20] studied the kinetics of pyrolysis and oxidation of anisole, mainly focusing on combustion intermediates of lignin and reaction rates. Rahimpor et al.[21] discuss anisole conversion in a plasma reactor for catalytic and non-catalytic reactions, but do not provide a mechanistic explanation for these steps. Prasomsri et al.[22] explored the effectiveness of anisole conversion in the presence of hydrocarbons during catalytic pyrolysis over HY and HZSM5 zeolite catalyst, although the mechanism of conversion was not explored. Several researcher claim conversion involves a "carbon pool" within the zeolite pores without providing a detailed explanation of the phenomenon.[4, 6] Guisnet and Gilson[1] claim that the conversion of high molecular weight hydrocarbons over zeolites occurs via the carbonium ions, but provide no details on how oxygenated compounds convert inside zeolite pores. The present study explores the radical and ionic mechanisms involved in the conversion of anisole and phenol monomers over zeolites to produce hydrocarbons.

Experimental section

Material

ZSM-5 zeolite catalyst powder (CBV 2314) in ammonia form with Si/Al mole ratio of 23 and surface area of 425 m^2/g was purchased from Zeolyst International. The catalyst was heated at 5 °C min^{-1} and calcined at 550^0C for 5 hours in a muffle furnace prior to use. The powder was

then pressed into pellets using a hydraulic press (Carver, hydraulic unit, USA). The pellets were crushed to form catalysts particles in the size range of 212 - 300µm. All reactants including ^{13}C carbon labeled anisole and phenol used in this analysis to validate mechanisms were purchased from Sigma Aldrich with nearly 100% purity (Anisole: 99%, Phenol: 99%, 1,2,3-trimethoxybenzene: 98% , Benzaldehyde: 99% , 1,4- benzoquinone: 98% , Hydroquinone: 99% , Catechol: 99% , Anisole-phenyl-$^{13}C_6$: 99% and 99 atom % , Phenol-1-^{13}C: 98% and 99 atom%).

Methods

A Frontier Tandem system with a micro-pyrolysis reactor and an ex-situ catalyst bed (**Figure 1**) was used for catalytic pyrolysis experiments.[6-8] Approximately 250µg of liquid monomer was placed in a deactivated stainless steel sample cup containing a small disc made of ultra clean, high quality fine glass fibers (Frontier, Auto-Rx disc). This disc adsorbs the monomers to prevent evaporation during the preparation step. The catalyst bed was loaded with 40 mg of prepared zeolite catalyst, which was deemed in preliminary experiments to be sufficient quantity for thorough contacting of the pyrolysis vapors with the zeolite. The monomers were pyrolyzed at 600ºC and the volatiles generated were transported through the catalyst bed, also maintained at 600ºC. This temperature is high enough to provide sufficient activation energy for reaction but low enough to prevent excessive formation of non-condensable gases.[13, 14] Volatiles were identified by the GC/MSD and quantified using GC/FID. Gases were identified by injecting known gases and quantified by injecting known gas mixture volumes via GC/TCD. After duplicate runs, the coked catalyst bed was analyzed for carbon content using an elemental analyzer (vario MICRO cube, Elementar, USA). Pyrolytic char (carbonaceous material produced in non-catalytic thermal conditions) content was calculated using residue mass in the

sample cup after pyrolysis, assuming 100% carbon in the char. A similar procedure was adopted for anisole and phenol carbon isotopes runs used for mechanisms validation purpose.

Non-catalytic pyrolysis runs were also performed for anisole and phenol using similar reaction conditions, without catalyst in the second reactor bed. Influence of water in phenol conversion was analyzed in an identical setup with a catalyst bed, by injecting 0.5µL, 1µL and 5µL quantities of water in to the sample cup, which consist of approximately 250µg of phenol and an adsorber disc prior to being pyrolyzed.

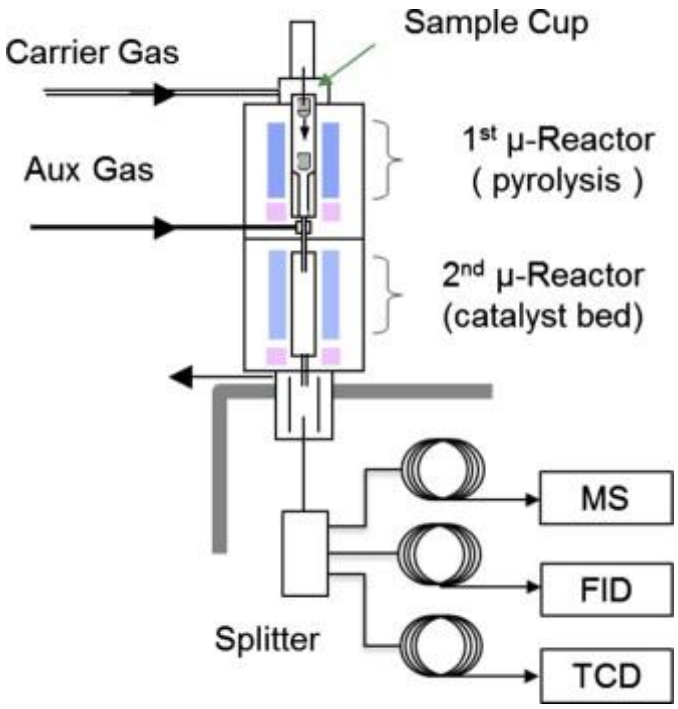

Figure 1. Schematic diagram of the micro-pyrolysis system used in this study

Results and discussion

As shown in **Table 1** anisole produced significantly higher carbon yield of aromatic hydrocarbons (58.4 % carbon) than phenol (29.0% carbon), which gives evidence that the type of

oxygen functionality attached to the aromatic ring plays an important role conversion over zeolites. Phenol produced significantly higher coke (56.4% carbon) than anisole (36.4% carbon). Phenol also produced a considerable amount of char (12.4% carbon) from non-catalytic polymerization in the cup. PAHs yield was 17.7% for phenol with only 12.8% for anisole. Most importantly, the selectivity of PAHs for phenol was 61.3% with only 22.9% for anisole. Contrary to the reported role of anisole promoting PAHs, these results indicated that the contribution from phenol for PAHs generation was significantly higher compared to anisole.[19] Gas yields were relatively small and similar for both cases.

Product selectivity was significantly different for these two monomers, as illustrated in **Table 1**. The main products from anisole were benzene and toluene, while from phenol they were benzene, naphthalene, and biphenyl. This indicates distinct mechanisms for their conversion over ZSM5 catalyst. Even though zeolites provide ionic influence to the reactions, predominantly radical-based mechanisms have been proposed for the catalytic conversion of these two monomers after investigating product formation routes, as explained later.[11, 23]

As proposed in this study, anisole conversion starts by producing phenol and methenium ion with the help of acid sites on the surface of the zeolite catalyst (**Figure 2)**. The methylene radical generated from anisole is thought to be stabilized in the form of methenium ion. Phenol then reacts with the methenium ion to form benzaldehyde with a dehydrogenation step. Next, benzaldehyde decarbonylates to benzene on the acid sites. Supporting these observations, Pramosri et al.[22] report phenol as the major intermediate generated from anisole over zeolites. Kim et al.[11] show that during fast pyrolysis methoxy functionality converts to a less extent to

Table 1. Product distribution for catalytic conversion of anisole and phenol (ex-situ catalysis, pyrolysis temperature = 600^0C, catalyst bed temperature = 600^0C, reactant loading = 0.25mg, catalyst CBV 2314, catalyst loading = 40mg)

Feedstock	Anisole	Phenol
Overall yield (%)		
CO	1.1 ± 0.1	1.0 ± 0.1
CO2	0.3 ± 0.1	0.2 ± 0.1
Catalytic coke	36.4 ± 0.8	56.4 ± 2.5
Pyrolytic char	0.0 ± 0.0	12.4 ± 0.1
Aromatics	58.45 ± 0.7	29.0 ± 1.2
Olefins	2.8 ± 0.2	2.8 ± 0.2
Total	99.1 ± 0.16	101.9 ± 3.8
Aromatics selectivity (%)		
Benzene	47.9 ± 0.5	34.2 ± 0.8
Toluene	21.9 ± 0.0	2.2 ± 0.2
C8 aromatics[a]	4.1 ± 0.0	0.4 ± 0.1
Naphthalene	9.5 ± 0.3	27.9 ± 0.6
Biphenyl	1.2 ± 0.1	11.7 ± 0.0
C9 aromatics[b]	3.2 ± 0.3	2.1 ± 0.1
$C10^+$ aromatics[c]	12.2 ± 0.3	21.7 ± 0.3
Olefin selectivity (%)		
Ethylene	55.1 ± 1.4	46.1 ± 1.8
Propylene	12.4 ± 2.0	23.0 ± 2.8

[a] C8 aromatics including xylenes andethylbenzene.

[b] C9 aromatics include indene and alkylbenzenes.

[c] $C10^+$ aromatics include alkylated naphthalenes and higher polyaromatic hydrocarbons (PAHs).

aldehyde functionality, as described above. The ionic influences of zeolites are expected to enhance this conversion significantly.

Next, methenium ion acts as an alkylating agent and reacts with benzene to produce toluene, xylenes and a small amount of naphthalenes as final products. These type of electrophilic aromatic substitution reactions under acidic conditions, such as in Friedel-Craft benzene alkylation, are commonly reported in the literature. [24, 25] It is also important to note that the production of methenium ions is not sufficient to completely convert phenol to benzene. The remainder of the phenol converts to additional naphthalene and benzene, as subsequently described. A similar pathway exists for conversion of cresol (the other major intermediate of anisole as shown in **Figure S1**) to toluene although not illustrated in **Figure 2**.

As shown in **Figure 3** phenol conversion is initiated by generation over the zeolite catalyst of aryl, phenoxy, hydroxyl and hydrogen radicals. Some of these recombine to produce products such as benzene, biphenyl, hydrogen and water. Although previous evidence for this mechanism was not found in the literature, we subsequently present experimental evidence in support of it. From here, the hydroxyl radicals combine with phenoxy radicals to form 1,4- benzoquinone as the major product intermediate. Rapport et al.[26] describe the formation of 1,4-benzoquinone from phenol under oxidative conditions via a dehydrogenation step . Similarly, dehydrogenation could explain 1,4-benzoquinone formation observed in our study. 1,4- benzoquinone then goes through ring opening defragmentation via cyclopenta-2,4-dien-1-one, eluting carbon monoxide and producing short lived biradicals that rapidly cyclize inside zeolite pores to form benzene, naphthalene and PAHs, as shown in **Figure 3.** Existence of these C_2H_2 and C_4H_4 bi-radicals has not been established in the literature; however, these might be in equilibrium with acetylene and

cyclobutadiene (or cumulene), respectively, or exist as surface intermediates.[27] This idea is supported by several previous studies that describe benzene formation starting from acetylene and converting via C_2H_2 and C_4H_4 radical intermediates, even at very mild reaction conditions.[28, 29, 30]

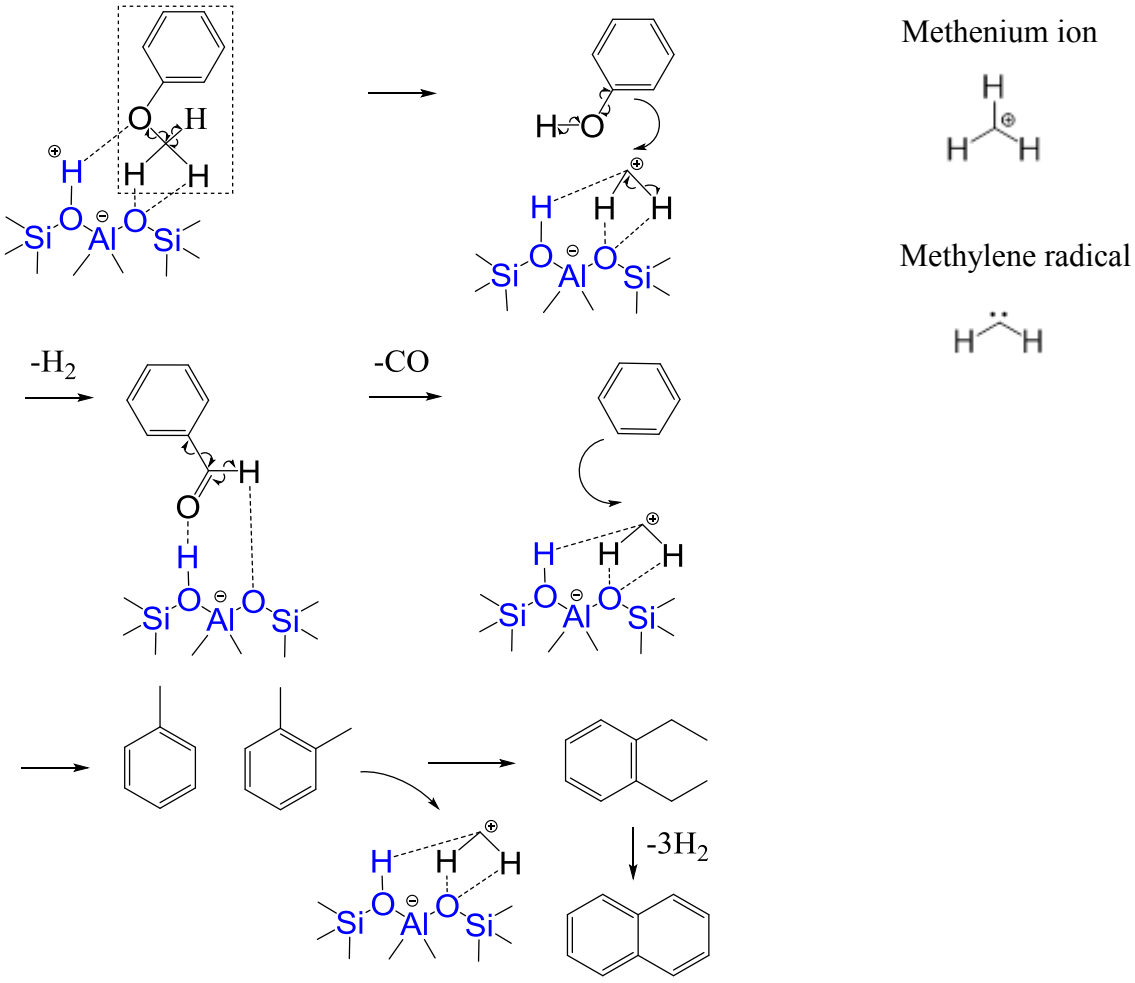

Figure 2. Proposed mechanism for conversion of anisole over zeolites at 600^0C (line 1: phenol and methenium ion formation, line 2: benzaldehyde decarbonylation, line 3: benzene alkylation in zeolites using methenium ions)

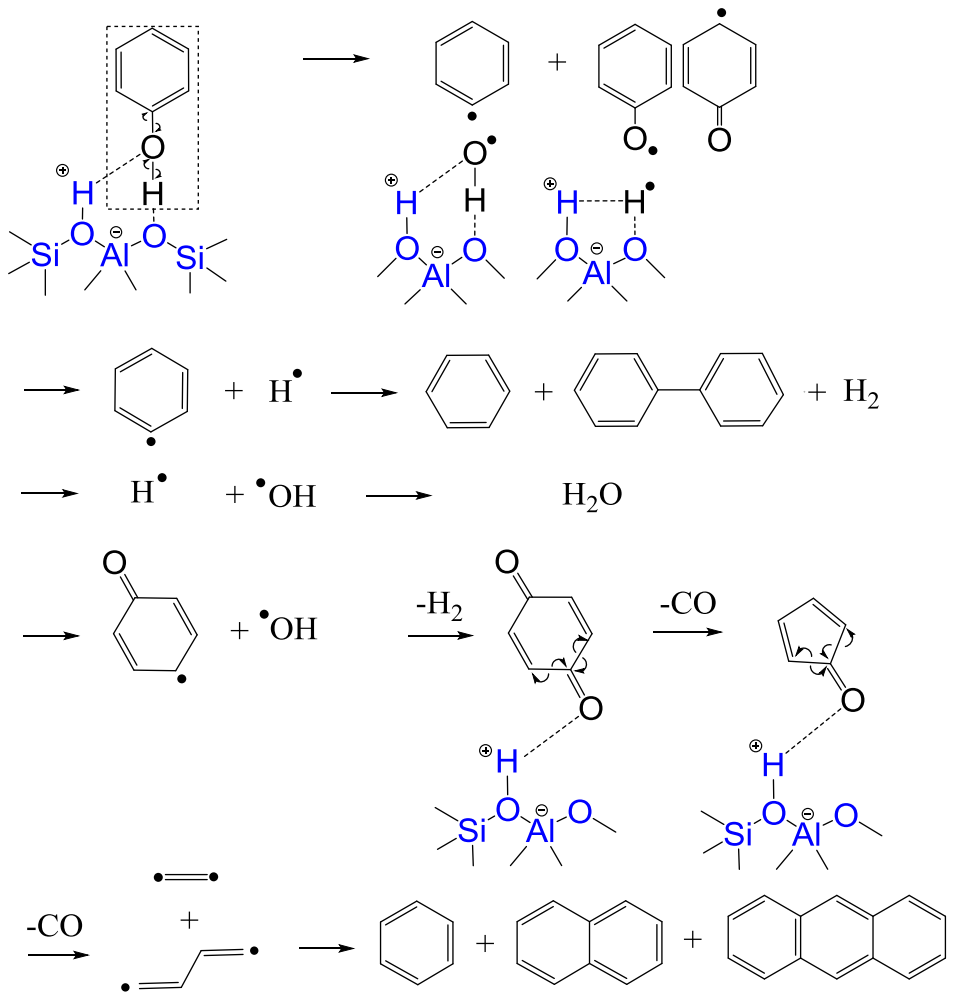

Figure 3. Proposed mechanisms for conversion of phenol over zeolites at 600^0C (line 1: aryl, phenoxy, hydroxyl and hydrogen radicals formation, line 2 & 3 : aryl, hydroxyl and hydrogen radicals recombination, line 4: 1,4- benzoquinone and cyclopenta-2,4-dien-1-one formation and ring fragmentation by decarbonylation, line 5: benzene, naphthalene and PAHs formation)

As illustrated in **Figure 3,** higher coke yield observed for phenol could be attributed to the tendency of ring fragmentation bi-radicals to cyclize to higher molecular weight PAHs. The higher ethylene selectivity for anisole could be a result of two methylene radicals combining, whereas higher propylene selectivity for phenol might result from aromatic ring defragmentation, as previously described. Although CO and CO2 can undergo secondary reactions such as water-gas shift and Boudouard reactions, their carbon yields are insufficient to explain mechanisms

proposed in this study. [31] The greater energy barrier associated with hydroxyl radical generation and high molecular coke formation can be attributed to lower conversion associated with phenol, while methenium ion assisted intermediate phenol conversion could explain the significantly higher conversion for anisole. [32]

Validation of the proposed mechanism for anisole and phenol conversion over zeolites

Proposed anisole conversion mechanism

At 600^0C, typical of fast pyrolysis, anisole shows very little decomposition, resulting in small amounts of phenol, benzaldehyde and cresols. According to the mechanism (**Figure 2**), anisole in the presence of zeolite catalyst first decomposes to phenol through the action of the surface acid sites. Because phenol has a smaller effective diameter, its kinetic hindrance through the zeolite pores would be reduced compared to anisole. [26, 33] As shown in **Figure S1** (see supplementary details)**,** anisole reacted over a coked catalyst bed (generated from five consecutive runs of 2 mg anisole over the catalyst) produces phenol as the major oxygenated intermediate. As catalysts fouled with coke have limited internal pore acidity and restricted access, this observation provides evidence that anisole initially convert to phenol over external surface acid sites while subsequent phenol conversion to aromatic hydrocarbons occurs mainly inside pores.[25, 26]

The step from phenol to benzene was experimentally validated by co-reacting phenol with 1,2,3- trimethoxybenzene (1:1 weight ratio), which is expected to generate methylene radicals that subsequently produce methenium ions over zeolites.[34] The net effect on benzene generation

Table 2. Product selectivity for catalytic conversion of anisole intermediates and 1,2,3-trimethoxybenzene methylene donor (ex situ catalysis, pyrolysis temperature = 600^0C, catalyst bed temperature = 600^0C, catalyst CBV 2314, catalyst loading = 40mg)

Feedstock	Phenol	1,2,3-Trimethoxybenzene	Phenol + 1,2,3-Trimethoxybenzene[a]	Benzaldehyde
Benzene	34.2 ± 0.8	36.4 ± 0.6	40.6 ± 0.5	95.5 ± 0.6
Toluene	2.2 ± 0.2	27.0 ± 0.0	13.0 ± 1.1	1.6 ± 0.4
C8 aromatics[b]	0.4 ± 0.1	5.9 ± 0.1	1.6 ± 0.1	0.6 ± 0.2
Naphthalene	27.9 ± 0.6	13.4 ± 0.1	20.2 ± 0.3	0.8 ± 0.1
Biphenyl	11.7 ± 0.0	0.4 ± 0.0	3.2 ± 0.5	0.7 ± 0.2
C9 aromatics[c]	2.1 ± 0.1	3.4 ± 0.1	2.4 ± 0.5	0.2 ± 0.1
C10+ aromatics[d]	21.7 ± 0.3	13.9 ± 0.5	22.1 ± 1.5	0.7 ± 0.1

[a] Sample contains approximately 500µg of phenol and 1,2,3- trimethoxybenzene mixture at 1:1 weight ratio.
[b] C8 aromatics including xylenes and ethylbenzene.
[c] C9 aromatics include indene and alkybenzenes.
[d] C10+ aromatics include alkylated naphthalenes and higher polyaromatic hydrocarbons (PAHs).

is shown in **Table 2** and **Figure 4**. When phenol was co-reacted with 1,2,3-trimethoxybenzene, benzene selectivity increased to 40.6%, compared to 34.2% for phenol alone and 36.4% for 1,2,3-trimethoxybenzene alone. **Figure 4** shows that the carbon conversion for benzene in the phenol-1,2,3-trimethoxybenzene combination is 20.3 %, significantly higher than theoretical carbon conversion as calculated from individual conversion percentages (15.2%). These observations show that phenol uses methenium ions produced from 1,2,3-trimethoxybenzene for benzene generation in a similar way as the anisole mechanism. The dramatic reduction of toluene selectivity (**Table 2**) for phenol and 1,2,3-trimethoxy benzene mixture, could be mainly due to the effect of phenol having very low selectivity for toluene. In addition, methylene radicals that

contribute to toluene generation for 1,2,3- trimethoxybenzene could be used up for phenol conversion to benzene, reducing toluene in the products for this mixture.

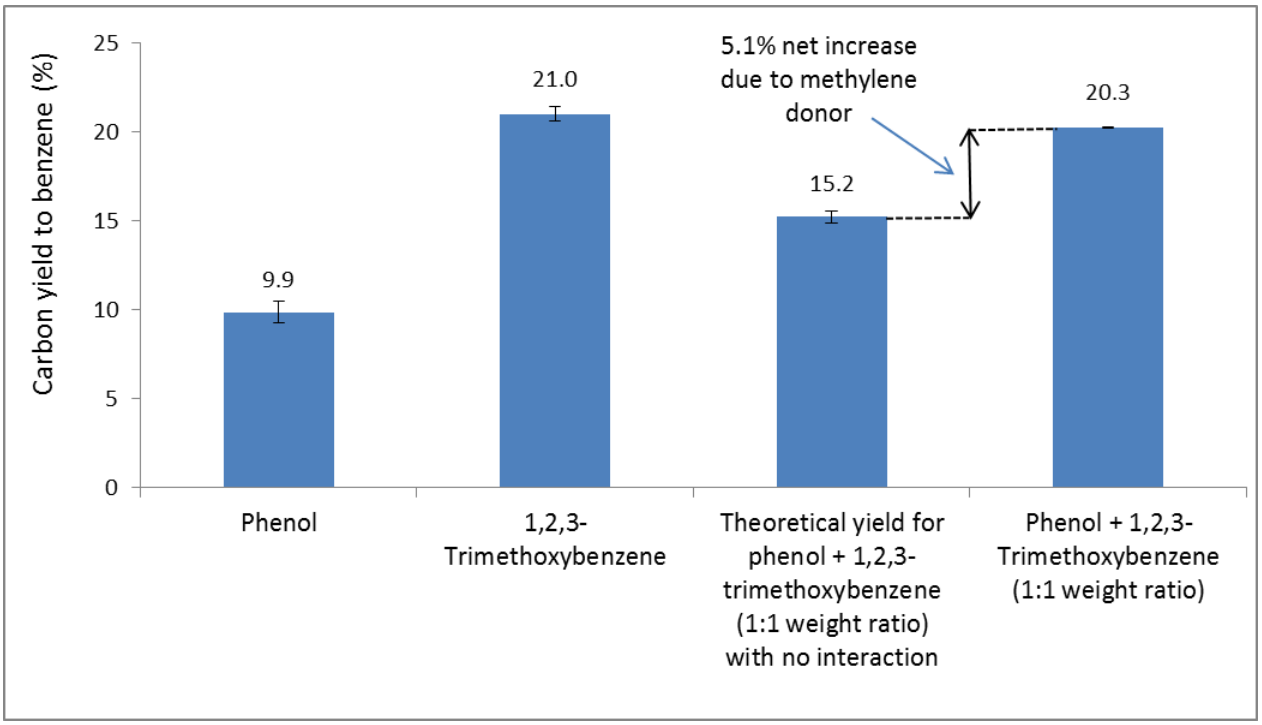

Figure 4. Comparative analysis of carbon yield of benzene from catalytic conversion of phenol alone and in the presence of a methylene donor (1,2,3- trimethoxybenzene)

Proposed phenol conversion mechanism

In phenol conversion, formation of biphenyl is evidence for the presence of aryl and hydroxyl radicals. A very high amount of symmetric biphenyl formation is seen as strong evidence of the radical reactions rather than ionic reactions. The presence of water in the MSD chromatograph for phenol (**Figure S2** in supplementary details) suggests the generation of hydrogen radicals during the reaction, assuming that hydroxyl radicals are generated as described above. Presences of hydrogen radicals imply the presence of phenoxy radicals.[32] Radical recombination is expected to produce benzene and hydrogen as reported for catalytic pyrolysis reactions over zeolites.[1]

Major ring opening step for phenol would be via 1,4- benzoquinone (**Figure 3**). This reaction is bi-molecular as phenoxy radical uses a hydroxyl radical from a different phenol molecule.[26] Resonance of the phenoxy radical can also generate 1,2-benzoquinone isomer similar to 1,4- benzoquinone generation (**Figure 3**) but zeolite pore hindrance would favor linear 1,4-benzoquinone as reported in other studies.[33] However it was not possible to experimentally observe 1,4- benzoquinone, which possibly converted inside zeolite pores. To validate this reaction step, 1,4- benzoquinone was reacted with zeolite under identical conditions. In this reaction, 1,4- benzoquinone generated a similar product distribution as phenol, producing mostly benzenes and naphthalene. Hydroquinone, corresponding phenolic derivative of 1,4-benzoquinone, also generate similar product distribution as phenol providing high product selectivity to benzene and naphthalene (**Table 3).** This implies that hydroquinone and phenol both go through the same intermediate 1,4- benzoquinone. However, 1,4-benzoquinone provide lower C10+ aromatics selectivity mainly due to lack of biphenyl and fluorene produced compared to phenol. Surprisingly, catechol **(Table 3)** produces significantly different product distribution than phenol mostly with hydrogenated monoaromatics, suggesting a conversion route close to a proposed secondary phenol ring opening mechanism (**Figure S3** in supplementary details).

Isotopic 13C labeled study for validating proposed mechanisms for anisole and phenol

Experiments were performed using ^{13}C labeled anisole (anisole-phenyl-$^{13}C_6$) and phenol (phenol-1-^{13}C) isotopes to further validate the major steps involved in the proposed mechanisms. For all pyrolysis runs, EI fragmentation patterns in MSD are assumed similar for both regular molecules and ^{13}C labeled isotopes. All calculations were performed after deducting the

estimated overlapping ion counts of the fragments generated from H cleavage in the EI fragmentation step.

Table 3. Product selectivity for conversion of 1,4 benzoquinone, hydroquinone and catechol over zeolite (volatilizing temperature = 600^0C, catalyst bed temperature = 600^0C, reactant loading = 0.25mg, catalyst CBV 2314, catalyst loading = 40mg)

Feedstock	Phenol	1,4-Benzoquinone	Hydroquinone	Catechol
Benzene	34.2 ± 0.8	37.1 ± 0.1	37.4 ± 0.5	40.8 ± 0.4
Toluene	2.2 ± 0.2	9.6 ± 0.2	12.9 ± 0.8	22.3 ± 1.3
C8 aromatics[a]	0.4 ± 0.1	1.2 ± 0.1	2.2 ± 0.4	4.5 ± 0.7
Naphthalene	27.9 ± 0.6	28.2 ± 0.3	30.0 ± 1.8	16.2 ± 1.1
Biphenyl	11.7 ± 0.0	1.9 ± 1.3	0.7 ± 0.0	0.6 ± 0.3
C9 aromatics[b]	2.1 ± 0.1	2.6 ± 0.3	0.7 ± 0.2	3.5 ± 0.1
C10+ aromatics[c]	21.7 ± 0.3	6.6 ± 1.2	16.1 ± 0.0	12.1 ± 0.3

[a] C8 aromatics including xylenes and ethylbenzene.
[b] C9 aromatics include indene and alkybenzenes.
[c] C10+ aromatics include alkylated naphthalenes and higher polyaromatic hydrocarbons (PAHs).

The MSD-EI spectrum for benzene produced from anisole (**Figure 5**) showed a major M+ peak at m/z= 84, probably coming from the benzene ring of anisole. During the production of benzene from anisole, the probability of benzene forming exclusively from ^{13}C carbons was 70% (**Figure 5**). This show that the anisole benzene ring is mostly preserved to produce benzene in the anisole conversion as illustrated in the anisole mechanism of **Figure 2**. Theoretically, a perfectly scrambled system of seven carbons with six ^{13}C carbons will only have a 14% probability of having all ^{13}C carbons in the benzene ring. However, for naphthalene, only 17% (m/z=138) of the total count are formed exclusively from ^{13}C carbon atoms, indicating a

contribution of the ^{12}C methoxy carbon atoms in naphthalene formation, as shown in **Figure 2**. Toluene and xylene (not illustrated) produced from anisole isotope has M+ equivalent to exactly six atomic mass units higher than the corresponding ions for regular ^{12}C anisole (**Figure 5)**. This indicates that ^{12}C carbon in the methoxy group of anisole apparently participates in alkylation of benzene to produce the toluene and xylenes, as illustrated in the anisole mechanism (**Figure 2**).

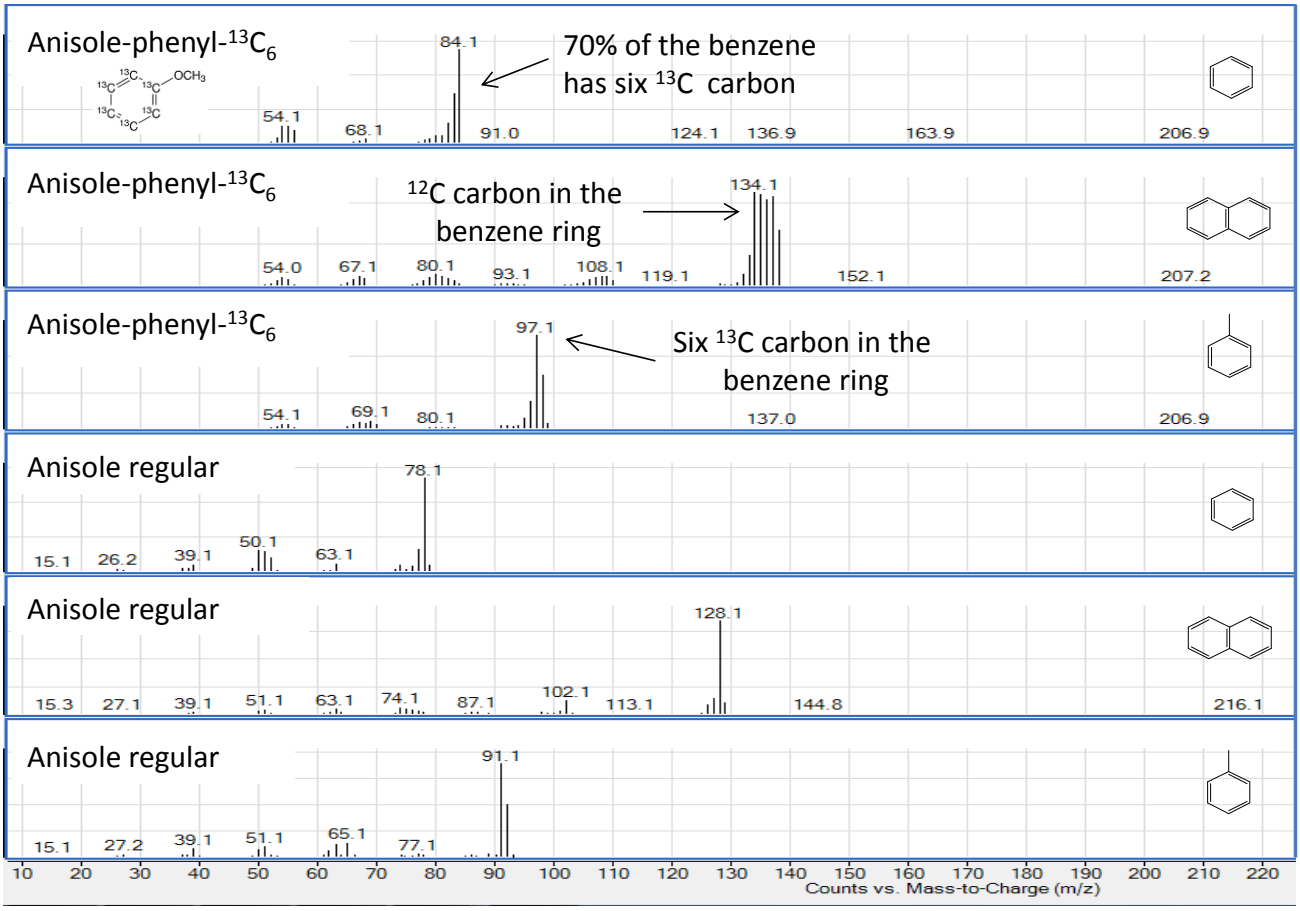

Figure 5. MSD-EI spectrum for benzene, naphthalene and toluene produced from anisole-phenyl-$^{13}C_6$ and regular anisole during catalytic pyrolysis over zeolites at 600^0C.

In preliminary runs with phenol isotope over zeolites, evolved phenol had only 45% of the original isotope (^{13}C position carbon in C-1) as apparent from MSD Electron Ionization (EI) patterns (see **Figure S5** in supplementary section for further details). One explanation for this phenomenon could be isomerization reactions of phenol on the external surface acid sites of the zeolite catalyst. For subsequent calculations, it was assumed that only 45% of the original phenol isotope was available for secondary phenol conversion reactions, assuming phenol isomerization occur initially over the external surface of the zeolite.

Reaction of phenol isotope over zeolites show that product benzene has a main M+ peak of m/z = 79, similar to phenol-1-^{13}C benzene ring (**Figure 6**). This imply that benzene is formed primarily (79%) by coupling of aryl and hydrogen radicals, as shown in the radical recombination step in the phenol mechanism (**Figure 3**). Around 13.9% (m/z=78) of the benzene is exclusively formed from ^{12}C carbons, possibly derived from the ring opening step described in the phenol mechanism of **Figure 3** (secondary benzene formation route). As indicated in **Figure 6,** 8.8 % of the naphthalene is exclusively formed from ^{12}C carbon atoms (m/z=128). This naphthalene generation step should have a similar bi-radical route as illustrated in **Figure 3**. If we assume all naphthalene was formed from benzene, the observed yield of 8.8% represents 98% of the theoretical maximum yield of 9.0%, calculated assuming perfect mechanism and 45% availability of original isotope (phenol-1-^{13}C) due to phenol isomerization. This value (8.8%) is 167% higher than the random naphthalene formed exclusively from ^{12}C (5.3%), calculated assuming arbitrary contributions from perfectly scrambled carbon atoms of phenol isotope molecule. These observations provide evidence that naphthalene formation on benzene ring mostly do not use C-1 carbon as it is lost as carbon monoxide similar to that for the phenol mechanism (**Figure 3)**.

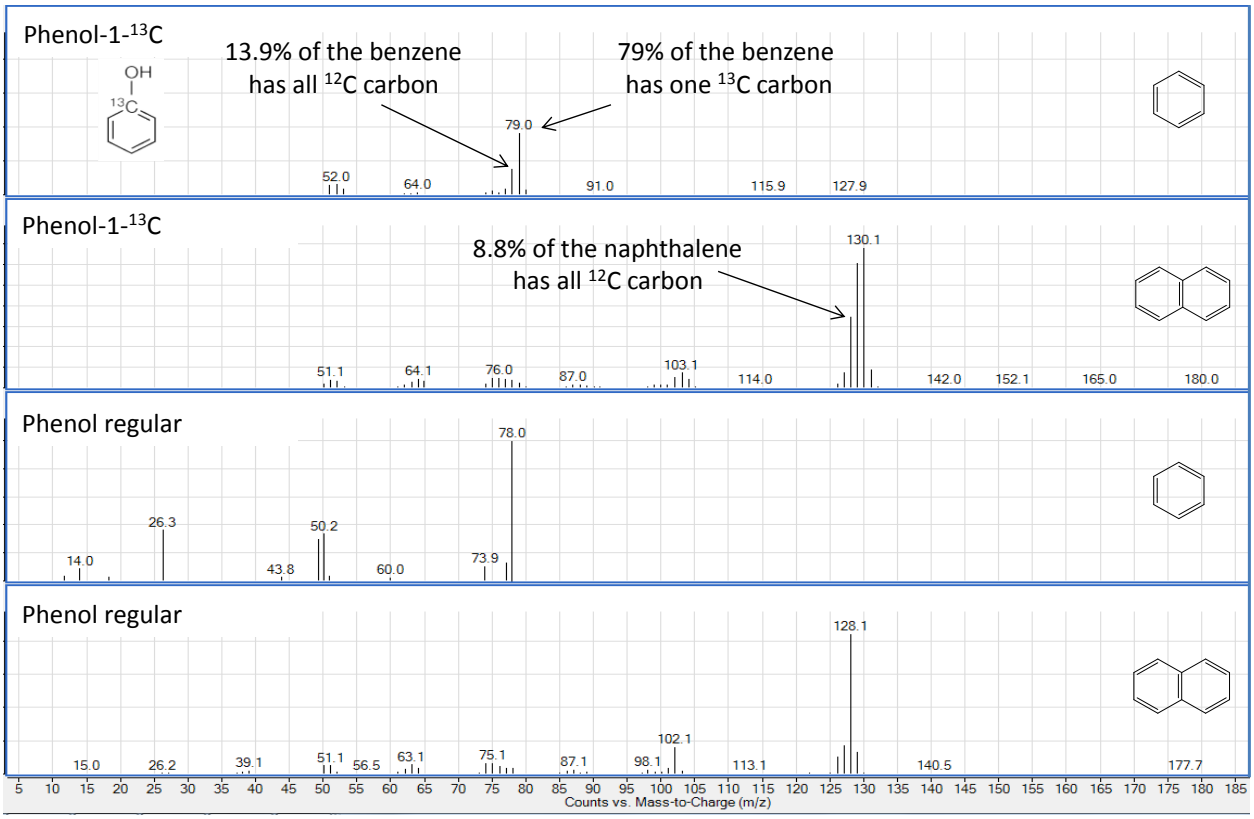

Figure 6. MSD-EI spectrum for benzene and naphthalene produced from phenol-1-^{13}C and regular phenol during catalytic pyrolysis over zeolites at 600^{0}C

<u>Understanding the conversion of phenol over zeolite in presence of water</u>

Since water is a major constituent of most biomass, its effect on reaction mechanisms should be considered. As shown in **Figure 7,** the introduction of water with the sample dramatically increased monoaromatic products and reduced PAHs, especially naphthalene and biphenyl. It is hypothesized that water increases the formation of hydrogen and hydroxyl radicals by shifting the equilibrium of the water-forming radical reaction. Hydrogen enhances saturation of double bonds in the fractionated intermediates, encouraging formation of monoaromatic compounds. Hydroxyl radicals enhance phenol ring-opening reactions while PAHs and coke generation are expected to decrease with increasing hydrogenation. For 1:20 phenol-to-water ratio, overall conversion to aromatic hydrocarbons increased to 43.7%. With enhanced hydrogenation,

conversion via phenol isomer 2,4- cylohexadienone (**Figure S3** in supplementary details) was also expected, which could generate more monoaromatics.

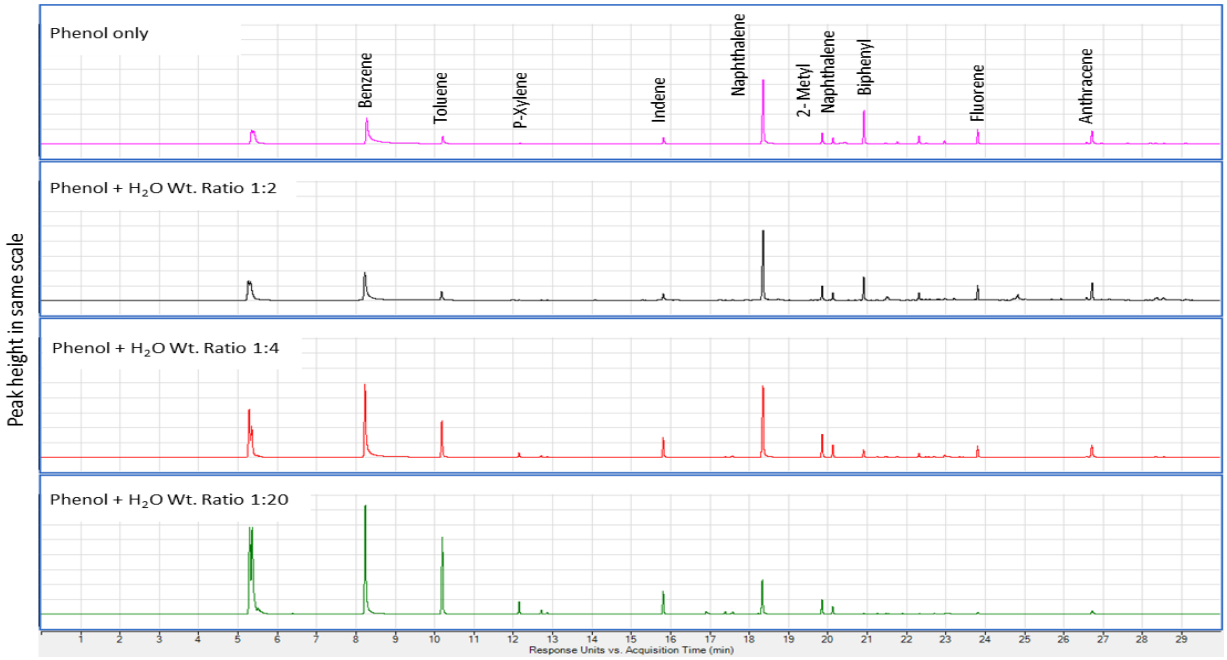

Figure 7. Comparative GC-FID spectra showing effect of water on conversion of phenol over zeolite at 600^0C

<u>Significance of the anisole and phenol conversion mechanisms</u>

Phenol readily polymerizes and dehydrates to char when heated even in the absence of zeolite catalyst. However, we found that in the presence of a methenium ion, the CO bond in phenol can be replaced with a carbon-carbon bond to form benzaldehyde, which readily converts to benzene over zeolite catalyst. Methenium ions generated were also identified as an alkylating agent for aromatic hydrocarbons produced inside zeolite pores. The proposed mechanism for anisole conversion over zeolites suggests that the carbon pool formed from anisole might consist of methenium ions on the acid sites of the catalyst

The ring opening reactions proposed for the conversion of phenol provides new insight into the naphthalenes and PAHs formation that lead to excessive coke during catalytic pyrolysis. The mechanisms for both phenol and anisole conversion have routes to high molecular weight PAHs. However dehydrogenation of phenol to form naphthalene only involves the removal of two hydrogen atoms, so coke might be expected to be more readily formed from phenol than anisole, which requires the loss of eight hydrogen atoms to form naphthalene. This study also indicated the influence of strong OH bond in phenol on PAHs and coke formation.

Water has a dramatic effect on phenol conversion, completely changing product distribution, as shown in **Figure 7.** Bio-oil contain large amount of water and considerable amount of phenols that could be used to produce aromatic hydrocarbons using zeolites as described in this study.

As a summary, study results inform us the importance of removing the phenolic hydroxyl functionalities which is a precursor for coke formation by converting them to beneficial methoxy functionality by the use of methylene donors. Basics understood from these mechanisms are expected to be useful in solving complex issues of phenolic monomers, oligomers and polymers in bio-oil and lignin.

Conclusion

Reaction mechanisms are proposed for the conversion of anisole and phenol over zeolites into aromatic compounds. The different product selectivities for these two phenolic reactants suggest distinctive reaction mechanisms. Anisole is thought to be converted to aromatic hydrocarbons via phenol and benzaldehyde intermediates, while phenol is mainly converted via 1,4- benzoquinone. Methenium ions and hydroxyl radicals are proposed as the most influential

intermediates for anisole and phenol conversion, respectively. The proposed anisole mechanism shows methenium ions convert phenol and alkylate aromatic hydrocarbons inside zeolite pores. Phenol mechanism illustrates how intermediate bi-radicals generate polyaromatic hydrocarbons (PAHs) in zeolites. Product selectivities of major intermediates under identical reaction conditions are used to validate the mechanisms proposed for anisole and phenol. Further validation of the proposed mechanisms was carried out by using anisole and phenol with ^{13}C carbon labeled isotopes. Addition of water increased the conversion of phenol mainly to monoaromatic compounds, probably due to high temperature hydrolysis of water to hydrogen and hydroxyl radicals.

Acknowledgement

The authors would like to acknowledge financial support from the U.S. Department of Agriculture (Contract No. 2011-68005-30411). The authors would also like to thank Gayan Abeykoon, Nuwan de Silva and Umayangani Wanninayake of the Chemistry Department of Iowa State University for helpful suggestions about reaction mechanisms.

Supplementary data

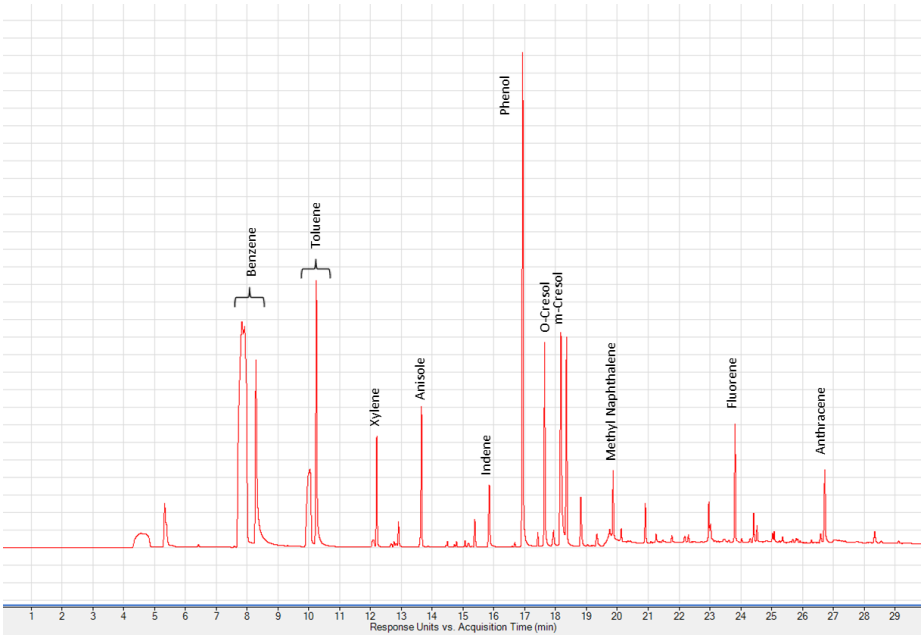

Figure S1. FID chromatogram showing intermediate peaks for anisole run over coked ZSM5 catalyst bed in pyrolysis at 600^{o}C (after five consecutive runs of 2mg anisole over the catalytic bed)

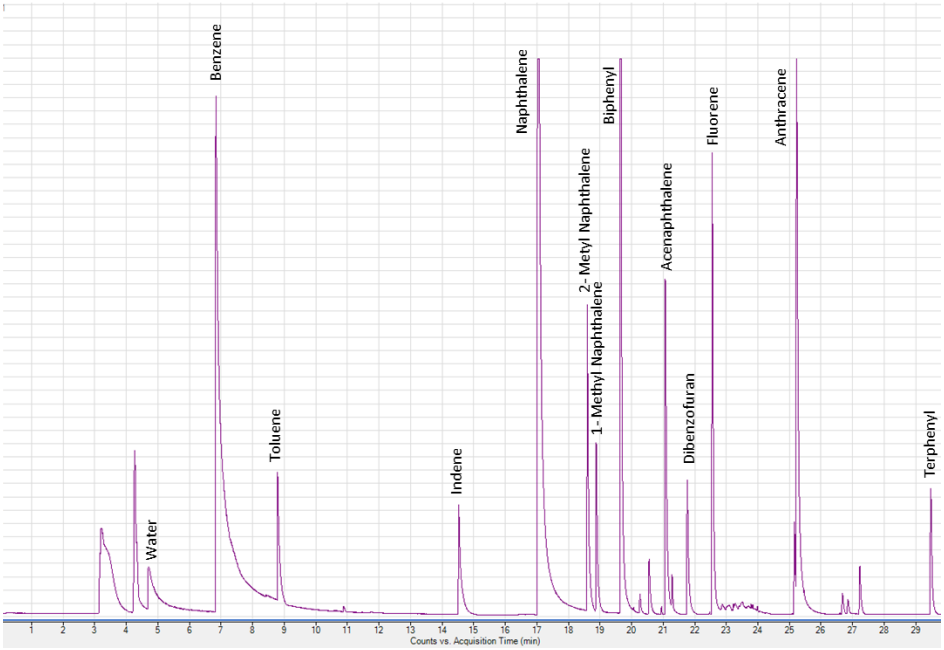

Figure S2. MSD chromatogram showing water and other aromatic products for phenol pyrolysis over zeolites at 600^{o}C

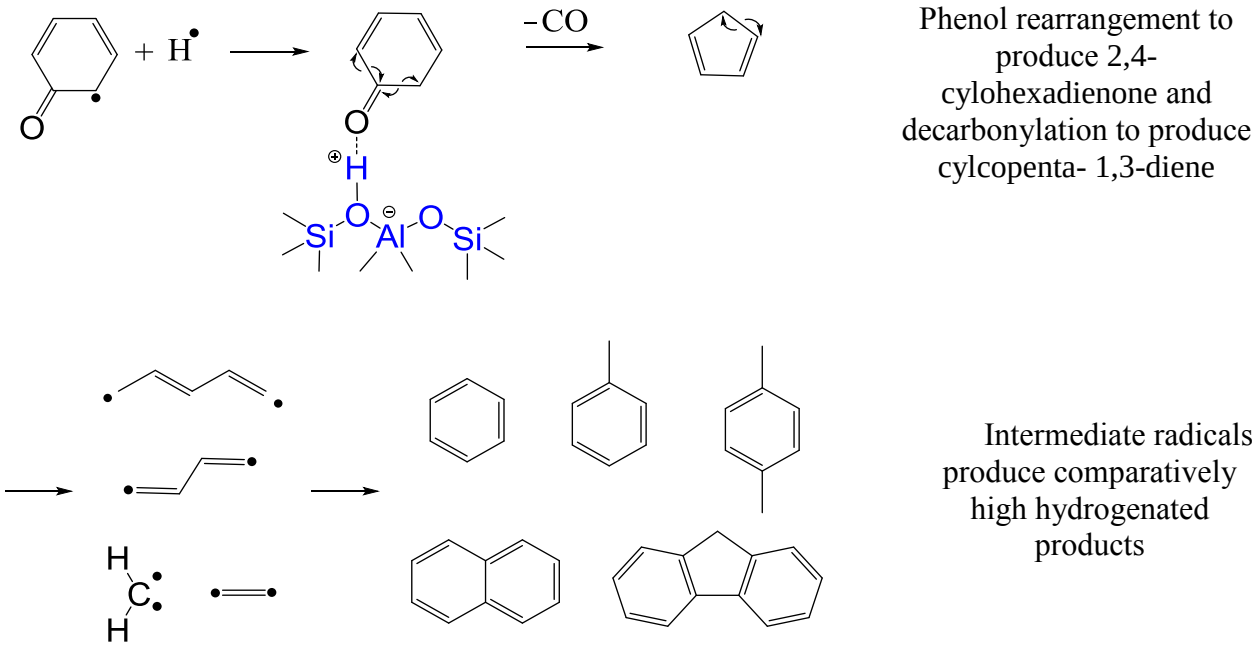

Figure S3. Proposed mechanism for secondary phenol conversion pathway via 2,4-cylohexadienone phenol isomer (thermal route)

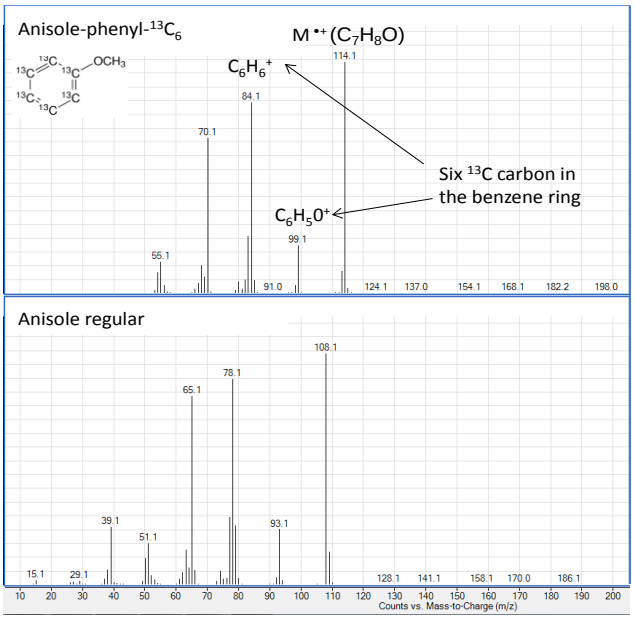

Figure S4. MSD-EI spectrum for anisole produced from anisole-phenyl-$^{13}C_6$ and regular anisole during catalytic pyrolysis over zeolites (anisole-phenyl-$^{13}C_6$ conformity test).

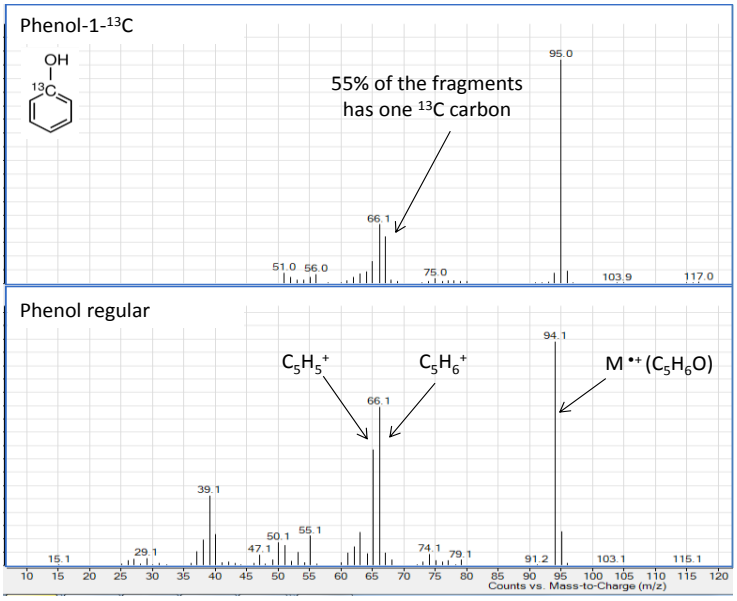

Figure S5. MSD-EI spectrum for phenol produced from phenol-1-^{13}C and regular phenol (phenol-1-^{13}C conformity test)

Reference

1. M. Guisnet and J. P. Gilson, *Zeolites for cleaner technologies*, Imperial College Press, 2002.
2. Y. T. Cheng, J. Jae, J. Shi, W. Fan and G. W. Huber, *Angew Chem Int Ed Engl*, 2012, **51**, 1387-1390.
3. A. J. Foster, J. Jae, Y.-T. Cheng, G. W. Huber and R. F. Lobo, *Applied Catalysis A: General*, 2012, **423-424**, 154-161.
4. T. R. Carlson, T. P. Vispute and G. W. Huber, *ChemSusChem*, 2008, **1**, 397-400.
5. T. R. Carlson, Y. T. Cheng, J. Jae and G. W. Huber, *Energy & Environmental Science*, 2011, **4**, 145.
6. K. Wang, J. Zhang, B. H. Shanks and R. C. Brown, *Green Chemistry*, 2015, **17**, 557-564.
7. K. Wang, K. H. Kim and R. C. Brown, *Green Chemistry*, 2014, **16**, 727-735.
8. K. Wang, P. A. Johnston and R. C. Brown, *Bioresource Technology*, 2014, **173**, 124-131.
9. B. L. S. Ivanova, B. Madani, J. P. Tessonnier, M. J. Ledoux, and C. Pham-Huu, *J. Phys. Chem.*, 2007, **111**, 4368 - 4374.
10. X. Bai, K. H. Kim, R. C. Brown, E. Dalluge, C. Hutchinson, Y. J. Lee and D. Dalluge, *Fuel*, 2014, **128**, 170-179.
11. K. H. Kim, X. Bai and R. C. Brown, *Journal of Analytical and Applied Pyrolysis*, 2014, **110**, 254-263.

12. T. Kotake, H. Kawamoto and S. Saka, *Journal of Analytical and Applied Pyrolysis*, 2014, **105**, 309-316.

13. Z. Ma, E. Troussard and J. A. van Bokhoven, *Applied Catalysis A: General*, 2012, **423-424**, 130-136.

14. X. Li, L. Su, Y. Wang, Y. Yu, C. Wang, X. Li and Z. Wang, *Front. Environ. Sci. Eng.*, 2012, **6**, 295-303.

15. R. Thilakaratne, T. Brown, Y. Li, G. Hu and R. Brown, *Green Chemistry*, 2014, **16**, 627-636.

16. R. Thilakaratne, M. M. Wright and R. C. Brown, *Fuel*, 2014, **128**, 104-112.

17. K. H. Kim, X. Bai and R. C. Brown, *Journal of Analytical and Applied Pyrolysis*, 2014, **110**, 254 - 263.

18. L. Zhu and J. W. Bozzelli, *The Journal of Physical Chemistry A*, 2003, **107**, 3696-3703.

19. A. V. Friderichsen, E. J. Shin, R. J. Evans, M. R. Nimlos, D. C. Dayton and G. B. Ellison, *Fuel*, 2000, **80**, 1747 - 1755.

20. M. Nowakowska, O. Herbinet, A. Dufour and P.-A. Glaude, *Combustion and Flame*, 2014, **161**, 1474-1488.

21. M. R. Rahimpour, A. Jahanmiri, P. Rostami, H. Taghvaei and B. C. Gates, *Energy & Fuels*, 2013, **27**, 7424-7431.

22. T. Prasomsri, A. T. To, S. Crossley, W. E. Alvarez and D. E. Resasco, *Applied Catalysis B: Environmental*, 2011, **106**, 204-211.

23. K. H. Kim, X. Bai, S. Cady, P. Gable and R. C. Brown, *ChemSusChem*, 2015.

24. F. Carey, *On-Line Learning Center for Organic Chemistry*, 1992.

25. G. A. Olah, *Accounts of Chemical Research*, 1971, **4**, 240-248.

26. Z. Rapport, ed., *The Chemistry of phenols*, Wiley, 2003.

27. J. A. Berson, in *Rearrangements in Ground and Excited States: Organic Chemistry: A Series of Monographs*, 2013, vol. 1, p. 311.

28. W. Sesselmann, B. Woratschek, G. Ertl, J. Küppers and H. Haberland, *Surface Science*, 1983, **130**, 245-258.

29. M. Kaltchev, D. Stacchiola, H. Molero, G. Wu, A. Blumenfeld and W. Tysoe, *Catalysis Letters*, 1999, **60**, 11-14.

30. I. M. Abdelrehim, N. A. Thornburg, J. T. Sloan, T. E. Caldwell and D. P. Land, *Journal of the American Chemical Society*, 1995, **117**, 9509-9514.

31. R. C. Brown and T. R. Brown, *Why are We Producing Biofuels?*, Brownia LLC, 2012.

32. S. J. Blanksby and G. B. Ellison, *Accounts of Chemical Research*, 2003, **36**, 255-263.

33. J. Li, E. Kennedy and M. Stockenhuber, *Catalysis Letters*, 2014, **144**, 9-15.

34. W. Wang, Y. Jiang and M. Hunger, *Catalysis Today*, 2006, **113**, 102-114.

CHAPTER 5

ENHANCING THE AROMATIC YIELD FROM COMBINED HOMOGENEOUS AND HETEROGENEOUS ACID-CATALYZED REACTIONS DURING CELLULOSE CATALYTIC PYROLYSIS

A manuscript in preparation

Rajeeva Thilakaratne, Thomas C. Hoff, Jean-Philippe Tessonnier, Robert C. Brown

Abstract

Here, we report a novel method to enhance aromatic yield from a combined homogeneous and heterogeneous acid-catalyzed pathway for cellulose conversion during pyrolysis. Impregnated sulfuric acid was used as the homogeneous catalyst. Silylated zeolites that has reduced strong Brønsted acid and intermediate extra-framework aluminum (EFAL) Lewis acid sites in the external surface of the catalyst was used as the heterogeneous acid catalyst.

Zeolite silylation had relatively minor influence on cellulose conversion, however acid impregnated cellulose (1wt% sulfuric acid) over silylated zeolites produced the highest aromatic yield reported in literature to date (47%). In contrast, pyrolysis of untreated cellulose over unsilylated zeolite yielded only 38% aromatics. This aromatic yield enhancement from acid impregnated cellulose over silylated zeolites was accompanied by a 19% increase in C1-C4 alkanes and olefins and a 52% reduction in coke production. Interestingly, a similar trend was observed for levoglucosan pyrolysis over silylated zeolites. These results imply that external surface acid sites promote coke generation possibly due to lack of spatial restriction,

combined with excessive dehydrogenation reactions. Acid impregnation reduced ring fragmentation in cellulose intermediates and enhanced smaller cyclic oxygenates that can conveniently diffuse into zeolite internal pores, where most of the aromatics are formed.

Using these results, we revisited the mechanism for cellulose conversion over zeolites. Because cellulose is the major constituent of biomass, optimizing levels of acid impregnation and zeolite silylation could offer an attractive pathway for biomass conversion over zeolites. Furthermore, this study suggests zeolite silylation is an attractive method for enhancing the conversion of carbohydrate derived monomers to aromatics.

Introduction

This study demonstrates a novel method to enhance aromatic yield from a combined homogeneous and heterogeneous acid-catalyzed pathway for cellulose conversion during pyrolysis. Silylated zeolites were used as the heterogeneous catalyst which manipulate external surface acidity of zeolites. Acid impregnation in cellulose was used to provide the homogeneous acidity. Furthermore, mechanistic insights on cellulose conversion to aromatics are also provided in this study.

Catalytic pyrolysis over zeolites is attractive for its ability to deoxygenate biomass-derived molecules without the use of hydrogen.[1-4] This approach to biomass conversion is inspired by the success of fluid catalytic cracking (FCC) in the petroleum industry to convert heavy hydrocarbons into fuel range molecules without resorting to expensive hydroprocessing.[5] However, carbon yields of hydrocarbons from catalytic cracking of biomass-derived molecules is relatively low, which is attributed to excessive coke formation.[2, 3, 6, 7] Coke is thought to form

on both the internal and external surfaces of the catalyst, creating a barrier to further conversion without frequent regeneration of the catalyst. Internal coke is attributed to acid-catalyzed dehydrogenation reactions. External coke formation is thought to result from both acid-catalyzed dehydrogenation and incompletely depolymerized polysaccharides and lignin, which dehydrate on the acid sites to coke.[3 7] Carbon loss due to coke formation is significant, which makes the process commercially unattractive at present.[8] Cellulose, as the major constituent of biomass, dominates the chemistry of catalytic pyrolysis.[9] Pure cellulose readily pyrolyzes to high yields of levoglucosan and lesser amounts of light oxygenated compounds.[10] Nevertheless, in the presence of zeolites, a significant portion of carbon in cellulose is converted to coke and non-condensable gases.[8] The chemistry of this phenomenon is not well established.

Silylated zeolites were examined as a catalyst to enhance selectivity of para-xylene from a mixture of xylenes[11] as well as from biomass pyrolysis.[12] Hoff et al.[13] showed that excessive mesoporosity in zeolites reduced cellulose conversation to aromatics indicating deleterious influence of external surface acid sites. Homogeneous acid impregnation was studied as a method to enhance levoglucosan from biomass pyrolysis. Dobele et al.[14] indicated how mineral acids help to reduce the degree of polymerization of cellulose during pyrolysis to enhance levolgucosan yield. In contrast, Kuzhiyil et al.[15] illustrated the role of acid impregnation in biomass on passivating alkali and alkaline earth metals that promote ring fragmentation reactions. Wang et al.[8] observed that catalytic pyrolysis of cellulose produced comparatively higher aromatic yield compared to lignin but did not provide a mechanistic explanation for this difference. In a separate study, Wang et al.[16] noted that oxygenates with smaller molecular diameters tended to form more hydrocarbons and less coke, which is consistent with exclusion of larger molecules from the pores of the zeolite catalysts. Karanjkar et al.[17] showed that

cellulose can be converted to aromatics with 39.5% yield over zeolites, the highest reported yield in literature to our knowledge. Many other researchers have studied pyrolysis of cellulose and levoglucosan over zeolites without providing convincing evidence for a specific mechanism for observed product yields.[2, 7, 18-21]

Experimental

Material

Cellulose was obtained from Sigma Aldrich with a particle size of 20 microns. ZSM5 zeolite in ammonium form (CBV 2314) with SiO_2/Al_2O_3 mole ratio of 23 and surface area of $425 m^2/g$ was purchased from Zeolyst International. The catalyst was heated at $5°C min^{-1}$ and calcined at 550^oC for 5 hours in a muffle furnace to obtain the protonic H-ZSM5 form of the catalyst prior to use. Surface modification to prepare silylated zeolites is described in the methods section. N-hexane (95 %w/w), tetraethylorthosilicate (TEOS) (98% w/w), and sulfuric acid (96.6%w/w) used for silylation treatment and acid impregnation were purchased from Fischer Scientific. Granulated Silica with mild silanol acidity (AEROPERL 300/30) that was used to model silanol acid sites was obtained from Evonik Industries with a particle size of 30μm and a total surface area of $300 m^2/g$.

Methods

Surface modification to prepare silylated zeolites

The silylation treatment coats the outer surface of the zeolite crystals with a layer of silica, thus suppressing the strong Brønsted and intermediate extra-framework aluminum (EFAL) Lewis acid sites on the external surface of the zeolite. TEOS was used as the silylation agent because it

is too large to diffuse inside the ZSM5 pores. Consequently, this treatment deactivates the external acid sites while leaving the bulk structure, chemical composition and internal pores of the zeolite intact.

For the first silylation treatment (sample ZSM5-T1), 2.0g of commercial zeolite was mixed with 0.06ml of TEOS in 40ml of hexane and stirred at 300rpm for 30min using an IKA RCT basic stir plate. The solution was then filtered using a 0.6 – 0.8µm glass microfiber Whatman filter and rinsed with excess hexane. The collected sample was dried at room temperature overnight. Finally, the resulting catalyst was calcined at 550^{o}C in a muffle furnace for 6 hours. This step removes any organic residue associated with TEOS treatment. A similar treatment was performed on ca. 0.5g of the ZSM5-T1 sample to obtain the ZSM5-T2 catalyst.

Catalyst characterization

Ammonia (NH_3) temperature programmed desorption (TPD) was performed using a Micromeritics Autochem II 2920 to probe acid site strength and relative amounts. Prior to analysis, zeolite powder (50mg) was pretreated at 550°C (heating ramp of 10°C/min) in 10 ml/min helium (He) for 1 hour to remove moisture. The zeolite was then saturated with NH_3 for 30min at 50°C using 20ml/min of 10vol% NH_3 in He. The sample was then purged at 100°C under flowing He for 30min. Desorption was recorded using a thermal conductivity detector (TCD) while heating from 100°C to 700°C (10°C/min). TCD curves were normalized using sample mass. TPD curves provide information on changes to the total (Brønsted, Lewis and silanol) acid site density (**Figure S1** in supplementary details). While NH_3 peaks do not differentiate between each type of acid site, Bate et al.[22] demonstrated a strong correlation between the highest temperature desorption peak and N-propylamine decomposition, suggesting

that this peak can be assigned to strong Brønsted acid sites, which are associated with framework aluminum atoms.[11] Other acid sites present include EFAL and silanols. Lewis acidity associated with EFAL originates from structure deformities of aluminium not in the zeolite framework.[11] Silanol acidity is a weak acid catalyst associated with the terminal OH groups attached to silicon atoms in the structure.[11]

Silylation treatment reduced strong Brønsted acid sites by approximately 16-17% for both ZSM5-T1 and ZSM5-T2 (**Table 1**). Intermediate acid sites (EFAL and intermediate Brønsted acids) were reduced by 18-28% in silylated zeolites with the ZSM5-T2 showing a slightly greater reduction than ZSM5-T1. This trend was expected as silica deposits reduce both Brønsted and EFAL acid sites on the external surface of zeolites. The silica treatment also moderately increased weak acid sites (silanol groups). In contrast, TPD analysis of granulated silica revealed only a relatively small number of weak acid sites.

Table 1. TCD ammonia peak areas for silylated zeolites and silica gel in TPD acidity analysis

Acid site type	**Untreated ZSM5**	**ZSM5-T1**	**ZSM5-T2**	**Granulated Silica[a]**
Weak (Silanol)	99.4	117.6	121.4	22.1
Moderate (EFAL and Brønsted)	196.7	161.5	142.6	-
Strong (Brønsted)	91.3	76.8	75.5	-

[a] For granulated EFAL and Brønsted acidity was not detected

The surface area and porosity of the silylated zeolites were measured by nitrogen physisorption at 77 K using a Micromeritics ASAP 2020 system. Samples (50-60mg) were first degassed at 200°C (5°C/min) for 12 hours under dynamic vacuum. The specific surface area was determined using the Brunauer-Emmett-Teller (BET) method. The *t*-plot method was used to discriminate

between microporous and mesoporous surface areas. The pore size distribution (PSD) was calculated from the adsorption branch of the isotherm using the BJH model with Faas correction.

This analysis showed that no significant change in surface area occurred during silylation of zeolites. Both microporous and mesoporous surface areas remained within 10% of the initial values (**Table 2**). For granulated silica, the supplier provided total surface area value was 300 m^2/g, approximately 69% of the total specific surface area for untreated zeolite samples (**Table 2**). According to PSD results in **Figure S2** in supplementary details, ZSM5-T1 showed slightly smaller mesopores compared to the parent ZSM5. This could be due to silica covering the external surface of the zeolite crystals, thus leading to narrower intercrystalline pores. However similar BET values (**Table 2**) obtained for specific surface areas corresponding to mesopores and micropores indicate that the silylation process did not block access to internal acid sites.

Table 2. BET surface areas for silylated zeolites and silica gel

	Untreated ZSM5	**ZSM5-T1**	**ZSM5-T2**	**Silica Gel**
BET total surface area (m^2/g)	436.8	456.8	427.7	300.00[a]
Micropore area (m^2/g)	326.6	333.2	329.6	-
External surface area (m^2/g)	110.2	123.6	110.8	-

[a] Supplier specified total surface area for granulated silica

Catalytic pyrolysis testing

A Frontier Tandem micropyrolysis reactor (3050) in in-situ mode (**Figure 1**) was used for all catalytic pyrolysis experiments.[8, 16, 23] Approximately 10mg of untreated cellulose (sieved size < 100 μm) was mixed with around 200mg of zeolites (sieved size < 50μm) in a vortex mixer with intermittent hand mixing to break agglomerates for approximately 5 minutes to create a

uniform mixture. Approximately 5.25mg of sample from this mixture was placed in a deactivated stainless steel sample cup to be loaded into the pyrolysis reactor operating at 600^{o}C.

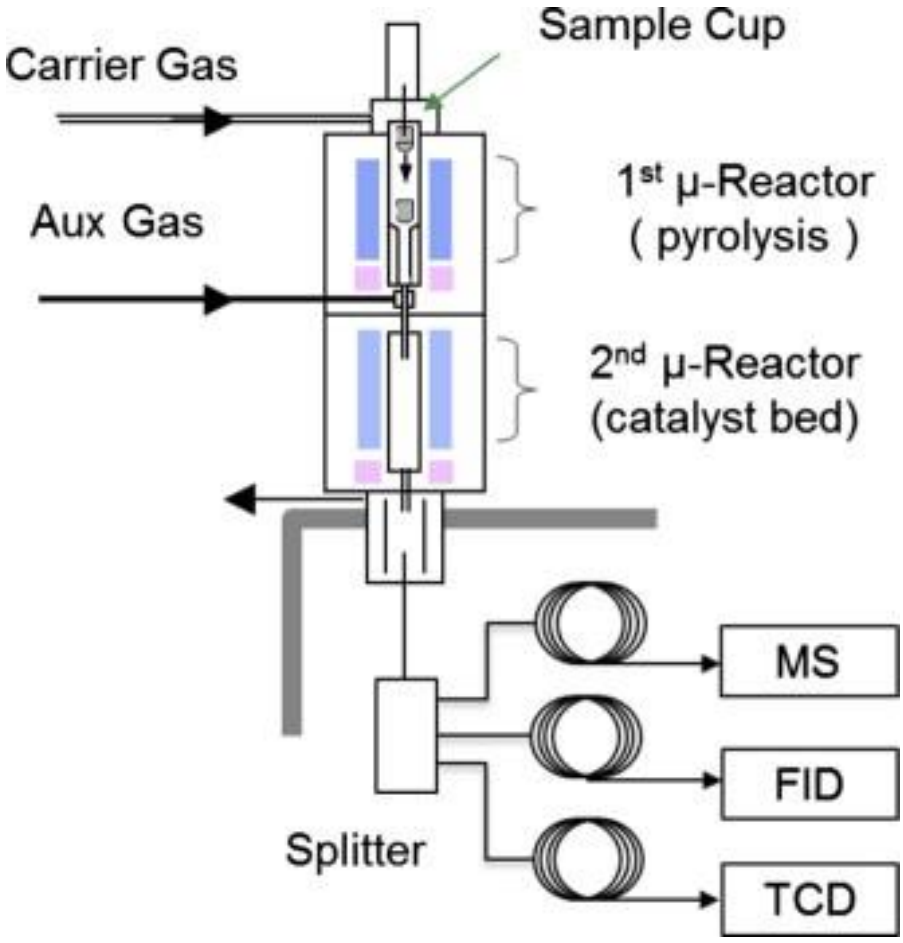

Figure 1. Schematic diagram of the micro-pyrolysis system used in this study

For some tests cellulose was impregnated with sulfuric acid (1wt% of cellulose) using a procedure similar to that employed by Kuzhiyil et al.[15] to evaluate the effect of a homogeneous acid catalyst acting in combination with the zeolite heterogeneous acid catalyst. Acid impregnation of 1wt% provided Brønsted acidity comparable to that found in the unsilylated zeolite (assuming all aluminum atoms are associated with a proton). Acid impregnated cellulose runs were performed in a similar method to unsilylated cellulose runs. Granulated silica runs to

evaluate the influence of silanol acid sites were also performed in an identical reaction setup. Approximately 3.75mg of this sample (which best illustrate the silanol activity) consist of granulated silica (~3.5mg) and untreated or acid impregnated cellulose (~250ug) was prepared in a similar way to the cellulose-zeolite mixture described above. Because levoglucosan is known to be the major product of pyrolysis of pure cellulose, some experiments volatilized levoglucosan at 600^{o}C in the presence of unsilylated zeolite, silylated zeolites and granulated silica. As it is difficult to mix levoglucosan uniformly (moisture absorbs when grinding to a fine powder) with zeolite or granulated silica, approximately 250µg of monomer sample was carefully placed in the bottom of the cup and about 5mg of catalyst were loaded on top before the sample was loaded into the pyrolysis reactor. In some tests untreated cellulose, acid impregnated cellulose, and levoglucosan were pyrolyzed without catalyst (in a similar pyrolysis reaction setup) to observe the non-catalytic reaction products.

Results and discussion

Catalytic pyrolysis of untreated cellulose

As shown in **Table 3**, the effect of silylation on aromatic yields is relatively modest and depends upon the level of silylation. For the mildest silylation treatment (ZSM5-T1), aromatics increase by 6% while coke yield decreases by 21%. For the most severe silylation treatment (ZSM5-T2) aromatics decrease by 11% and coke increases by 10% compared to the unsilylated zeolite. ZSM5-T1 and ZSM5-T2 increase the gas yields of cellulose by 12% and 6% respectively. These results suggest that maintaining an intermediate level of external acid sites (ZSM5-T1 opposed to ZSM5 and ZSM5-T2) is somewhat beneficial in cellulose conversion to aromatics. The increase in silylation of the surface of zeolites (that is, a decrease in acid sites)

increased selectivity toward aromatics with lower kinetic diameter (like benzene, toluene and naphthalene) and decreased selectivity for aromatics with higher kinetic diameter like C8 aromatics (mostly xylenes) and C10+ aromatics (mostly alkylated naphthalenes). These results suggest that aromatics with higher kinetic diameter preferentially form over the external surface of the zeolites due to lack of spatial restriction. This preference could also be due to pore size restrictions of silylated zeolites reducing formation of aromatics with higher kinetic diameter.

Table 3. Cellulose conversion over silylated zeolites during catalytic pyrolysis

	Cellulose + Unsilylated ZSM5	**Cellulose + ZSM5-T1**	**Cellulose + ZSM5-T2**	**Acid Impregnated Cellulose + Unsilylated ZSM5**	**Acid Impregnated Cellulose + ZSM5-T1**
Aromatic yield (%)	37.9±0.4	40.3±0.6	33.6±0.6	30.3±0.7	46.9±0.6
Total gas yield (%)	32.5±0.6	36.3±0.4	34.3±0.3	29.9±0.2	38.8±0.7
CO (%)	20.1±0.3	22.1±0.2	22.1±0.1	16.9±0.5	15.0±0.2
CO_2 (%)	6.2±0.2	6.6±0.1	5.7±0.1	6.8±0.1	8.1±0.3
C1-C4 olefins [a] (%)	5.3±0.3	6.2±0.1	5.3±0.1	5.9±0.2	12.1±0.1
C1-C4 alkanes [b] (%)	0.3±0.0	0.3±0.0	0.3±0.0	0.1±0.0	0.3±0.0
Coke [c] (%)	29.6±1.0	23.4±1.0	32.1±0.9	39.8±0.9	14.3±1.3
Aromatic selectivity (%)					
Benzene	16.2±0.1	16.5±0.1	18.7±0.1	17.7±0.5	15.3±0.3
Toluene	30.2±0.1	32.0±0.1	34.6±0.0	30.0±0.7	35.5±0.3
C8 aromatics [d]	21.2±0.1	19.1±0.1	16.7±0.1	20.9±0.3	27.6±0.6
C9 aromatics [e]	3.6±0.0	2.6±0.0	2.1±0.0	3.0±0.3	1.8±0.1
Naphthalene	9.1±0.1	12.1±0.0	15.4±0.1	10.4±0.4	8.1±0.2
$C10^+$ aromatics [f]	19.7±0.3	17.7±0.3	12.6±0.0	18.0±0.9	11.7±1.3

[a] C1-C4 olefins include ethylene, propylene, and butylene
[b] C1-C4 alkanes include methane and ethane
[c] Calculated by difference
[d] C8 aromatics include xylenes and ethylbenzene
[e] C9 aromatics include indene and alkylbenzenes
[f] $C10^+$aromatics include alkylated naphthalenes and higher polyaromatic hydrocarbons (PAHs)

The relatively small effect of external acid sites on aromatic yields suggests that most cellulose pyrolysis products are small enough to diffuse into the pores of zeolite without the need for additional decomposition on the external acid sites. However, it is well known that the major product of fast pyrolysis of pure cellulose is levoglucosan,[24] which is thought to have a kinetic diameter too large to enter the pores of zeolites.[16] To test this assumption, levoglucosan was pyrolyzed in the presence of unsilylated zeolites, silylated zeolites, and granulated silica as described later in this study.

Catalytic pyrolysis of acid impregnated cellulose

Sulfuric acid impregnated cellulose was pyrolyzed over unsilylated and silylated zeolites (ZSM5-T1) to evaluate the effect of combined homogeneous and heterogeneous acid catalysts. Pyrolysis of acid impregnated cellulose (1wt %) in the absence of zeolite catalyst showed significant amount of dehydrated products such as levoglucosenone, furfural, and furan compared to levoglucosan obtained from pure cellulose (**Figure 2**). This observation is consistent with Kuzhiyil et al.[15] indicating higher dehydrated products from acid impregnated cellulose. Over granulated silica, both untreated and acid impregnated cellulose showed similar dehydrated products possibly due to dehydration activity imposed by homogeneous and silanol acid sites (**Figure 2**). However, untreated cellulose showed considerably higher (125% increase in peak area) ring fragmented products compared to acid impregnated cellulose (**Figure 2**). Furthermore, levoglucosenone and furfural peak areas for acid impregnated cellulose were considerably increased (around 104% and 19% respectively) compared to peak areas obtained for untreated cellulose. This suggests that homogenous acidity possibly help to increase the ring products by converting thermally fragile levoglucosan to more robust dehydrated products such

as levoglucosenone and furfural. In this analysis, only qualitative indication of the activity of the silanol acid sites were observed due to differences in acid site densities, structure, and convoluted influences of other stronger acid sites between silanols in external surface and granulated silica.

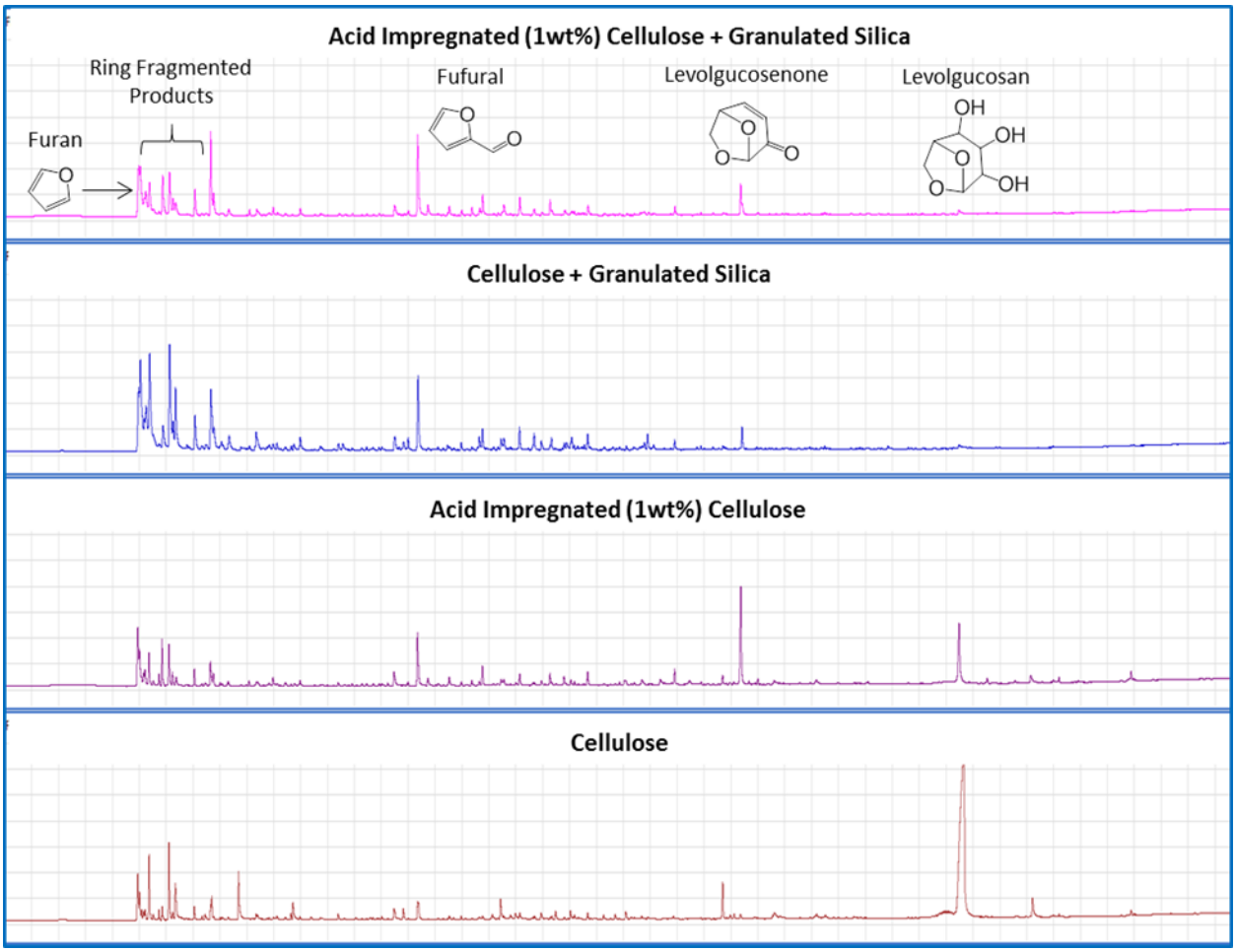

Figure 2. Cellulose and levoglucosan conversion during pyrolysis at 600^{o}C in the absence of zeolites

Incidentally, the homogeneous Brønsted or heterogeneous silanol acidity does not produce discernable amounts of aromatics as occurs for the zeolites. Rather, aromatic formation requires a strong dehydrogenation to accumulate the carbon pools attributed to hydrocarbon formation in

zeolites.[25,26] Unlike strong zeolite acid sites that produce aromatics, homogeneous Brønsted acid sites stop short at these dehydrated intermediates, probably due to sulfuric acid decomposition at temperatures over 300^{o}C. Distinguishable sulfur dioxide peak that appear in acid impregnated cellulose runs during pyrolysis provide evidence for this decomposition of sulfuric acid as mentioned above (**Figure S3**).

Interestingly, 1wt% acid impregnated cellulose over silylated zeolites produce 47% aromatics with a 24% increase compared to untreated cellulose (**Table 3).** To our knowledge, this is the highest reported aromatic yield obtained from cellulose to date. This result is consistent with the expectation that smaller cellulose-derived molecules such as levoglucosenone, furfural, and furan have improved access to the internal pores of zeolites, where most aromatics are formed. It is also in accordance with a recent study that showed zeolite structural changes that improve pore diffusion enhance conversion of cellulose to aromatics.[13] On the other hand, increased dehydrated cyclic intermediates due to reduced ring fragmentation could be the major reason for higher aromatic yields with acid impregnated cellulose compared to untreated cellulose pyrolysis over silylated zeolites. This observation is in accordance with Wang et al.[27] that showed how alkali and alkaline earth metals reduce aromatic yield in biomass catalytic pyrolysis by enhancing ring-fragmented products. Even though effectiveness of homogeneous acids and silanol acids cannot be directly compared, these results imply that homogeneous acids may contribute in direct dehydrating cellulose to produce higher amount of dehydrated cyclic oxygenates. In contrast, silanol acid sites on the external surface probably only convert primary products of the cellulose due to comparatively reduced accessibility. Here, sulfuric acid decomposition at higher temperatures could potentially reduce unwanted cracking, dehydrogenation, and coke generation for cellulose. Surprisingly, acid impregnated cellulose

provides only a 30% increase in aromatics over unsilylated zeolites indicating the negative influence of strong external surface acid sites of the zeolites. This phenomenon is analyzed further in the next section when levoglucosan conversion over unsilylated zeolites, silylated zeolites, and granulated silica are investigated.

The acid impregnated cellulose over silylated zeolites (**Table 3)** show higher selectivity for hydrogen rich aromatics (toluene and xylene with H:C ratio of 1.25 and 1.3 respectively) compared to other unsilylated zeolites runs. This provides signs of lower dehydrogenation prevailing in this method. These runs also showed increase in hydrogen rich gas (H:C ratio of 2 to 4) production (by 19%) while reducing coke dramatically (by 52%), providing further evidence of the lower dehydrogenation in this scenario. Both acid impregnated runs showed significantly lower CO yield following the trend of lower fragmented products, however CO_2 increased somewhat, possibly derived from carboxylic acids formed in slightly acidic reaction conditions.

Catalytic pyrolysis of levoglucosan

Similar to what was observed for cellulose, granulated silica runs for levoglucosan in an identical reaction setup showed dehydrated oxygenates (mainly levoglucosenone and furfural) as the major products, however with considerably smaller peak areas compared to levoglucosan pyrolysis without granulated silica (**Figure 4**). This could be due to either thermal cracking (insufficient dehydration) to produce other ring fragmented products or excessive inter-molecular condensation reactions to produce coke.

As shown in **Table 4**, levoglucosan pyrolyzed in the presence of silylated zeolites showed a significant increase in aromatics. The aromatic yield was on average 76% higher than the untreated zeolites experiments (**Table 4**). Dramatic coke reduction (57%) for levoglucosan over silylated zeolites clearly indicates the deleterious contribution of strong external surface acid sites in unsilylated zeolites in producing coke. Even though levoglucosan and acid impregnated cellulose runs over silylated zeolites provide similar aromatic yields, these results cannot be directly compared as levoglucosan is a primary product of cellulose, combined with the fact that different methods were used for pyrolysis. Nevertheless, these results provide evidence that silanol acid sites contributes in a beneficial way in converting levoglucosan to smaller oxygenates that can diffuse into zeolite pores. However, these silanol acid sites might not be as effective as homogeneous acids as explained previously.

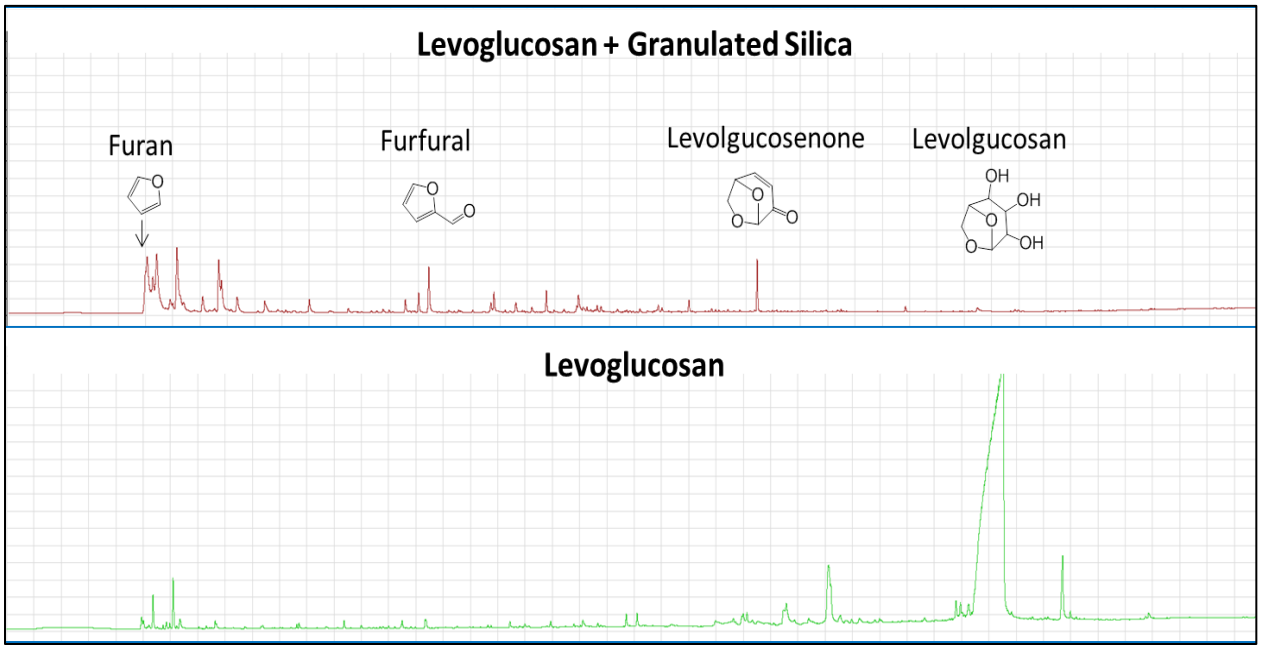

Figure 4. FID chromatograms for levoglucosan conversion during pyrolysis at 600^{o}C in the absence of zeolites

Table 4. Levoglucosan conversion during catalytic pyrolysis over zeolites

	Levoglucosan + ZSM5	**Levoglucosan + ZSM5-T1**
Aromatic yield (%)	26.2±0.7	46.0±0.9
Total gas yield (%)	31.9±1.4	36.1±2.5
CO (%)	17.7±0.6	16.6±1.1
CO_2 (%)	7.4±0.2	7.4±0.6
C1-C4 olefins[a] (%)	5.7±0.7	9.0±0.8
C1-C4 alkanes[b] (%)	0.2±0.0	0.6±0.0
Coke[c] (%)	41.9±2.1	17.9±3.4
Aromatic Selectivity (%)		
Benzene	21.4±0.7	15.6±0.2
Toluene	28.3±0.3	32.4±0.1
C8 aromatics[d]	15.4±0.6	24.5±0.6
C9 aromatics[e]	2.0±0.3	2.0±0.1
Naphthalene	16.5±0.4	11.7±0.3
C10+ aromatics[f]	16.5±1.2	13.8±0.7

[a] C1-C4 olefins include ethylene, propylene, and butylene
[b] C1-C4 alkanes include methane and ethane
[c] Calculated by difference
[d] C8 aromatics include xylenes and ethylbenzene
[e] C9 aromatics include indene and alkylbenzenes
[f] $C10^+$ aromatics include alkylated naphthalenes and higher polyaromatic hydrocarbons (PAHs)

Following the trend observed for acid impregnated cellulose over silylated zeolites, levoglucosan over silylated zeolites, increased toluene and xylene yields while reducing benzene, naphthalene, and higher PAHs (**Table 4**) providing signs of less dehydrogenation. On a different perspective, reactions that promote cyclic aromatics were reduced and reactions that promote alkylation were increased over silylated zeolites. Total gas yields were also increased (by 13%) for levoglucosan over silylated zeolites, similar to what was observed for acid impregnated cellulose experiments over silylated zeolites (**Table 4**). CO and CO_2 yields were relatively unaltered with a small reduction of CO and CO_2 for silylated zeolites (**Table 4**). These

reductions indicate slightly less cracking over silylated zeolites. Apparently, the deoxygenation route for these two catalysts has not changed considerably. Overall these results indicate that, for untreated zeolites, strong acid sites on the external surface promote large coke molecule formation possibly due to lower spatial restriction assisted by dehydrogenation compared to internal pores.

Mechanistic analysis for cellulose conversion over zeolites

Using the carbon yield values, we constructed elemental balance (CHO) of the cellulose and levoglucosan reactions using several assumptions as hydrogen and oxygen balance was difficult to obtain with the adsorption of water onto the catalysts. For untreated zeolites, we assumed the coke was 100% carbon with negligible hydrogen and oxygen content. For silylated zeolites we assumed no net hydrogen production from the reaction. These assumptions were necessary to obtain realistic numbers for an elemental balance for these two reactions. Stoichiometric equations that fulfil these requirements are shown below for 1 mol of a cellulose monomer unit or levoglucosan reacted.

Untreated cellulose conversion over unsilylated zeolites

$C_6H_{10}O_5 \rightarrow$ 2.27 Aromatic (H/C=1.01) + 1.21 CO + 0.37 CO_2 + 1.78 Coke (100% carbon)

+ 0.34 Gases (H/C=2.05) + 4.24 H_2O +1.27 H_2 ……..……(1)

Acid impregnated conversion over silylated zeolites

$C_6H_{10}O_5 \rightarrow$ 2.81 Aromatic (H/C=1.05) + 0.90 CO + 0.49 CO_2 + 0.86 Coke (O/C=0.42)

+ 0.74 Gases (H/C=2.02) + 3.85 H_2O ……..……(2)

Levoglucosan conversion over unsilylated zeolites

$C_6H_{10}O_5 \rightarrow$ 1.57 Aromatic (H:C=1.01) + 1.06 CO + 0.44 CO_2 + 2.54 Coke (100% carbon)

+ 0.35 Gases (H:C=2.03) + 4.24 H_2O +2.21 H_2 ……..……(3)

Levoglucosan conversion over silylated zeolites

$C_6H_{10}O_5 \rightarrow$ 2.76 Aromatic (H:C=1.05) + 1.00 CO + 0.44 CO_2 + 1.07 Coke (O:C=0.15)

+ 0.57 Gases (H:C=2.06) + 4.11 H_2O ……..….(4)

H:C ratio of the aromatics and gases are indicated with brackets for each undefined products. Note that there is significant oxygen content in the coke from silylated zeolite runs with acid impregnated cellulose (O:C=0.42) and levoglucosan (O:C=0.15) that balances the stoichiometry of the reaction. Coke produced from acid impregnated cellulose over silylated zeolites possibly contain a considerable amount of condensation products from cellulose which contain oxygen. The mole balances provide further evidence of considerable dehydrogenation (2.21 and 1.27 moles of H_2 produced for untreated cellulose and levoglucosan respectively) over unsilylated zeolite runs. Water yield remained relatively similar for all cases except for acid impregnated cellulose, primarily due to oxygen in the coke.

A mechanism was proposed from the observed results, depicting dominant reactions over different acid sites for cellulose conversion (**Figure 3**). Cellulose conversion starts with depolymerizing into levoglucosan under non-catalytic reaction conditions. Then silanol acid sites located in the external surface or homogeneous Brønsted acid sites convert the levoglucosan into levoglucosenone through a dehydration step which has the lowest energy requirement.[28] Under more severe conditions, levoglucosenone undergo decarbonylation and dehydrogenation reactions to produce cyclic furans such as furfural and furan.[28, 29] As reported in literature (also as shown in the mechanism), these energetic reactions ideally occur over stronger acid sites;

however as indicated in the granulated silica runs, severe reaction conditions prevailing at 600^{o}C are sufficient to convert levoglucosan to furans (**Figure 2**). [19, 30] These furanic intermediates react further over stronger acid sites to produce aromatics via C_2H_2 and CH_2 radical intermediates.[25] These conversion steps were derived from our previous study, which showed how oxygenates decarbonylate over strong Brønsted acid sites to produce short lived radical intermediates, which eventually convert to aromatics and coke.[25] When space is not restricted such as on the external surface of the zeolites, aromatics grows larger to produce PAHs and coke. This conversion is assisted by further dehydrogenation of CH_2 radicals (that promote alkylation) to C_2H_2 radicals (that promote PAH production) over strong acid sites on untreated zeolite external surfaces. Higher dehydrogenation (**Table 3 and 4**, **Reaction 1 and 3**) and lower alkylated aromatic products (**Table 3 and 4**) result from untreated zeolites provide evidence to the conversion step mentioned above. When space is restricted such as in zeolite internal pores the products cannot grow larger than mostly double ring aromatics, even over strong acid sites. These phenomena result in lower coke generation over silylated zeolites with deactivated acid sites on the external surface. It is important to note that the proposed mechanism is only intended to show major steps predicted in cellulose conversion reactions.

Significance of the study

Catalytic pyrolysis tests conducted in this study indicate how silanol, and other strong acid sites (EFAL and Brønsted) have different roles in converting cellulose over zeolites. Silanol acid sites help mostly to dehydrate intermediate levoglucosan to smaller oxygenates such levoglucosenone, furfural, and furan promoting diffusion into zeolite pores where the majority of aromatics form. In contrast, stronger Brønsted and intermediate EFAL acid sites promote further decarbonylation, dehydrogenation, and ring fragmentation to produce radical

intermediates that generate aromatics, polyaromatics, and coke. Most importantly, this study indicates that external surfaces allow excessive coke generation due to lower spatial restriction compared to internal pores, as observed in the levoglucosan experiments over silylated zeolites. This coke generation explanation is thoroughly supported by the strong dehydrogenation observed over external surface acid sites. Spatial restriction and prominent hydrogen transfer reactions are likely to suppress coke generation inside zeolite internal pores. Acid impregnation in cellulose helped to enhance smaller cyclic oxygenates that diffuse effectively into zeolite pores, while decreasing ring fragmentation products detrimental to aromatic yield. Acid impregnation combined with zeolite silylation provides an ideal homogenous-heterogeneous alternative to detrimental external surface acid sites in zeolites. Using this method, we were able to achieve the highest reported yield of aromatics (47%) so far from cellulose.

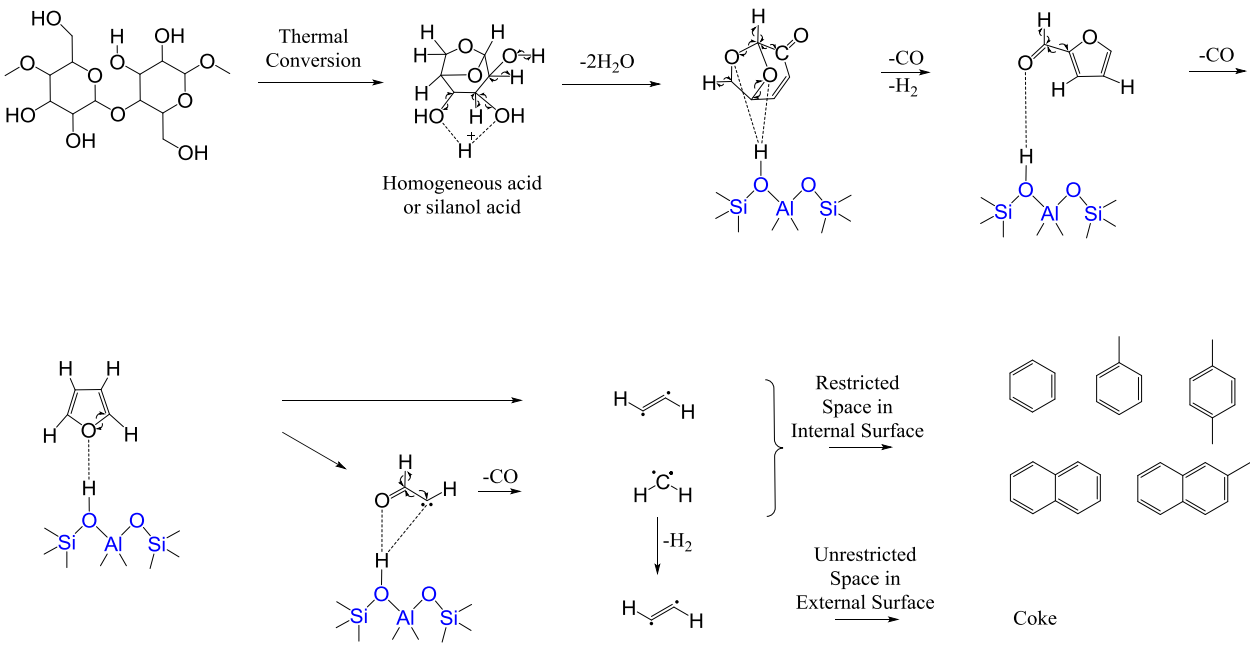

Figure 3. Proposed mechanism for levoglucosan conversion over zeolites during catalytic pyrolysis at 600^{o}C

With the ability of neutralizing the detrimental influence of alkali and alkaline earth metals in biomass, optimized levels of acid impregnation could prove beneficial in whole biomass conversion to aromatics during catalytic pyrolysis.[20] The influence of sulfuric acid decomposition on zeolites might be minimal with possible oxidized sulfur (SO_2 or SO_3) resulting from decomposition at higher temperatures. Moreover, zeolite silylation treatment can be beneficial in converting carbohydrate derived monomers to useful aromatics, reducing unwanted coke generation.

Conclusion

This study illustrates a combined homogeneous and heterogeneous acid-catalyzed methodology for cellulose conversion during pyrolysis using mineral acids and silylated zeolites respectively. Silylation in zeolites reduced the coke generation from cellulose mainly originating from strong external surface acid sites in zeolites. Moreover, acid impregnation in cellulose proved beneficial in producing higher amount of smaller cyclic oxygenates that can penetrate into zeolite internal pores where the majority of the conversion occurs. As a result, acid impregnated cellulose over silylated zeolites provide the highest aromatic yield reported for cellulose to date.

Acknowledgement

The authors would like to acknowledge financial support from the Iowa Energy Center (IEC Grant No. 13-01). The authors would also like to thank Jake Lindstrom, Xianglan Bai, Marge Rover, Patrick Johnston, and Patrick Hall from the Bioeconomy Institute for their useful inputs in discussions related to this study.

Supplementary data

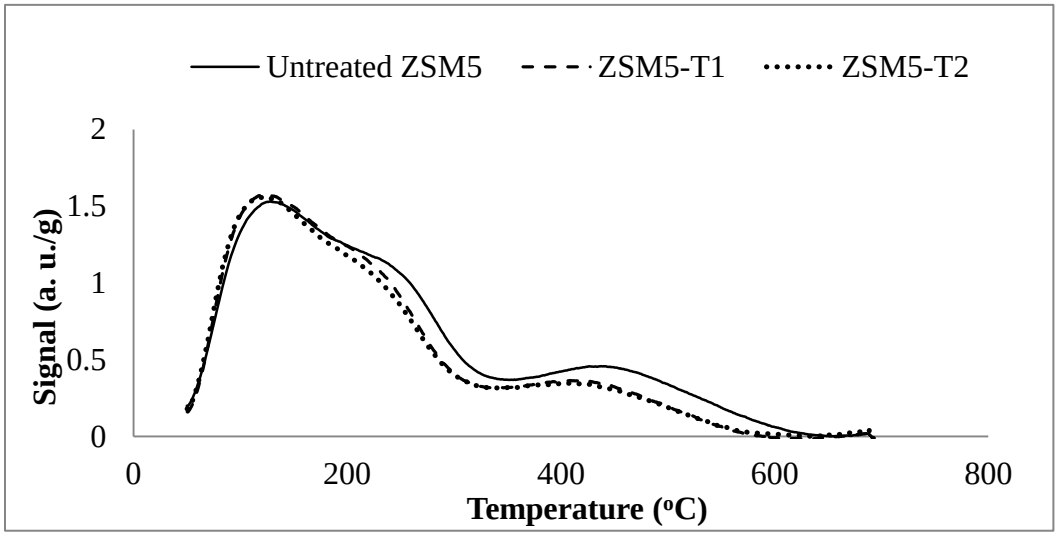

Figure S1. TCD ammonia peaks for TPD acidity analysis of silylated zeolites

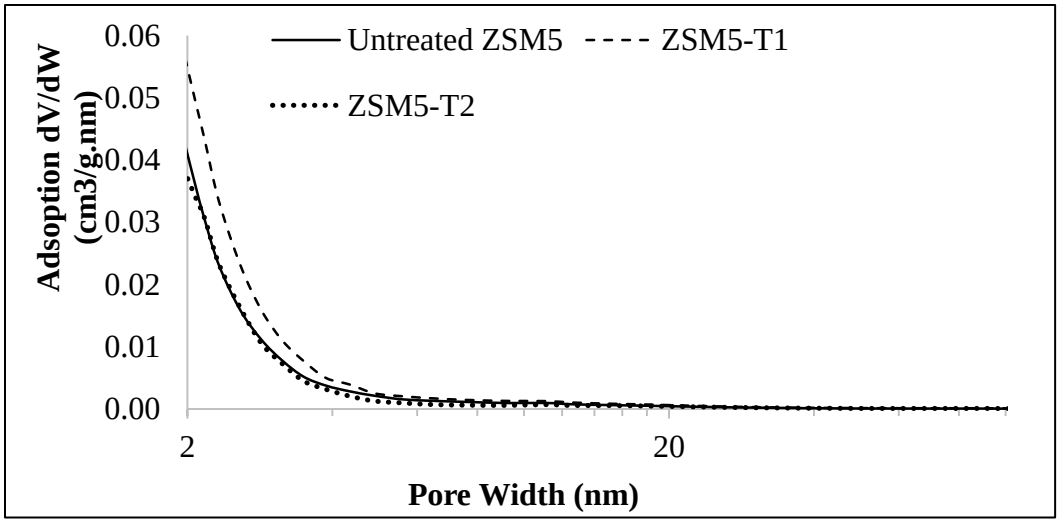

Figure S2. Pore size distribution (PSD) for silylated zeolites calculated using the adsorption branch of the isotherm using the BJH model with Faas correction

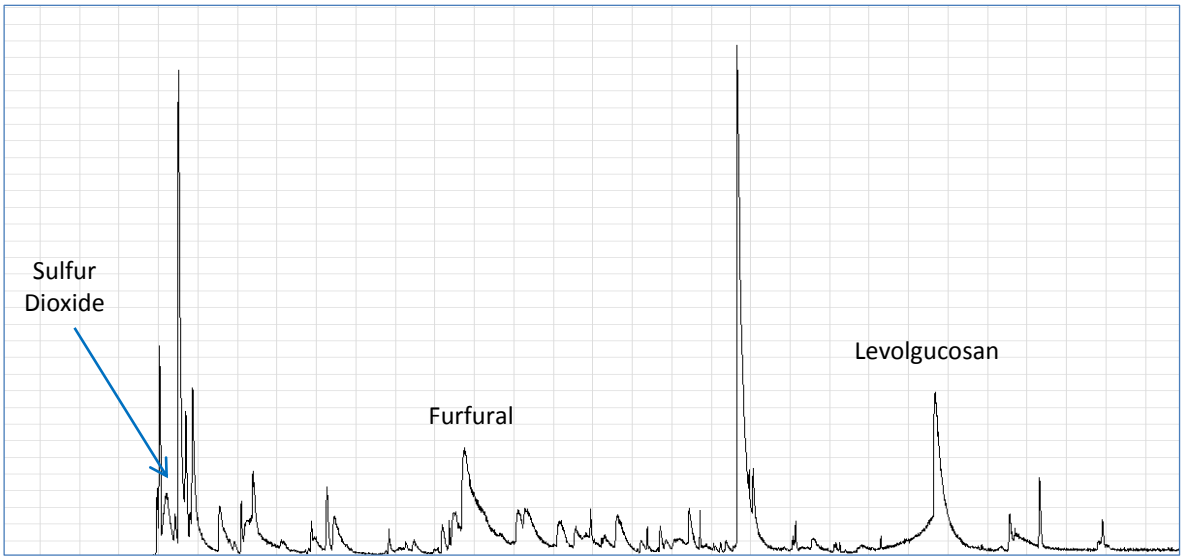

Figure S3. MSD chromatogram showing sulfur dioxide and other primary products of non-catalytic pyrolysis of acid impregnated cellulose at 600^{o}C

Reference

1. Y. Yu, X. Li, L. Su, Y. Zhang, Y. Wang and H. Zhang, *Applied Catalysis A: General*, 2012, **447–448**, 115-123.
2. X. Li, L. Su, Y. Wang, Y. Yu, C. Wang, X. Li and Z. Wang, *Front. Environ. Sci. Eng.*, 2012, **6**, 295-303.
3. C. A. Mullen and A. A. Boateng, *Fuel Processing Technology*, 2010, **91**, 1446-1458.
4. R. Thilakaratne, T. Brown, Y. Li, G. Hu and R. Brown, *Green Chemistry*, 2014, **16**, 627-636.
5. R. A. Meyer, in *Handbook of Petroleum Refining Processes*, McGraw Hill, New York, 3rd edn., 2004, ch. 3, p. 68.
6. J. Piskorz, P. Majerski, D. Radlein and A. C. Scott, *Fuels Energy & Fuels* 1989, **3**, 723,726.
7. Z. Ma and J. A. van Bokhoven, *ChemCatChem*, 2012, **4**, 2036-2044.
8. K. Wang, K. H. Kim and R. C. Brown, *Green Chemistry*, 2014, **16**, 727-735.
9. R. C. Brown and T. R. Brown, *Why are We Producing Biofuels?*, Brownia LLC, 2012.
10. P. R. Patwardhan, J. A. Satrio, R. C. Brown and B. H. Shanks, *Bioresource Technology*, 2009, **101**, 4646-4655.
11. M. Guisnet and J. P. Gilson, *Zeolites for cleaner technologies*, Imperial College Press, 2002.
12. Y. T. Cheng, Z. Wang, C. J. Gilbert, W. Fan and G. W. Huber, *Angew Chem Int Ed Engl*, 2012, **51**, 11097-11100.

13. Thomas C. Hoff, David W. Gardner, Rajeeva Thilakaratne, Kaige Wang, Thomas W. Hansen, Robert C. Brown and J.-P. Tessonnier, *ChemSusChem*, 2016, **9**, 1-12.

14. G. Dobele, T. Dizhbite, G. Rossinskaja, G. Telysheva, D. Meier, S. Radtke and O. Faix, *Journal of Analytical and Applied Pyrolysis*, 2003, **68-69**, 197-211.

15. N. Kuzhiyil, D. Dalluge and R. Brown, *Bioresource Technology*, 2011, **Submitted**.

16. K. Wang, J. Zhang, B. H. Shanks and R. C. Brown, *Green Chemistry*, 2015, **17**, 557-564.

17. P. U. Karanjkar, R. J. Coolman, G. W. Huber, M. T. Blatnik, S. Almalkie, S. M. de Bruyn Kops, T. J. Mountziaris and W. C. Conner, *Aiche Journal*, 2014, **60**, 1320-1335.

18. Z. Luo, S. Wang and X. Guo, *Journal of Analytical and Applied Pyrolysis*, 2012, **95**, 112-117.

19. Z. Ma, E. Troussard and J. A. van Bokhoven, *Applied Catalysis A: General*, 2012, **423–424**, 130-136.

20. S. Kudo, Z. Zhou, K. Norinaga and J.-i. Hayashi, *Green Chemistry*, 2011, **13**, 3306.

21. A. J. Foster, J. Jae, Y.-T. Cheng, G. W. Huber and R. F. Lobo, *Applied Catalysis A: General*, 2012, **423-424**, 154-161.

22. S. A. Bates, W. N. Delgass, F. H. Ribeiro, J. T. Miller and R. Gounder, *Journal of Catalysis*, 2014, **312**, 26-36.

23. K. Wang, P. A. Johnston and R. C. Brown, *Bioresource Technology*, 2014, **173**, 124-131.

24. P. R. Patwardhan, J. A. Satrio, R. C. Brown and B. H. Shanks, *Journal of Analytical and Applied Pyrolysis*, 2009, **86**, 323-330.

25. R. Thilakaratne, J.-P. Tessonnier and R. C. Brown, *Green Chemistry*, 2016.

26. T. R. Carlson, T. P. Vispute and G. W. Huber, *ChemSusChem*, 2008, **1**, 397-400.

27. K. Wang, J. Zhang, B. H. Shanks and R. C. Brown, *Applied Energy*, 2015, **148**, 115-120.

28. J. Hon, S. I. Woo and S.-E. Park, *Recent Advances and New Horizons in Zeolite Science and Technology*, Elsevier, 1996.

29. M. Käldström, N. Kumar, T. Heikkilä, M. Tiitta, T. Salmi and D. Y. Murzin, *ChemCatChem*, 2010, **2**, 539-546.

30. H. Kawamoto, S. Saito, W. Hatanaka and S. Saka, *Journal of Wood Science*, 2007, **53**, 127-133.

CHAPTER 6

CONCLUSIONS AND FUTURE WORK

Conclusion

Various aspects of catalytic pyrolysis of biomass were investigated in this study. First, analysis performed on woody biomass catalytic pyrolysis for transportation fuels shed insights into the process, energy conversion, economics and uncertainty of this pathway. Following chapter on microalgae conversion for transportation fuels during catalytic pyrolysis, payed special focus on thermal and mechanical dewatering techniques and on using process heat for partial dewatering of microalgae. The study also showed the undesirable influence of the lower product yield in commercializing this process. Phenolic monomer conversion analysis over zeolites indicated the detrimental influence of hydroxyl functionality that promote coke generation and beneficial influence of methoxy functionality that reduce coke and enhance aromatic alkylation. Moreover, this study proposed a novel mechanism for coke and aromatic formation over zeolites. Mechanistic study performed on cellulose conversion over zeolites showed that, external surface acid site promote coke due to lack of spatial restriction compared to internal pores acid sites. Homogenous acid impregnation in cellulose has being identified as a method that enhance aromatic yield when combined with silylated zeolites.

Future Work

The results of this dissertation study have opened new avenues to be investigated in future. First, techno-economic models developed in these studies can be expanded and updated for newer technologies and for updated conversion data available. The knowledge gathered from the techno-economic analyses can be used to develop simplified surrogate models that can be used as a tool to screen emerging technologies. Second, reaction mechanisms obtained for simple phenolic monomers can be expanded to more complex lignin derived monomers as well as for whole lignin conversion over zeolites, using similar approach provided in this study. As suggested in cellulose conversion study, process optimization can be performed for acid impregnation and zeolite silylation to obtain even higher cellulose conversion to aromatics than this study reports. The methods proposed in this study could be expanded to whole biomass conversion for improving aromatic yields.

Finally, as these experimental analyses were performed in micro-scale reactors, it is recommended to carry out the proceeding analyses in pilot scale units to understand the influence of heat and mass transfer influences of these conversions. Another area of potential interest would be hydropyrolysis, which can repress coke generation further to enhance biomass conversion to biofuels.